UNIVERSITÀ DELLA CALABRIA

DOTTORATO DI RICERCA IN MECCANICA COMPUTAZIONALE
SCUOLA DI DOTTORATO DI SCIENZA E TECNICA "B.TELESIO"
XXIV CICLO

SETTORE SCIENTIFICO DISCIPLINARE ICAR-08

Tesi di Dottorato

Non-conventional approaches
to statical and dynamical analysis
of geometrically nonlinear structures

Gabriella La Sala

Dissertazione presentata per il conseguimento del titolo di Dottore di
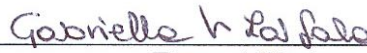Ricerca in Meccanica Computazionale

Novembre 2011

Università della Calabria

Data: Cosenza, Novembre 2011

Autore: **Gabriella Vincenzina La Sala**

Titolo: **Non-conventional approaches to statical and dynamical analysis of geometrically nonlinear structures**

Dipartimento: **Modellistica per l'Ingegneria**

(firma)

Firma dell'autore

Supervisore:

(firma)

Prof. Salvatore Lopez

Coordinatore:

(firma)

Prof. Raffaele Casciaro

Contents

Abstract

The purpose of the work presented in this thesis is to implement two innovative approaches in order to analyze elastic instability problems both in statical and in dynamical field. The proposed formulations have their main feature in the possibility of describing large rotations without the use of rotation matrices in order to overcome complex manipulations required to obtain conservative descriptions and well-posed transformation matrices.

The basis is a total Lagrangian description, where the rigid body motions (translations and rotations) are separated from the total deformation that consequently can be treated using the small-deformation linearized theory.

The principal difference between the suggested two models concerns the chosen parameterization of finite rotations, with distances applied to two- and three-dimensional finite elements in the first and slopes applied to two node finite element beams in the second one.

The theoretical features of the the approaches are presented and their main items are discussed referring to some implementations to planar and spatial beam and thin plate models. An incursion into dynamics has also been performed.

The present approach is featured by the fact that the formulation is simple, the expressions in the equations of the nonlinear system are explicit and computationally efficient, and the analysis is robust and economical.

A large amount of numerical analysis is performed and the good agreement with the results reported in the literature shows the accuracy and capability of the proposed approaches for numerical implementations.

Chapter 1

Introduction

1.1 General remarks

In such cases, linear finite element models are not able to predict the structural response accurately. Hence, the development of efficient and accurate nonlinear finite element models becomes crucial. In fact buckling and post-buckling phenomena exist widely in slender elastic structures, and this always leads structures to experience large displacements and large rotations.

The so-called geometrically exact structural theory, capable of representing finite rotations and finite displacements, has been examined in numerous studies. In this theory, geometrical approximations, such as the linearization of rotation parameters, are not employed.

1.2 Background and literature review

In the computational mechanics community, initial interest in the finite rotations was stirred by the work of Argyris. However, it is only with the development of the so called geometrically exact structural theories which make use of finite rotations, that the urgent need has arisen to address the pertinent computational issues.

There exist various formulations for the description of large translations and large rotations in nonlinear finite element analysis. These formulations had been separated into three categories: the total Lagrangian formulation, updated Lagrangian formulation or corotational formulation. In the total Lagrangian formulation, the motion of a body is defined with respect to the initial configuration, whereas in the updated Lagrangian formulation the motion is defined with respect to the latest configuration. About the corotational formulation, it is motivated by the fact that provides a framework in which standard linear structural elements can be utilized, and therefore, it has become popular in many practical applications. The evolution of the

corotational approach can be traced by referring to the works of Belytschko and Hsieh [8], Argyris [3], Rankin and Nour-Omid [68], Cardona and Geradin [16], Crisfield [19], Peng and Crisfield [67] and Pacoste [66], Ibrahimbegović et al [35].

The origin of the corotational description of motion has its roots in the polar decomposition theorem. According to this theorem, the total deformation of a continuous body can be decomposed into rigid body motion and relative deformation. In the derivation of the finite element, this decomposition is achieved by attaching a local coordinate system to each element so that it rotates with the average rigid body rotation of the element. In this way, the finite rigid body motion part is eliminated from the total displacements. The remaining relative deformation, which is assumed to be small with respect to the local frame, is used for the calculation of strains and element internal nodal forces. As a consequence, the linear beam theory can be used for describing the relative deformation. The geometrical non-linearity induced by the large rigid-body motion is introduced in the transformation matrices relating local and global quantities.

These techniques, however, have to be supported by a robust and economical definition of the rotated local reference system. Basically, the corotational approach suffers from the singularities in the transformation matrices for several angles and requires complex manipulations to overcome nonconservative descriptions due to the noncommutativity of rotations. The interpolation of rotations to measure deformations then requires the use of incremental solution procedures when large rotations are considered. In effect, small rotation increments are hypothesized for the linearization of the configuration space. Consequently, small steps in the continuation process are allowed and a slow convergence is intrinsic to the formulation.

1.3   Finite rotations in 3D space

One of the central issues in the development of a non-linear structural element is the treatment of finite 3D rotations. A general three-dimensional non-linear formulation is not a simple extension of a two-dimensional formulation because fully three-dimensional finite rotations, that are not vector quantities, have to be accounted for .

Plane rotations are easy. A rotation in, say, the $\{x_1, x_2\}$ plane, is defined by just a scalar: the rotation angle θ about x_3. Plane rotations commute: $\theta_1 + \theta_2 = \theta_2 + \theta_1$, because the θs are numbers.

The study of spatial 3D rotations is more difficult. The subject is dominated by a fundamental theorem of Euler: *The general displacement of a rigid body with one point fixed is a rotation about some axis which passes*

through that point.

A consequence of the Euler theorem is that: any rotation θ of a rigid body with a fixed point O about a fixed axis $\vec{\omega}$ can be decomposed into three rotations about three given non-coplanar axes. On the contrary, the final orientation of the rigid body after a finite number of rotations is equivalent to a unique rotation about a unique axis. Determination of the angle and axis is called the *orientation kinematics* of rigid bodies.

Thus spatial rotations have both magnitude (the angle of rotation), and direction (the axis of rotation). These are nominally the same two attributes that categorize vectors. Finite 3D rotations, however, do not obey the laws of vector calculus, although infinitesimal rotations do. Most striking is commutation failure: switching two successive rotations does not yield the same answer unless the rotation axis is kept fixed.

Various possibilities for selecting the parameters for finite rotation representation are placed in practical implementations of computational schemes involving large rotations (direction cosine matrices or orthogonal matrices, Euler angles, quaternions or Euler parameters, Rodrigues' parameters or Gibbs vectors, conformal rotation vectors and rotation vectors); however, only a few of them are fundamentally distinct. Detailed accounts of most used of these parametrizations are presented in the following.

Rotation matrix representation

Generally, the applied rotation analysis of rigid bodies is done by matrix calculus. As we said there are two inherent problems in representing rotations, both related to incontrovertible properties of rotations:

- rigid-body rotations do not commute;

- rigid-body rotations cannot map smoothly in three-dimensional Euclidean space.

The noncommutativity of rotations force us to obey the order of rotations. The lack of a smooth mapping in three-dimensional Euclidean space means we cannot smoothly represent every kind of rotation by using only one set of three numbers. Any set of three rotational coordinates contains at least one geometric orientation where the coordinates are singular, at which at least two coordinates are undefined or not unique. This is the reason why we sometimes describe rotations by using four numbers. We may only use three-number systems and expect to see singularities or use other numbers and cope with the redundancy. The choice depends on the application and method of calculation. For computer applications, the redundancy is not a problem, so

most algorithms use representations with extra numbers. However, engineers prefer to work with the minimum set of numbers.

Within the framework of matrix algebra, finite rotations can be represented in two ways:

- As $3x3$ real orthogonal matrices R called *rotators*. (An abbreviation for *rotation tensor*.

- As $3x3$ real skew-symmetric matrices W called *spinors*. (An abbreviation for *spin tensor*.

Following the notations according to which superscript on a vector denotes the frame in which the vector is expressed, we can indicate as r^G the position vector expressed in frame $G(OXYZ)$ and r^P the position vector expressed in frame $P(Oxyz)$.

In this context a *rotator* R is a linear operator that transforms r^P to r^G when the directional cosines of the axes of the coordinate frames P and G are known:

$$r^G = R\,r^P. \tag{1.1}$$

The *spinor* W corresponds to the vector $\vec{\omega}$, which, along with angle θ, can be utilized to describe a rotator:

$$R[\theta] = I cos\theta + \vec{\omega}\vec{\omega}^T vers\theta + W sin\theta. \tag{1.2}$$

where

$$vers\theta = versin\theta = 1 - cos\theta = 2sin^2(\theta/2) \tag{1.3}$$

and W is the skew-symmetric matrix associated to the vector $\vec{\omega}$

$$W = \begin{bmatrix} 0 & -\omega_3 & \omega_2 \\ \omega_3 & 0 & -\omega_1 \\ -\omega_2 & \omega_1 & 0 \end{bmatrix}$$

In other words, let the body frame $P(Oxyz)$ rotate θ about a fixed line in the global frame $G(OXYZ)$ that is indicated by a unit vector $\vec{\omega}$ with directional cosines $\omega_1, \omega_2, \omega_3$, so that $\omega = \omega_1\vec{i} + \omega_2\vec{j} + \omega_3\vec{k}$. This is called the *axis-angle representation* of a rotation. Two parameters are needed to define the axis of rotation that goes through O and one parameter is needed to define the amount of rotation about the axis. So, an angle-axis rotation needs three independent parameters to be defined. The angle-axis transformation matrix R that transforms the coordinates of the body frame $P(Oxyz)$ to the

associated coordinates in the global frame $G(OXYZ)$ is expressed by the done relation (1.2).

The angle-axis rotation equation (1.2) is also called the *Rodriguez rotation formula* or the Euler-Lexell-Rodriguez formula. It is sometimes reported in the literature as the following equivalent forms:

$$I + W\sin\theta + 2W^2\sin^2(\theta/2),$$
$$I + 2W\sin(\theta/2)[I\cos(\theta/2) + W\sin(\theta/2)],$$
$$I + W\sin\theta + W^2 vers\theta, \tag{1.4}$$
$$[I - \vec{\omega}\vec{\omega}^T]\cos\theta + W\sin\theta + \vec{\omega}\vec{\omega}^T,$$
$$I + W^2 + W\sin\theta - W^2\cos\theta,$$

A rotator is a function of a spinor, so R can be expanded in a Taylor series of W:

$$R = I + c_1 W + c_2 W^2 + c_3 W^3 + ... \tag{1.5}$$

However, because of Cayley-Hamilton theorem ([26]), all powers of order 3 or higher can be eliminated. Therefore, R is a quadratic function of W:

$$R[\theta] = I + a(\lambda W) + b(\lambda W)^2. \tag{1.6}$$

where λ is the spinor normalization factor and $a = a(\theta)$ and $b = b(\theta)$ are scalar functions of the rotation angle θ.

Table 1.3 presents some representations of rotator R as a function of the coefficients a, b and the spinor λW used by different author.

a	b	λ	R
$\sin\theta$	$\sin^2(\theta/2)$	1	$I + \sin\theta W + 2\sin^2(\theta/2)W^2$
$2\cos^2(\theta/2))$	$2\cos^2(\theta/2)$	$\tan(\theta/2)$	$I + 2\cos^2(\theta/2)[\tan(\theta/2)W + \tan^2(\theta/2)W^2]$
$2\cos(\theta/2)$	2	$\sin(\theta/2)$	$I + \cos(\theta/2)\sin(\theta/2)W + 2\sin^2(\theta/2)W^2]$
$1/\theta\sin\theta$	$1/(\theta^2)\sin^2(\theta/2)$	θ	$I + \sin\theta W + 2\sin^2(\theta/2)W^2$

Tab. 1.1: Rotator R as a function of Spinor W.

In conclusion we can summarize that for many purposes the rotation matrix representation, based on directional cosines, is the most useful representation method of rigid-body rotations; however the primary disadvantage of rotation matrices is that there are so many numbers, which often make

rotation matrices hard to interpret. As an alternative we have the axis-angle representation, described by the Rodriguez formula, where a rotation is expressed by the magnitude of rotation, θ, with the positive right-hand direction about the axis of rotation $\vec{\omega}$. Angle-axis representation has also some shortcomings. First, the rotation axis is indeterminate when $\theta = 0$. Second, the angle-axis rotation represents a two-to-one mapping system because $R_{-\omega,-\theta} = R_{\omega,\theta}$. Third, it is redundant because for any integer k we have $R_{\omega,\theta+2k\Pi} = R_{\omega,\theta}$. However, all of these problems can be improved to some extent by restricting θ to some suitable range such as $[0, \Pi]$ or $[-\Pi/2, \Pi/2]$. The angle-axis representation is also not an efficient method to find the composition of rotations and determine the equivalent angle-axis of rotations.

Euler Parameters and Quaternion

As we said in the previous section any orientation of a local frame $P(0xyz)$ relative to a global frame $G(0XYZ)$ can be achieved by a rotation θ about an axis ω. An effective way to find the angle θ and the axis $\vec{\omega}$ is the Euler parameters e_0, e_1, e_2, e_3 such that e_0 is a scalar and e_1, e_2, e_3 are component of a vector $\vec{e}$:

$$
\begin{aligned}
e_0 &= cos(\theta/2), \\
\vec{e} = e_1\vec{i} + e_2\vec{j} + e_3\vec{k} &= \vec{\omega}sin(\theta/2),
\end{aligned}
\tag{1.7}
$$

so

$$
e_1^2 + e_2^2 + e_3^2 + e_0^2 = e_0^2 + \vec{e}^T\vec{e} = 1
\tag{1.8}
$$

Using the Euler parameters, the transformation matrix R to satisfy the equation $r^G = R r^P$ is

$$
R = R_{\vec{\omega},\theta} = (e_0^2 - \vec{e}^2)I + 2\vec{e}\vec{e}^T + 2e_0\tilde{e}
\tag{1.9}
$$

where $\tilde{e}$ is the skew-symmetric matrix associated with $\vec{e}$.

Euler parameters provide a well-suited, redundant, and nonsingular rotation description for arbitrary and large rotations. It is redundant because there are four parameters and a constraint equation to define the required three parameters of angle-axis rotation.

Quaternions, with special rules for addition and multiplication, use four numbers to represent rotations. A rotation quaternion is a unit quaternion that may be expressed by Euler parameters or the angle and axis of rotations:

$$
e(\theta,\vec{\omega}) = e_0 + \vec{e} = e_0 + e_1\vec{i} + e_2\vec{j} + e_3\vec{k} = cos(\theta/2) + sin(\theta/2)\vec{\omega}.
\tag{1.10}
$$

Euler parameters are the elements of rotation quaternions. There is a direct conversion between rotation quaternions and Euler parameters, which in turn are related to angle-axis parameters. We can obtain the angle θ and axis $\vec{\omega}$ of rotation from Euler parameters or rotation quaternion $e(\theta, \vec{\omega})$ by

$$\theta = 2tan^{-1}(|\vec{e}|/e_O),$$
$$\omega = \vec{e}/|\vec{e}|, \tag{1.11}$$

Unit quaternions provide a suitable base for describing rigid-body rotations, although they need normalization. In general, quaternions offer superior computational efficiency in most applications.

It is interesting to know that Leonhard Euler (1707-1783) was the first to derive the Rodriguez formula, while Benjamin Rodriguez (1795-1851) was the first to discover the Euler parameters. William Hamilton (1805-1865) introduced quaternions, although Friedrich Gauss (1777-1855) discovered them but never published.

1.4   Objectives, scope and outline

In this thesis we suggest an alternative to the standard parametrization of finite rotations by means of two different approaches based on a total Lagrangian description. We confine our attention to the case in which the material behavior stays within the linear elastic range, thus implying small deformational strains but arbitrarily large rotations. In both of these formulations we avoid the use of rotation matrices and angle measures in order to overcome all described difficulties in their management while preserving robustness, simplicity and inexpensiveness of the analysis.

In a first alternative, called *lengths based method* and applied to low order finite element, attention is given to the possibility of drawing out only the contributions due to the deformations from the complete nonlinear strain tensor. In the context of decoupling the rigid boby motion from the elastic response, the aim is to find for each deformative mode a characteristic measure that is an invariant to the rotations. In such a way the linear deformation modes become reciprocally independent and then they can be summed up in the strain tensor definition. The invariant measures have been computed, then, by requiring for each of them the following two features: not zero for the examined defomative mode and equal to zero for the other modes in the initial configuration; independent of the rigid kinematics value. Therefore a selective based definition of the strain tensor, used in order to avoid shear-locking problems, is effected by the linear definition of deformations because it is element reference system independent.

In the second proposed approach, called *projectors based method* and based on the Euler-Bernoulli beam theory, rigid and deformative modes are referred to the nodes of the element. The nonlinear rigid motion is recovered by referring to three unit and mutually orthogonal vectors attached to the nodes of the beam element. All nine components of such vectors in the global inertial frame of reference are assumed as unknown. As will be demonstrated, the rotational degree of freedom of the element is reduced to only three by six well-posed constraint conditions. Afterward, as above, for each deformative mode, a characteristic measure that is an invariant of the rotations is defined. We note that, boundary conditions on rotations are simply imposed by assuming as known the related nodal slopes while applied moments are modelled as forces following the motions.

To get an overview of the general structure of this thesis, the contents of the chapters are presented in the following. In Chapter 2 and 3 we describe the theoretical features of the lengths and projectors method respectively. We underline the methodology and the appropriacy of the proposed approaches as well as their limitations. In Chapter 4 we discuss the application of both methods to the dynamical field. Finally in Section 5 and 6 several numerical examples are presented to validate the proposed formulations both in statical and in dynamical field.

Chapter 2

Lengths based method

In the geometrically nonlinear structural mechanics context, the aim of this chapter is to present an alternative small strains - finite displacements description by a potential energy based finite element formulation without the use of rotation matrices. In particular the proposed approach is based on definitions of only relative lengths (hence the name *Lengths based method*) applied to low-order elements while the robustness and inexpensiveness of the analysis and the possibility to study the finite element in the linear field are preserved.

Continuum based beam and plate elements in two- and three-dimensional applications are proposed. In our context, the actual configuration of the element results rigidly translated and rotated and deformed according to the selected linear modes. The aim is to find, for each deformative mode, a characteristic measure that is an invariant to the rotations (the so called *Deformative Invariant*). In such a way the linear deformation modes become reciprocally independent and then they can be summed up in the strain tensor definition. Besides, in order to avoid shear-locking phenomena, a selectively based definition of the strain tensor is carried out; for example, the contribution of the hourglass modes to the shearing strains can be omitted.

The main feature of the proposed technique, then, is represented by an effective description of the finite kinematics without the use of rotation parameterizations keeping the possibility of obtaining good elemental performances by a selective choice of the mode contributions.

In this chapter we first describe the chosen linear deformative basis for the analyzed bilinear 4-node and trilinear 8-node elements, afterwards we discuss the suggested approach to identify the deformative invariants and to simplify the strain tensor definition. Finally the description of the statical equilibrium equations and of the related solution algorithms is presented.

2.1 Linear kinematical basis in the 4-node and 8-node elements

In this section we describe the used kinematical basis for the considered 4-node and 8-node elements. We consider in the element the referential coordinates ξ, η, ζ and the displacements vector $\mathbf{u}^T = \{u(\xi,\eta,\zeta), v(\xi,\eta,\zeta), w(\xi,\eta,\zeta)\}$.

2.1.1 Two-dimensional 4-node element

We refer to a rectangular $2h_\xi$, $2h_\eta$ 4-node element centered in the origin $O = (0,0)$ of the (ξ,η) reference system (see Figure 2.1).
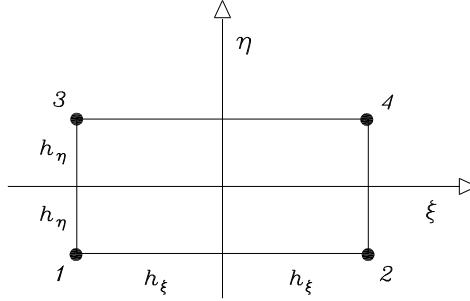

Fig. 2.1: Two-dimensional 4-node element: definition.

By using the classical bilinear interpolation

$$
\begin{aligned}
u(\xi,\eta) &= a_0 + a_1\xi + a_2\eta + a_3\xi\eta, \\
v(\xi,\eta) &= b_0 + b_1\xi + b_2\eta + b_3\xi\eta,
\end{aligned}
\tag{2.1}
$$

we obtain the following strain expressions:

$$
\begin{aligned}
\varepsilon_{\xi\xi} &= u_{,\xi}(\xi,\eta) = a_1 + a_3\eta, \\
\varepsilon_{\eta\eta} &= v_{,\eta}(\xi,\eta) = b_2 + b_3\xi, \\
\varepsilon_{\xi\eta} &= \tfrac{1}{2}\left[u_{,\eta}(\xi,\eta) + v_{,\xi}(\xi,\eta)\right] = \tfrac{1}{2}\left[a_2 + a_3\xi + b_1 + b_3\eta\right].
\end{aligned}
\tag{2.2}
$$

Now, we express the strains (2.2) into a basis of the three rigid and of five deformative motions. By following the order of the polynomial expansion, the strains are connected with the classical parameters:

$$
\begin{aligned}
e_1 &= a_1, \\
e_2 &= b_2, \\
e_3 &= a_2 + b_1, \\
e_4 &= a_3, \\
e_5 &= b_3,
\end{aligned}
\tag{2.3}
$$

11

by the position:

$$
\left\{
\begin{array}{c}
u_{,\xi} \\
v_{,\eta} \\
\frac{1}{2}(u_{,\eta} + v_{,\xi})
\end{array}
\right\}
=
\left[
\begin{array}{ccccc}
1 & 0 & 0 & \eta & 0 \\
0 & 1 & 0 & 0 & \xi \\
0 & 0 & \frac{1}{2} & \frac{1}{2}\xi & \frac{1}{2}\eta
\end{array}
\right]
\left\{
\begin{array}{c}
e_1 \\
e_2 \\
e_3 \\
e_4 \\
e_5
\end{array}
\right\} .
\qquad (2.4)
$$

We constrain the rigid motions by the following conditions in O:

$$
\begin{aligned}
& u(0,0) = a_0 = 0, \\
& v(0,0) = b_0 = 0, \\
& \omega(0,0) = \frac{1}{2}(u_{,\eta} - v_{,\xi})\Big|_{(0,0)} = \frac{1}{2}(a_2 - b_1) = 0,
\end{aligned}
\qquad (2.5)
$$

where $\omega(0,0)$ is the rotation of the element around the center O.
For each chosen $e_i \neq 0$ and with $e_j = 0 \ \forall j \neq i$ we can compute the displacements field (2.1) related to the i-th mode by imposing equations (2.5).

The first mode is here linked to the value $e_1 = E_\xi$. Then, the deformative parameter E_ξ is a constant that defines the linear expansion in the ξ direction. It follows that the correspondent strains are:

$$
\begin{cases}
u_{,\xi} = E_\xi \\
v_{,\eta} = 0 \\
\frac{1}{2}[u_{,\eta} + v_{,\xi}] = 0
\end{cases}
\qquad (2.6)
$$

and the consecutive displacements field is represented by:

$$
\begin{aligned}
& u(\xi, \eta) = E_\xi \xi, \\
& v(\xi, \eta) = 0.
\end{aligned}
\qquad (2.7)
$$

Similarly to the previous case, we can obtain the other modes by referring to the deformative parameters E_η, S, H_ξ, H_η as we can see below.

The second deformative mode, that is the expansion motion along the η direction, described by the deformative parameter E_η, is obtained by the position $e_2 = E_\eta$ which leads to the system:

$$
\begin{cases}
u_{,\xi} = 0 \\
v_{,\eta} = E_\eta \\
\frac{1}{2}[u_{,\eta} + v_{,\xi}] = 0
\end{cases}
$$

whose solution is:

$$
\begin{aligned}
& u(\xi, \eta) = 0 \\
& v(\xi, \eta) = E_\eta \eta.
\end{aligned}
\qquad (2.8)
$$

12

The third deformative mode, that is the shearing motion in the $\xi\eta$ plan, is obtained by referring to the deformative parameters S by the position $e_3 = S$, dove S. So we obtain the following strain expressions:

$$\begin{cases} u_{,\xi} = 0 \\ v_{,\eta} = 0 \\ \dfrac{1}{2}[u_{,\eta} + v_{,\xi}] = S \end{cases}$$

The resulting displacement field is:

$$\begin{aligned} u(\xi,\eta) &= S\eta \\ v(\xi,\eta) &= S\xi. \end{aligned} \tag{2.9}$$

The fourth and fifth deformative modes, linked to the value $e_4 = H_\xi$ e $e_5 = H_\eta$, define the hourglass motion in the plan $\xi\eta$ along the ξ and η direction respectively. The corresponding systems and solutions are as follows:

$$\begin{cases} u_{,\xi} = H_\xi\eta \ \ v_{,\eta} = 0 \\ \dfrac{1}{2}[u_{,\eta} + v_{,\xi}] = H_\xi\xi \end{cases}$$

$$\begin{aligned} u(\xi,\eta) &= H_\xi\xi\eta \\ v(\xi,\eta) &= 0, \end{aligned} \tag{2.10}$$

$$\begin{cases} u_{,\xi} = 0 \\ v_{,\eta} = H_\eta\xi \\ \dfrac{1}{2}[u_{,\eta} + v_{,\xi}] = H_\eta\eta \end{cases}$$

$$\begin{aligned} u(\xi,\eta) &= 0 \\ v(\xi,\eta) &= H_\eta\xi\eta. \end{aligned} \tag{2.11}$$

Mechanical and kinematics description of the motions is summarized in Table 2.1.1 while the related deformative modes are shown in Figure 2.2.

2.1.2 Three-dimensional 8-node element

We refer now to a $2h_\xi$, $2h_\eta$, $2h_\zeta$ 8-node element still centered in the origin $O = (0,0,0)$ of the (ξ,η,ζ) reference system (see Figure 2.3) and to the classical trilinear interpolation

$$\begin{aligned} u(\xi,\eta,\zeta) &= a_0 + a_1\xi + a_2\eta + a_3\zeta + a_4\xi\eta + a_5\xi\zeta + a_6\eta\zeta + a_7\xi\eta\zeta, \\ v(\xi,\eta,\zeta) &= b_0 + b_1\xi + b_2\eta + b_3\zeta + b_4\xi\eta + b_5\xi\zeta + b_6\eta\zeta + b_7\xi\eta\zeta, \\ w(\xi,\eta,\zeta) &= c_0 + c_1\xi + c_2\eta + c_3\zeta + c_4\xi\eta + c_5\xi\zeta + c_6\eta\zeta + c_7\xi\eta\zeta. \end{aligned} \tag{2.12}$$

$e_1 = E_\xi$	expansion motion along the ξ direction $u(\xi,\eta) = E_\xi\xi, \quad v(\xi,\eta) = 0$
$e_2 = E_\eta$	expansion motion along the η direction $u(\xi,\eta) = 0, \quad v(\xi,\eta) = E_\eta\eta$
$e_3 = S_{\xi\eta}$	shearing motion in the $\xi\eta$ plan $u(\xi,\eta) = S\eta, \quad v(\xi,\eta) = S\xi$
$e_4 = H_\xi$	hourglass motion in the plan $\xi\eta$ along the ξ direction $u(\xi,\eta) = H_\xi\xi\eta, \quad v(\xi,\eta) = 0$
$e_5 = H_\eta$	hourglass motion in the plan $\xi\eta$ along the η direction $u(\xi,\eta) = 0, \quad v(\xi,\eta) = H_\eta\xi\eta$

Tab. 2.1: Four-node element: definitions of the deformative modes.

The following strain expressions are obtained:

$$
\begin{aligned}
\varepsilon_{\xi\xi} &= u_{,\xi}(\xi,\eta,\zeta) = a_1 + a_4\eta + a_5\zeta + a_7\eta\zeta, \\
\varepsilon_{\xi\eta} &= \frac{1}{2}\left[u_{,\eta}(\xi,\eta,\zeta) + v_{,\xi}(\xi,\eta,\zeta)\right] \\
&= \frac{1}{2}\left[(a_2 + b_1) + a_4\xi + b_4\eta + (a_6 + b_5)\zeta + a_7\xi\zeta + b_7\eta\zeta\right], \\
\varepsilon_{\xi\zeta} &= \frac{1}{2}\left[u_{,\zeta}(\xi,\eta,\zeta) + w_{,\xi}(\xi,\eta,\zeta)\right] \\
&= \frac{1}{2}\left[(a_3 + c_1) + a_5\xi + c_6\zeta + (c_4 + a_6)\eta + a_7\xi\eta + c_7\eta\zeta\right], \quad (2.13) \\
\varepsilon_{\eta\eta} &= v_{,\eta}(\xi,\eta,\zeta) = b_2 + b_4\xi + b_6\zeta + b_7\xi\zeta, \\
\varepsilon_{\eta\zeta} &= \frac{1}{2}\left[v_{,\zeta}(\xi,\eta,\zeta) + w_{,\eta}(\xi,\eta,\zeta)\right] \\
&= \frac{1}{2}\left[(b_3 + c_2) + b_6\eta + c_6\zeta + (b_5 + c_4)\xi + b_7\xi\eta + c_7\xi\zeta\right], \\
\varepsilon_{\zeta\zeta} &= w_{,\zeta}(\xi,\eta,\zeta) = c_3 + c_5\xi + c_6\eta + c_7\xi\eta.
\end{aligned}
$$

Similarly to the two-dimensional case see in the previous section, the strains (2.13) are referred to the basis of the six rigid and eighteen deformative motions. These latter are obtained by the position

$$\varepsilon = \mathbf{L}\mathbf{e}, \qquad (2.14)$$

where

$$\varepsilon^{\mathbf{T}} = \{\varepsilon_{\xi\xi},\ \varepsilon_{\xi\eta},\ \varepsilon_{\xi\zeta},\ \varepsilon_{\eta\eta},\ \varepsilon_{\eta\zeta},\ \varepsilon_{\zeta\zeta}\}, \qquad (2.15)$$
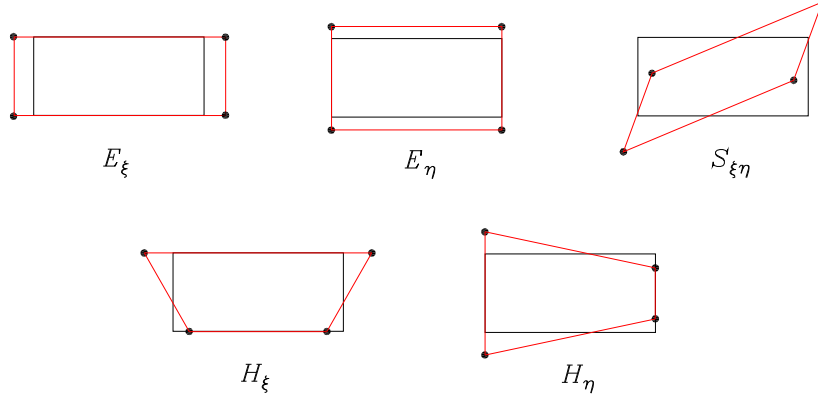
Fig. 2.2: Four-node element: representations of the linear deformative modes.

$$
\mathbf{L} =
\begin{bmatrix}
1 & 0 & 0 & 0 & 0 & 0 & \eta & 0 & 0 & 0 & 0 & \zeta & 0 & 0 & 0 & \eta\zeta & 0 & 0 \\
0 & 0 & 0 & \frac{1}{2} & 0 & 0 & \frac{1}{2}\xi & 0 & 0 & \frac{1}{2}\eta & 0 & 0 & 0 & 0 & \frac{1}{2}\zeta & \frac{1}{2}\xi\zeta & \frac{1}{2}\eta\zeta & 0 \\
0 & 0 & 0 & 0 & 0 & \frac{1}{2} & 0 & 0 & \frac{1}{2}\zeta & 0 & 0 & \frac{1}{2}\xi & 0 & \frac{1}{2}\eta & 0 & \frac{1}{2}\xi\eta & 0 & \frac{1}{2}\eta\zeta \\
0 & 1 & 0 & 0 & 0 & 0 & 0 & \zeta & 0 & \xi & 0 & 0 & 0 & 0 & 0 & 0 & \xi\zeta & 0 \\
0 & 0 & 0 & 0 & \frac{1}{2} & 0 & 0 & \frac{1}{2}\eta & 0 & 0 & \frac{1}{2}\zeta & 0 & \frac{1}{2}\xi & 0 & 0 & 0 & \frac{1}{2}\xi\eta & \frac{1}{2}\xi\zeta \\
0 & 0 & 1 & 0 & 0 & 0 & 0 & 0 & \xi & 0 & \eta & 0 & 0 & 0 & 0 & 0 & 0 & \xi\eta
\end{bmatrix}
\tag{2.16}
$$

and

$$
\begin{aligned}
\mathbf{e}^T =\{ & a_1 \quad b_2 \quad c_3 \quad a_2 + b_1 \quad a_3 + c_1 \quad b_3 + c_2 \quad a_4 \quad b_6 \quad c_5 \quad b_4 \\
& c_6 \quad a_5 \quad b_5 + c_4 \quad c_4 + a_6 \quad a_6 + b_5 \quad a_7 \quad b_7 \quad c_7 \}.
\end{aligned}
\tag{2.17}
$$

By constraining the rigid motions we have the following conditions in the O center point:

$$
\begin{aligned}
u(0,0,0) &= a_0 = 0, \\
v(0,0,0) &= b_0 = 0, \\
w(0,0,0) &= c_0 = 0, \\
\omega_{\xi\eta}(0,0,0) &= \tfrac{1}{2}(u_{,\eta} - v_{,\xi})\big|_{(0,0,0)} = \tfrac{1}{2}(a_2 - b_1) = 0, \\
\omega_{\eta\zeta}(0,0,0) &= \tfrac{1}{2}(v_{,\zeta} - w_{,\eta})\big|_{(0,0,0)} = \tfrac{1}{2}(b_3 - c_2) = 0, \\
\omega_{\zeta\xi}(0,0,0) &= \tfrac{1}{2}(w_{,\xi} - u_{,\zeta})\big|_{(0,0,0)} = \tfrac{1}{2}(c_1 - a_3) = 0,
\end{aligned}
\tag{2.18}
$$

where $\omega_{\xi\eta}$, $\omega_{\eta\zeta}$ and $\omega_{\zeta\xi}$ are the rotations around to the ζ, ξ and η axes, respectively. Here the eighteen deformative mode of three-dimensional element
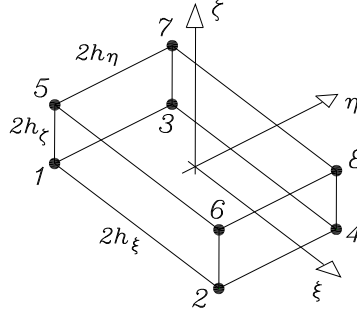
Fig. 2.3: Three-dimensional 8-node element: definition.

can be summarized: for each deformative mode we list the associated deformative parameter, the corresponding deformation, the system of differential equations in terms of strains and the connected displacement field.

- $e_1 = E_\xi$: expansion motion along the ξ direction

    - associated strain system

    $$\begin{cases} u_{,\xi} = E_\xi \\ \dfrac{1}{2}\left[u_{,\eta} + v_{,\xi}\right] = 0 \\ \dfrac{1}{2}\left[u_{,\zeta} + w_{,\xi}\right] = 0 \\ v_{,\eta} = 0 \\ \dfrac{1}{2}\left[v_{,\zeta} + w_{,\eta}\right] = 0 \\ w_{,\zeta} = 0 \end{cases}$$

    - displacement field

    $$\begin{aligned} u(\xi, \eta, \zeta) &= E_\xi \xi \\ v(\xi, \eta, \zeta) &= 0 \\ w(\xi, \eta, \zeta) &= 0; \end{aligned}$$

    (2.19)

- $e_2 = E_\eta$: expansion motion along the η direction

16

– associated strain system

$$
\begin{cases}
u_{,\xi} = 0 \\
\dfrac{1}{2}\left[u_{,\eta} + v_{,\xi}\right] = 0 \\
\dfrac{1}{2}\left[u_{,\zeta} + w_{,\xi}\right] = 0 \\
v_{,\eta} = E_\eta \\
\dfrac{1}{2}\left[v_{,\zeta} + w_{,\eta}\right] = 0 \\
w_{,\zeta} = 0
\end{cases}
$$

– displacement field

$$
\begin{aligned}
u(\xi,\eta,\zeta) &= 0 \\
v(\xi,\eta,\zeta) &= E_\eta \eta \\
w(\xi,\eta,\zeta) &= 0;
\end{aligned}
\tag{2.20}
$$

- $e_3 = E_\zeta$: expansion motion along the ζ direction

    – associated strain system

$$
\begin{cases}
u_{,\xi} = 0 \\
\dfrac{1}{2}\left[u_{,\eta} + v_{,\xi}\right] = 0 \\
\dfrac{1}{2}\left[u_{,\zeta} + w_{,\xi}\right] = 0 \\
v_{,\eta} = 0 \\
\dfrac{1}{2}\left[v_{,\zeta} + w_{,\eta}\right] = 0 \\
w_{,\zeta} = E_\zeta
\end{cases}
$$

– displacement field

$$
\begin{aligned}
u(\xi,\eta,\zeta) &= 0 \\
v(\xi,\eta,\zeta) &= 0 \\
w(\xi,\eta,\zeta) &= E_\zeta \zeta;
\end{aligned}
\tag{2.21}
$$

- $e_4 = S_{\xi\eta}$: shearing motion in the $\xi\eta$ plan

    – associated strain system

$$
\begin{cases}
u_{,\xi} = 0 \\
\dfrac{1}{2}\left[u_{,\eta} + v_{,\xi}\right] = S_{\xi\eta} \\
\dfrac{1}{2}\left[u_{,\zeta} + w_{,\xi}\right] = 0 \\
v_{,\eta} = 0 \\
\dfrac{1}{2}\left[v_{,\zeta} + w_{,\eta}\right] = 0 \\
w_{,\zeta} = 0
\end{cases}
$$

17

– displacement field

$$u(\xi, \eta, \zeta) = \frac{1}{2} S_{\xi\eta} \eta$$
$$v(\xi, \eta, \zeta) = \frac{1}{2} S_{\xi\eta} \xi \qquad (2.22)$$
$$w(\xi, \eta, \zeta) = 0;$$

- $e_5 = S_{\xi\zeta}$: shearing motion in the $\xi\zeta$ plan

    – associated strain system

$$\begin{cases} u_{,\xi} = 0 \\ \dfrac{1}{2}[u_{,\eta} + v_{,\xi}] = 0 \\ \dfrac{1}{2}[u_{,\zeta} + w_{,\xi}] = S_{\xi\zeta} \\ v_{,\eta} = 0 \\ \dfrac{1}{2}[v_{,\zeta} + w_{,\eta}] = 0 \\ w_{,\zeta} = 0 \end{cases}$$

    – displacement field

$$u(\xi, \eta, \zeta) = \frac{1}{2} S_{\xi\zeta} \zeta$$
$$v(\xi, \eta, \zeta) = 0 \qquad (2.23)$$
$$w(\xi, \eta, \zeta) = \frac{1}{2} S_{\xi\zeta} \xi;$$

- $e_6 = S_{\eta\zeta}$: shearing motion in the $\eta\zeta$ plan

    – associated strain system

$$\begin{cases} u_{,\xi} = 0 \\ \dfrac{1}{2}[u_{,\eta} + v_{,\xi}] = 0 \\ \dfrac{1}{2}[u_{,\zeta} + w_{,\xi}] = 0 \\ v_{,\eta} = 0 \\ \dfrac{1}{2}[v_{,\zeta} + w_{,\eta}] = S_{\eta\zeta} \\ w_{,\zeta} = 0 \end{cases}$$

    – displacement field

$$u(\xi, \eta, \zeta) = 0$$
$$v(\xi, \eta, \zeta) = \frac{1}{2} S_{\eta\zeta} \zeta \qquad (2.24)$$
$$w(\xi, \eta, \zeta) = \frac{1}{2} S_{\eta\zeta} \eta;$$

- $e_{10} = H_{\xi\eta}$: hourglass motion in the plan $\xi\eta$ along the ξ direction

  - associated strain system

  $$\begin{cases} u_{,\xi} = H_{\xi\eta}\eta \\ \dfrac{1}{2}\left[u_{,\eta} + v_{,\xi}\right] = \dfrac{1}{2}H_{\xi\eta}\xi \\ \dfrac{1}{2}\left[u_{,\zeta} + w_{,\xi}\right] = 0 \\ v_{,\eta} = 0 \\ \dfrac{1}{2}\left[v_{,\zeta} + w_{,\eta}\right] = 0 \\ w_{,\zeta} = 0 \end{cases}$$

  - displacement field

  $$\begin{aligned} u(\xi,\eta,\zeta) &= H_{\xi\eta}\xi\eta \\ v(\xi,\eta,\zeta) &= 0 \\ w(\xi,\eta,\zeta) &= 0; \end{aligned} \qquad (2.25)$$

- $e_{11} = H_{\eta\xi}$: hourglass motion in the plan $\xi\eta$ along the η direction

  - associated strain system

  $$\begin{cases} u_{,\xi} = 0 \\ \dfrac{1}{2}\left[u_{,\eta} + v_{,\xi}\right] = \dfrac{1}{2}H_{\eta\xi}\eta \\ \dfrac{1}{2}\left[u_{,\zeta} + w_{,\xi}\right] = 0 \\ v_{,\eta} = H_{\eta\xi}\eta \\ \dfrac{1}{2}\left[v_{,\zeta} + w_{,\eta}\right] = 0 \\ w_{,\zeta} = 0 \end{cases}$$

  - displacement field

  $$\begin{aligned} u(\xi,\eta,\zeta) &= 0 \\ v(\xi,\eta,\zeta) &= H_{\eta\xi}\xi\eta \\ w(\xi,\eta,\zeta) &= 0; \end{aligned} \qquad (2.26)$$

- $e_{12} = H_{\xi\zeta}$: hourglass motion in the plan $\xi\zeta$ along the ξ direction

  - associated strain system

  $$\begin{cases} u_{,\xi} = H_{\xi\zeta}\zeta \\ \dfrac{1}{2}\left[u_{,\eta} + v_{,\xi}\right] = 0 \\ \dfrac{1}{2}\left[u_{,\zeta} + w_{,\xi}\right] = \dfrac{1}{2}H_{\xi\zeta}\xi \\ v_{,\eta} = 0 \\ \dfrac{1}{2}\left[v_{,\zeta} + w_{,\eta}\right] = 0 \\ w_{,\zeta} = 0 \end{cases}$$

– displacement field

$$
\begin{aligned}
u(\xi,\eta,\zeta) &= H_{\xi\zeta}\xi\zeta \\
v(\xi,\eta,\zeta) &= 0 \\
w(\xi,\eta,\zeta) &= 0;
\end{aligned} \tag{2.27}
$$

- $e_{13} = H_{\zeta\xi}$: hourglass motion in the plan $\xi\zeta$ along the ζ direction

  – associated strain system

$$
\begin{cases}
u_{,\xi} = 0 \\
\dfrac{1}{2}\left[u_{,\eta} + v_{,\xi}\right] = 0 \\
\dfrac{1}{2}\left[u_{,\zeta} + w_{,\xi}\right] = \dfrac{1}{2}H_{\zeta\xi}\zeta \\
v_{,\eta} = 0 \\
\dfrac{1}{2}\left[v_{,\zeta} + w_{,\eta}\right] = 0 \\
w_{,\zeta} = H_{\zeta\xi}\xi
\end{cases}
$$

  – displacement field

$$
\begin{aligned}
u(\xi,\eta,\zeta) &= 0 \\
v(\xi,\eta,\zeta) &= 0 \\
w(\xi,\eta,\zeta) &= H_{\zeta\xi}\xi\zeta;
\end{aligned} \tag{2.28}
$$

- $e_{14} = H_{\eta\zeta}$: hourglass motion in the plan $\eta\zeta$ along the η direction

  – associated strain system

$$
\begin{cases}
u_{,\xi} = 0 \\
\dfrac{1}{2}\left[u_{,\eta} + v_{,\xi}\right] = 0 \\
\dfrac{1}{2}\left[u_{,\zeta} + w_{,\xi}\right] = 0 \\
v_{,\eta} = H_{\eta\zeta}\zeta \\
\dfrac{1}{2}\left[v_{,\zeta} + w_{,\eta}\right] = \dfrac{1}{2}H_{\eta\zeta}\eta \\
w_{,\zeta} = 0
\end{cases}
$$

  – displacement field

$$
\begin{aligned}
u(\xi,\eta,\zeta) &= 0 \\
v(\xi,\eta,\zeta) &= H_{\eta\zeta}\eta\zeta \\
w(\xi,\eta,\zeta) &= 0;
\end{aligned} \tag{2.29}
$$

- $e_{15} = H_{\zeta\eta}$: hourglass motion in the plan $\eta\zeta$ along the ζ direction

– associated strain system

$$
\begin{cases}
u_{,\xi} = 0 \\
\dfrac{1}{2}\left[u_{,\eta} + v_{,\xi}\right] = 0 \\
\dfrac{1}{2}\left[u_{,\zeta} + w_{,\xi}\right] = 0 \\
v_{,\eta} = 0 \\
\dfrac{1}{2}\left[v_{,\zeta} + w_{,\eta}\right] = \dfrac{1}{2}H_{\zeta\eta}\zeta \\
w_{,\zeta} = H_{\zeta\eta}\eta
\end{cases}
$$

– displacement field

$$
\begin{aligned}
u(\xi, \eta, \zeta) &= 0 \\
v(\xi, \eta, \zeta) &= 0 \\
w(\xi, \eta, \zeta) &= H_{\zeta\eta}\eta\zeta;
\end{aligned}
\tag{2.30}
$$

- $e_7 = T_\zeta$: torsional motion around the ζ axis

    – associated strain system

$$
\begin{cases}
u_{,\xi} = 0 \\
\dfrac{1}{2}\left[u_{,\eta} + v_{,\xi}\right] = \dfrac{1}{2}T_\zeta\zeta \\
\dfrac{1}{2}\left[u_{,\zeta} + w_{,\xi}\right] = 0 \\
v_{,\eta} = 0 \\
\dfrac{1}{2}\left[v_{,\zeta} + w_{,\eta}\right] = 0 \\
w_{,\zeta} = 0
\end{cases}
$$

– displacement field

$$
\begin{aligned}
u(\xi, \eta, \zeta) &= \dfrac{1}{2}T_\zeta\eta\zeta \\
v(\xi, \eta, \zeta) &= \dfrac{1}{2}T_\zeta\xi\zeta \\
w(\xi, \eta, \zeta) &= -\dfrac{1}{2}T_\zeta\xi\eta;
\end{aligned}
\tag{2.31}
$$

- $e_8 = T_\eta$: torsional motion around the η axis

    – associated strain system

$$
\begin{cases}
u_{,\xi} = 0 \\
\dfrac{1}{2}\left[u_{,\eta} + v_{,\xi}\right] = 0 \\
\dfrac{1}{2}\left[u_{,\zeta} + w_{,\xi}\right] = \dfrac{1}{2}T_\eta\eta \\
v_{,\eta} = 0 \\
\dfrac{1}{2}\left[v_{,\zeta} + w_{,\eta}\right] = 0 \\
w_{,\zeta} = 0
\end{cases}
$$

21

– displacement field

$$
\begin{aligned}
u(\xi, \eta, \zeta) &= \frac{1}{2} T_\eta \eta \zeta \\
v(\xi, \eta, \zeta) &= -\frac{1}{2} T_\eta \xi \zeta \\
w(\xi, \eta, \zeta) &= \frac{1}{2} T_\eta \xi;
\end{aligned}
\tag{2.32}
$$

- $e_9 = T_\xi$: torsional motion around the ξ axis

    – associated strain system

$$
\begin{cases}
u_{,\xi} = 0 \\
\frac{1}{2} [u_{,\eta} + v_{,\xi}] = 0 \\
\frac{1}{2} [u_{,\zeta} + w_{,\xi}] = 0 \\
v_{,\eta} = 0 \\
\frac{1}{2} [v_{,\zeta} + w_{,\eta}] = \frac{1}{2} T_\xi \xi \\
w_{,\zeta} = 0
\end{cases}
$$

    – displacement field

$$
\begin{aligned}
u(\xi, \eta, \zeta) &= -\frac{1}{2} T_\xi \eta \zeta \\
v(\xi, \eta, \zeta) &= \frac{1}{2} T_\xi \xi \zeta \\
w(\xi, \eta, \zeta) &= \frac{1}{2} T_\xi \xi \eta;
\end{aligned}
\tag{2.33}
$$

- $e_{16} = N_\xi$: non-physical motion around the ξ axis

    – associated strain system

$$
\begin{cases}
u_{,\xi} = N_\xi \eta \zeta \\
\frac{1}{2} [u_{,\eta} + v_{,\xi}] = \frac{1}{2} N_\xi \xi \zeta \\
\frac{1}{2} [u_{,\zeta} + w_{,\xi}] = \frac{1}{2} N_\xi \xi \eta \\
v_{,\eta} = 0 \\
\frac{1}{2} [v_{,\zeta} + w_{,\eta}] = 0 \\
w_{,\zeta} = 0
\end{cases}
$$

    – displacement field

$$
\begin{aligned}
u(\xi, \eta, \zeta) &= N_\xi \xi \eta \zeta \\
v(\xi, \eta, \zeta) &= 0 \\
w(\xi, \eta, \zeta) &= 0;
\end{aligned}
\tag{2.34}
$$

- $e_{17} = N_\eta$: non-physical motion around the η axis

  – associated strain system

$$\begin{cases} u_{,\xi} = 0 \\ \dfrac{1}{2}\left[u_{,\eta} + v_{,\xi}\right] = \dfrac{1}{2}N_\eta\eta\zeta \\ \dfrac{1}{2}\left[u_{,\zeta} + w_{,\xi}\right] = 0 \\ v_{,\eta} = N_\eta\xi\zeta \\ \dfrac{1}{2}\left[v_{,\zeta} + w_{,\eta}\right] = \dfrac{1}{2}N_\eta\xi\eta \\ w_{,\zeta} = 0 \end{cases}$$

  – displacement field

$$\begin{aligned} u(\xi,\eta,\zeta) &= 0 \\ v(\xi,\eta,\zeta) &= N_\eta\xi\eta\zeta \\ w(\xi,\eta,\zeta) &= 0; \end{aligned} \qquad (2.35)$$

- $e_{18} = N_\zeta$: non-physical motion around the ζ axis

  – associated strain system

$$\begin{cases} u_{,\xi} = 0 \\ \dfrac{1}{2}\left[u_{,\eta} + v_{,\xi}\right] = 0 \\ \dfrac{1}{2}\left[u_{,\zeta} + w_{,\xi}\right] = \dfrac{1}{2}N_\zeta\eta\zeta \\ v_{,\eta} = 0 \\ \dfrac{1}{2}\left[v_{,\zeta} + w_{,\eta}\right] = \dfrac{1}{2}N_\zeta\xi\zeta \\ w_{,\zeta} = N_\zeta\xi\eta \end{cases}$$

  – displacement field

$$\begin{aligned} u(\xi,\eta,\zeta) &= 0 \\ v(\xi,\eta,\zeta) &= 0 \\ w(\xi,\eta,\zeta) &= N_\zeta\xi\eta\zeta; \end{aligned} \qquad (2.36)$$

In the Tables 2.1.2-2.1.2 we summarize,for each referred base mode, the deformative parameter and the displacements field. Representations of these modes are shown in the Figures 2.4-2.8.

23

$e_1 = E_\xi$	expansion motion along the ξ direction
	$u(\xi,\eta) = E_\xi\xi, \quad v(\xi,\eta) = 0$
$e_2 = E_\eta$	expansion motion along the η direction
	$u(\xi,\eta) = 0, \quad v(\xi,\eta) = E_\eta\eta$
$e_3 = S_{\xi\eta}$	shearing motion in the $\xi\eta$ plan
	$u(\xi,\eta) = S\eta, \quad v(\xi,\eta) = S\xi$
$e_4 = H_\xi$	hourglass motion in the plan $\xi\eta$ along the ξ direction
	$u(\xi,\eta) = H_\xi\xi\eta, \quad v(\xi,\eta) = 0$
$e_5 = H_\eta$	hourglass motion in the plan $\xi\eta$ along the η direction
	$u(\xi,\eta) = 0, \quad v(\xi,\eta) = H_\eta\xi\eta$

Tab. 2.2: Four-node element: definitions of the deformative modes.
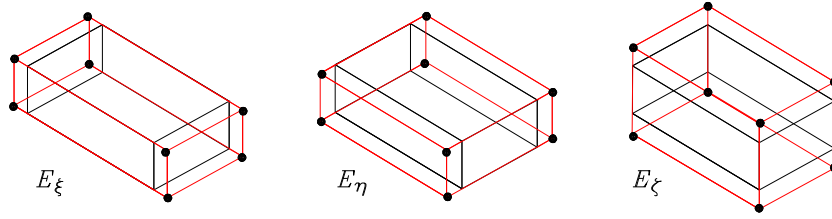
Fig. 2.4: Eight-node element: representations of the expansion modes.

$e_4 = S_{\xi\eta}$	shearing motion in the $\xi\eta$ plan
	$u(\xi,\eta,\zeta) = \frac{1}{2}S_{\xi\eta}\eta, \quad v(\xi,\eta,\zeta) = \frac{1}{2}S_{\xi\eta}\xi, \quad w(\xi,\eta,\zeta) = 0$
$e_5 = S_{\eta\zeta}$	shearing motion in the $\eta\zeta$ plan
	$u(\xi,\eta,\zeta) = 0, \quad v(\xi,\eta,\zeta) = \frac{1}{2}S_{\eta\zeta}\zeta, \quad w(\xi,\eta,\zeta) = \frac{1}{2}S_{\eta\zeta}\eta$
$e_6 = S_{\zeta\xi}$	shearing motion in the $\zeta\xi$ plan
	$u(\xi,\eta,\zeta) = \frac{1}{2}S_{\zeta\xi}\zeta, \quad v(\xi,\eta,\zeta) = 0, \quad w(\xi,\eta,\zeta) = \frac{1}{2}S_{\zeta\xi}\xi$

Tab. 2.3: Eight-node element: definitions of the shearing modes.

2.2 Deformative invariants definitions

We consider a generic configuration of the element. This configuration, therefore, results rigidly translated, rotated and deformed according to the modes described in the previous section. Now, for each deformative mode, we identify a measure with the following two features: not zero for the examined mode and equal to zero for the other modes in the initial configuration; in-
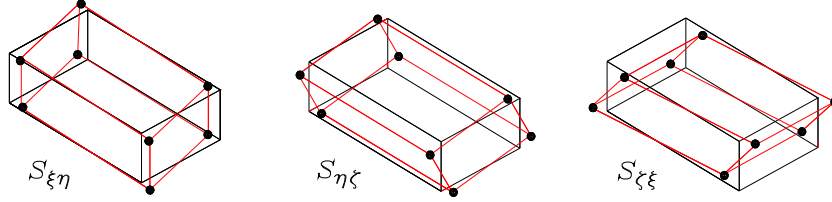
Fig. 2.5: Eight-node element: representations of the shearing modes.

$e_7 = H_{\xi\eta}$	hourglass motion in the $\xi\eta$ plan along the ξ direction
	$u(\xi,\eta,\zeta) = H_{\xi\eta}\xi\eta, \quad v(\xi,\eta,\zeta) = 0, \quad w(\xi,\eta,\zeta) = 0$
$e_8 = H_{\eta\zeta}$	hourglass motion in the $\eta\zeta$ plan along the η direction
	$u(\xi,\eta,\zeta) = 0, \quad v(\xi,\eta,\zeta) = H_{\eta\zeta}\eta\zeta, \quad w(\xi,\eta,\zeta) = 0$
$e_9 = H_{\zeta\xi}$	hourglass motion in the $\zeta\xi$ plan along the ζ direction
	$u(\xi,\eta,\zeta) = 0, \quad v(\xi,\eta,\zeta) = 0, \quad w(\xi,\eta,\zeta) = H_{\zeta\xi}\xi\zeta$
$e_{10} = H_{\eta\xi}$	hourglass motion in the $\xi\eta$ plan along the η direction
	$u(\xi,\eta,\zeta) = 0, \quad v(\xi,\eta,\zeta) = H_{\eta\xi}\xi\eta, \quad w(\xi,\eta,\zeta) = 0$
$e_{11} = H_{\zeta\eta}$	hourglass motion in the $\eta\zeta$ plan along the ζ direction
	$u(\xi,\eta,\zeta) = 0, \quad v(\xi,\eta,\zeta) = 0, \quad w(\xi,\eta,\zeta) = H_{\zeta\eta}\eta\zeta$
$e_{12} = H_{\xi\zeta}$	hourglass motion in the $\zeta\xi$ plan along the ξ direction
	$u(\xi,\eta,\zeta) = H_{\xi\zeta}\xi\zeta, \quad v(\xi,\eta,\zeta) = 0, \quad w(\xi,\eta,\zeta) = 0$

Tab. 2.4: Eight-node element: definitions of the hourglass modes.

$e_{13} = T_\xi$	torsional motion around the ξ axis
	$u(\xi,\eta,\zeta) = -\frac{1}{2}T_\xi\eta\zeta, \quad v(\xi,\eta,\zeta) = \frac{1}{2}T_\xi\xi\zeta, \quad w(\xi,\eta,\zeta) = \frac{1}{2}T_\xi\xi\eta$
$e_{14} = T_\eta$	torsional motion around the η axis
	$u(\xi,\eta,\zeta) = \frac{1}{2}T_\eta\eta\zeta, \quad v(\xi,\eta,\zeta) = -\frac{1}{2}T_\eta\xi\zeta, \quad w(\xi,\eta,\zeta) = \frac{1}{2}T_\eta\xi\eta$
$e_{15} = T_\zeta$	torsional motion around the ζ axis
	$u(\xi,\eta,\zeta) = \frac{1}{2}T_\zeta\eta\zeta, \quad v(\xi,\eta,\zeta) = \frac{1}{2}T_\zeta\xi\zeta, \quad w(\xi,\eta,\zeta) = -\frac{1}{2}T_\zeta\xi\eta$

Tab. 2.5: Eight-node element: definitions of the torsional modes.

dependent of the rigid kinematics value. Then, such a measure uniquely describes the deformation associated with the mode itself in the generic configuration. So, these definitions make the deformative modes reciprocally independent and then, they can be summed up in the strain tensor defini-
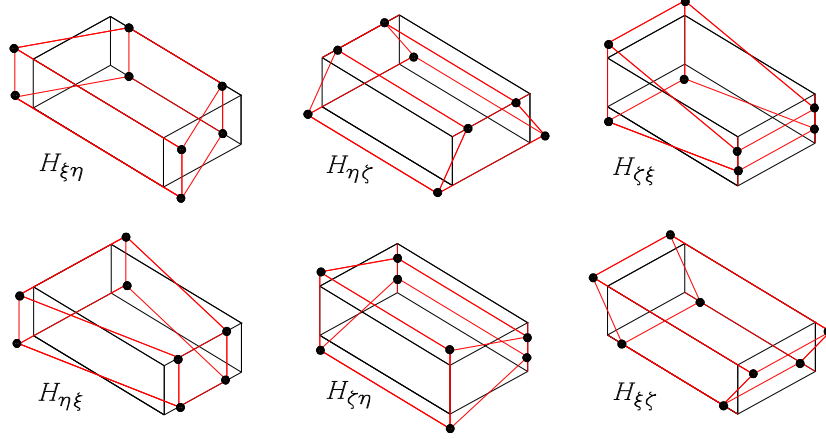
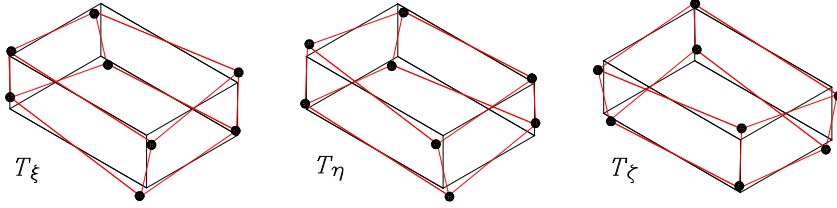**Fig. 2.6:** Eight-node element: representations of the hourglass modes.

Fig. 2.7: Eight-node element: representations of the torsional modes.

$e_{16} = N_\xi$	non-physical motion around the ξ axis
	$u(\xi,\eta,\zeta) = N_\xi \xi\eta\zeta, \quad v(\xi,\eta,\zeta) = 0, \quad w(\xi,\eta,\zeta) = 0$
$e_{17} = N_\eta$	non-physical motion around the η axis
	$u(\xi,\eta,\zeta) = 0, \quad v(\xi,\eta,\zeta) = N_\eta \xi\eta\zeta, \quad w(\xi,\eta,\zeta) = 0$
$e_{18} = N_\zeta$	non-physical motion around the ζ axis
	$u(\xi,\eta,\zeta) = 0, \quad v(\xi,\eta,\zeta) = 0, \quad w(\xi,\eta,\zeta) = N_\zeta \xi\eta\zeta$

Tab. 2.6: Eight-node element: definitions of the non-physical modes.

tions.

The measures just described, denoted in the following as *deformative invariants*, represent here relative distances between points of the generic configuration and they are in function of the unknown elemental parameters.
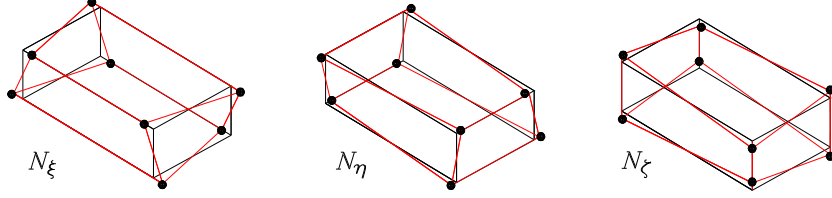
Fig. 2.8: Eight-node element: representations of the non-physical modes.

We refer to the Euclidean distance $\mathcal{D}(p_i, p_j)$ between the points p_i, p_j of the element in the generic configuration:

$$\mathcal{D}(p_i, p_j) = \sqrt{\left[\xi_i^p + u_i^p - \xi_j^p - u_j^p\right]^2 + \left[\eta_i^p + v_i^p - \eta_j^p - v_j^p\right]^2 + \left[\zeta_i^p + w_i^p - \zeta_j^p - w_j^p\right]^2}. \tag{2.37}$$

In (3.8) ξ_i^p, η_i^p and ζ_i^p are, respectively, the initial ξ, η and ζ coordinates of the point p_i while u_i^p, v_i^p and w_i^p are the respective displacements.

2.2.1 Two-dimensional 4-node element

In this section we define the deformative invariant for two-dimensional 4-node elements. As an example, we refer to the two-dimensional ξ extensional mode. In particular we underline how to describe the related characteristic measure and that it represents an invariant in respect to the deformation fields.
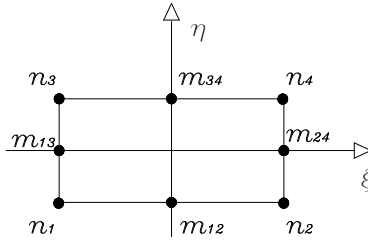

Fig. 2.9: Two-dimensional 4-node element: reference points definition.

We consider (see Figure 2.9) the distance $\mathcal{D}(m_{13}, m_{24})$ between the middle points m_{13} and m_{24} of the segments n_1-n_3 and n_2-n_4 connecting the n_i nodes of the element. We note that this distance is an invariant, in the first order approximation, in respect to the remaining η extensional, shearing, ξ and η hourglass modes as shown in Figures 2.10(a), 2.10(b), 2.10(c) and 2.10(d), respectively. As we can verify, the examined $\mathcal{D}(m_{13}, m_{24})$ distance changes only if the actual configuration of the element involves also the ξ

27

extensional deformation (see Figure 2.10(e)) In the following we define the invariants by basing our measures only on nodal distances.

Then, a possible choice for the invariant $\mathcal{I}E_\xi$ related to the deformative parameter E_ξ is:

$$\mathcal{I}E_\xi = \mathcal{D}(m_{13}, m_{24}) - 2h_\xi. \qquad (2.38)$$

This invariant, therefore, represents the difference between the actual $\mathcal{D}(m_{13}, m_{24})$ and the initial $2h_\xi$ distances. Of course, this difference is equal to the ξ expansion of the element. So, the following relation is valid:

$$\mathcal{I}E_\xi = 2E_\xi h_\xi. \qquad (2.39)$$

By equating the two invariant representations (2.38) e (2.39) we can determine the deformative parameter as a function of the kinematic parameters.

Similarly to the expansion mode we can define the invariant expression for the other deformative mode too. As a result the used definitions of the invariants and their dependence on the related deformative parameters are given. In particular, the already seen extensional, shearing and hourglass modes was considered:

- expansion motion along the ξ direction:

$$\mathfrak{I}E_\xi = \mathfrak{D}(m_{13}, m_{24}) - 2h_\xi, \qquad E_\xi = \frac{\mathfrak{I}E_\xi}{2h_\xi};$$

- expansion motion along the η direction:

$$\mathfrak{I}E_\eta = \mathfrak{D}(m_{12}, m_{34}) - 2h_\eta, \qquad E_\eta = \frac{\mathfrak{I}E_\eta}{2h_\eta};$$

- shearing motion in the $\xi\eta$ plan:

$$\mathfrak{I}S = \mathfrak{D}(n_1, n_4) - \mathfrak{D}(n_2, n_3), \qquad S = \frac{\mathfrak{I}S\sqrt{(h_\xi)^2 + (h_\eta)^2}}{8h_\eta h_\xi};$$

- hourglass motion in the plan $\xi\eta$ along the ξ direction:

$$\mathfrak{I}H_\xi = \mathfrak{D}(n_1, n_2) - \mathfrak{D}(n_3, n_4), \qquad H_\xi = \frac{\mathfrak{I}H_\xi}{4h_\xi h_\eta};$$

- hourglass motion in the plan $\xi\eta$ along the η direction:

$$\mathfrak{I}H_\eta = \mathfrak{D}(n_1, n_3) - \mathfrak{D}(n_2, n_4), \qquad H_\eta = \frac{\mathfrak{I}H_\eta}{4h_\eta h_\xi};$$
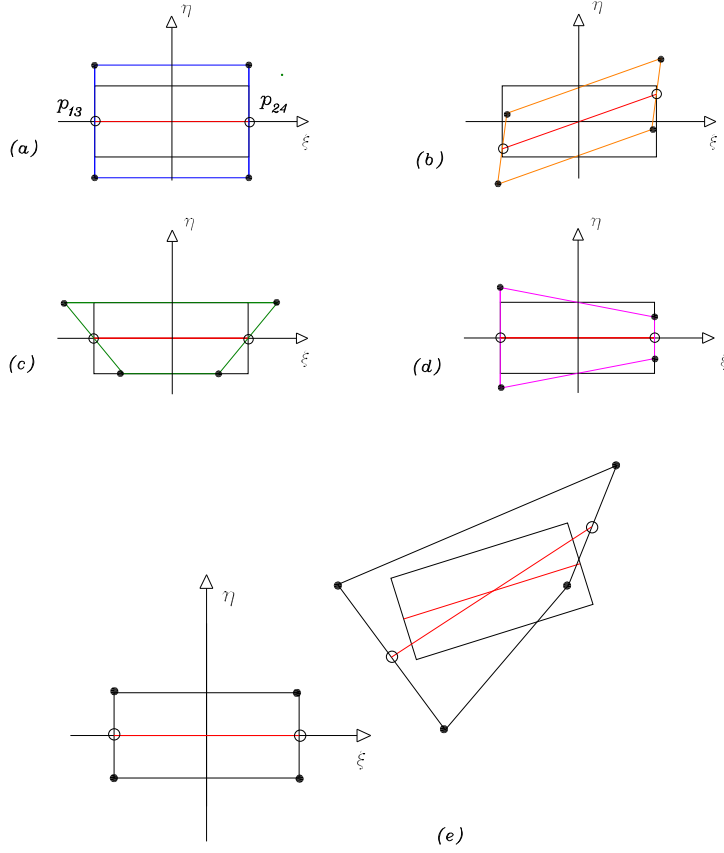
Fig. 2.10: Two-dimensional 4-node element: examination of the $\mathcal{I}E_\xi$ invariant.

2.2.2 Three-dimensional 8-node element

We extend, at present, the formulation obtained in the previous two-dimensional case to the three-dimensional 8-node element. The deformative parameters are the ones defined in Section . The definitions of the numbering of the nodes are referred to the Figure 2.11 where g_i is the central point of the i face. In the following we summarize the definitions of the invariants and their dependence on the related deformative parameters.

- Deformative invariants related to extensional modes:

$$\mathfrak{I}E_\xi = \mathfrak{D}(g_1, g_2) - 2h_\xi, \quad E_\xi = \frac{\mathfrak{I}E_\xi}{2h_\xi};$$
$$\mathfrak{I}E_\eta = \mathfrak{D}(g_3, g_4) - 2h_\eta, \quad E_\eta = \frac{\mathfrak{I}E_\eta}{2h_\eta};$$
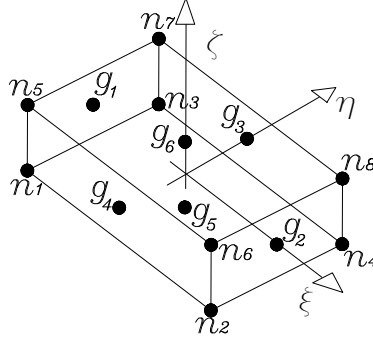$$\mathfrak{I}E_\zeta = \mathfrak{D}(g_5, g_6) - 2h_\zeta, \quad E_\zeta = \frac{\mathfrak{I}E_\zeta}{2h_\zeta}.$$

29

Fig. 2.11: Three-dimensional 8-node element: reference points definition.

- Deformative invariants related to shearing modes:

$$\Im S_{\xi\eta} = \mathfrak{D}(n_1, n_4) + \mathfrak{D}(n_5, n_8) - \mathfrak{D}(n_2, n_3) - \mathfrak{D}(n_6, n_7), \quad S_{\xi\eta} = \frac{\Im S_{\xi\eta}\sqrt{(h_\xi)^2 + (h_\eta)^2}}{16 h_\xi h_\eta};$$

$$\Im S_{\xi\zeta} = \mathfrak{D}(n_1, n_6) + \mathfrak{D}(n_3, n_8) - \mathfrak{D}(n_2, n_5) - \mathfrak{D}(n_4, n_7), \quad S_{\xi\zeta} = \frac{\Im S_{\xi\zeta}\sqrt{(h_\xi)^2 + (h_\zeta)^2}}{16 h_\xi h_\zeta};$$

$$\Im S_{\eta\zeta} = \mathfrak{D}(n_2, n_8) + \mathfrak{D}(n_1, n_7) - \mathfrak{D}(n_4, n_6) - \mathfrak{D}(n_3, n_5), \quad S_{\eta\zeta} = \frac{\Im S_{\eta\zeta}\sqrt{(h_\eta)^2 + (h_\zeta)^2}}{16 h_\eta h_\zeta}.$$

- Deformative invariants related to torsion modes:

$$\Im T_{\zeta} = \mathfrak{D}(n_2, n_3) + \mathfrak{D}(n_5, n_8) - \mathfrak{D}(n_1, n_4) - \mathfrak{D}(n_6, n_7), \quad T_{\zeta} = \frac{\Im T_{\zeta}\sqrt{(h_\xi)^2 + (h_\eta)^2)}}{16 h_\xi h_\eta h_\zeta};$$

$$\Im T_{\eta} = \mathfrak{D}(n_2, n_5) + \mathfrak{D}(n_3, n_8) - \mathfrak{D}(n_1, n_6) - \mathfrak{D}(n_4, n_7), \quad T_{\eta} = \frac{\Im T_{\eta}\sqrt{(h_\xi)^2 + (h_\zeta)^2}}{16 h_\xi h_\eta h_\zeta};$$

$$\Im T_{\xi} = \mathfrak{D}(n_2, n_8) + \mathfrak{D}(n_3, n_5) - \mathfrak{D}(n_1, n_7) - \mathfrak{D}(n_4, n_6), \quad T_{\xi} = \frac{\Im T_{\xi}\sqrt{(h_\eta)^2 + (h_\zeta)^2}}{16 h_\xi h_\eta h_\zeta}.$$

- Deformative invariants related to hourglass modes:

$$\Im H_{\xi\eta} = \mathfrak{D}(n_3, n_4) + \mathfrak{D}(n_7, n_8) - \mathfrak{D}(n_1, n_2) - \mathfrak{D}(n_5, n_6), \quad H_{\xi\eta} = \frac{\Im H_{\xi\eta}}{8 h_\xi h_\eta};$$

$$\Im H_{\eta\xi} = \mathfrak{D}(n_2, n_4) + \mathfrak{D}(n_6, n_8) - \mathfrak{D}(n_1, n_3) - \mathfrak{D}(n_5, n_7), \quad H_{\eta\xi} = \frac{\Im H_{\eta\xi}}{8 h_\xi h_\eta};$$

$$\Im H_{\xi\zeta} = \mathfrak{D}(n_5, n_6) + \mathfrak{D}(n_7, n_8) - \mathfrak{D}(n_1, n_2) - \mathfrak{D}(n_3, n_4), \quad H_{\xi\zeta} = \frac{\Im H_{\xi\zeta}}{8 h_\xi h_\zeta};$$

$$\Im H_{\zeta\xi} = \mathfrak{D}(n_2, n_6) + \mathfrak{D}(n_4, n_8) - \mathfrak{D}(n_1, n_5) - \mathfrak{D}(n_3, n_7), \quad H_{\zeta\xi} = \frac{\Im H_{\zeta\xi}}{8 h_\xi h_\zeta};$$

$$\Im H_{\eta\zeta} = \mathfrak{D}(n_5, n_7) + \mathfrak{D}(n_6, n_8) - \mathfrak{D}(n_1, n_3) - \mathfrak{D}(n_2, n_4), \quad H_{\eta\zeta} = \frac{\Im H_{\eta\zeta}}{8 h_\eta h_\zeta};$$

$$\Im H_{\zeta\eta} = \mathfrak{D}(n_3, n_7) + \mathfrak{D}(n_4, n_8) - \mathfrak{D}(n_1, n_5) - \mathfrak{D}(n_2, n_6), \quad H_{\zeta\eta} = \frac{\Im H_{\zeta\eta}}{8 h_\eta h_\zeta}.$$

- Deformative invariants related to non-physical modes:

$$\Im N_{\xi} = \mathfrak{D}(n_1, n_2) + \mathfrak{D}(n_7, n_8) - \mathfrak{D}(n_3, n_4) - \mathfrak{D}(n_5, n_6), \quad N_{\xi} = \frac{\Im N_{\xi}}{8 h_\xi h_\eta h_\zeta};$$

$$\Im N_{\eta} = \mathfrak{D}(n_1, n_3) + \mathfrak{D}(n_6, n_8) - \mathfrak{D}(n_2, n_4) - \mathfrak{D}(n_5, n_7), \quad N_{\eta} = \frac{\Im N_{\eta}}{8 h_\xi h_\eta h_\zeta};$$

$$\Im N_{\zeta} = \mathfrak{D}(n_1, n_5) + \mathfrak{D}(n_4, n_8) - \mathfrak{D}(n_2, n_6) - \mathfrak{D}(n_3, n_7), \quad N_{\zeta} = \frac{\Im N_{\zeta}}{8 h_\xi h_\eta h_\zeta}.$$

We note that, the definition of the invariant for each deformative mode has been found by inspection of some characteristic distances between points of the element. However, an inverse process is also practicable. In effect, the expressions of the invariants can be defined a priori in function of the nodal displacements. To compute these unknown displacements, we define a linear algebraic system for each invariant. The equations of the linear system are obtained by imposing zero value for all invariant expressions except the value of the considered one. In this way, by constraining also the rigid motions of the element, the kinematics related to the invariant mode is completely determined by the computed nodal displacements. In this sense, as we will see in details in the next section, the approach arises systematically and it acquires generality in the isoparametric elements field.

2.3   Quadrilateral and hexahedral geometries

For generic quadrilateral and hexahedral elements, we refer to the same measures of the invariants given in the previously section. This assumption, however, is consistent if the invariant definition requirements are satisfied. Here we proceed in such a way that the requirements are satisfied in a constructive manner. In effect, in respect to the invariants specification of the previous section carried out by inspection of the modes, here we adopt the related general inverse procedure. In the following, Greek subscript denotes the deformative component with range 1..5 for the two-dimensional and 1..18 for the three-dimensional case, respectively. Latin subscript, instead, denotes the elemental kinematical parameter q_i that can assume 1..8 and 1..24 values. The m subscript, finally, is used to identify the node.
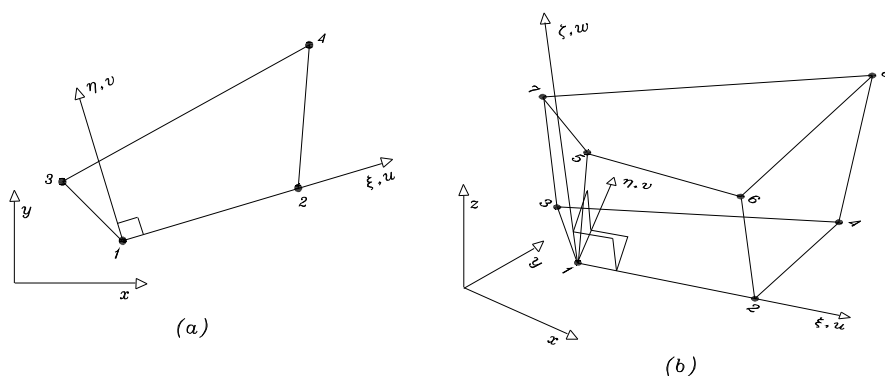

Fig. 2.12: Quadrilateral and hexahedral elements: topological definition.

Let the nodal distances based measures $\mathcal{M}_\alpha = \mathcal{D}_\alpha(n_m)$ for the assumed invariants given. The distances are then computed in function of the ξ_m, η_m and ζ_m local nodal coordinates and of the u_m, v_m and w_m local nodal displacements. Topological definitions are given in Figure 2.12(a) and Figure 2.12(b) for the four-node and eight-node element, respectively. In particular, for the three-dimensional space, η axis was placed in the plane defined by n_1, n_2 and n_3 nodes.

Having obtained the expression $\mathcal{M}_\alpha(u_m, v_m, w_m)$, the following elemental kinematics

$$u(\xi, \eta) = a_1\xi + a_3\eta + a_4\xi\eta, \qquad v(\xi, \eta) = a_3\xi + a_2\eta + a_5\xi\eta, \qquad (2.40)$$

and

$$\begin{aligned}
u(\xi, \eta, \zeta) &= a_1\xi + a_4\eta + a_6\zeta + a_7\xi\eta + a_{14}\xi\zeta + a_{12}\eta\zeta + a_{16}\xi\eta\zeta, \\
v(\xi, \eta, \zeta) &= a_4\xi + a_2\eta + a_5\zeta + a_{10}\xi\eta + a_8\xi\zeta + a_{15}\eta\zeta + a_{17}\xi\eta\zeta, \qquad (2.41) \\
w(\xi, \eta, \zeta) &= a_6\xi + a_5\eta + a_3\zeta + a_{13}\xi\eta + a_{11}\xi\zeta + a_9\eta\zeta + a_{18}\xi\eta\zeta,
\end{aligned}$$

are considered for the 4-node and 8-node cases, respectively. Expressions (2.40) and (2.41) are obtained from the (2.1) and (2.12) displacement interpolations by depriving them of the rigid motions and represent, therefore, only the deformative kinematics. Nodal displacements $u_m(a_\alpha)$, $v_m(a_\alpha)$, $w_m(a_\alpha)$, then, are in function of the a_α unknown parameters. By insertion of such nodal displacements in the definitions of the distances, the nonlinear $\mathcal{M}_\alpha(a_\beta)$ measures are obtained. Of course, being in the linear deformative assumptions,

$$\mathcal{L}\mathcal{M}_\alpha(a_\beta) = \mathbf{L}\,\mathbf{a} = \sum_\beta \frac{\partial \mathcal{M}_\alpha}{\partial a_\beta}(0)\,a_\beta \qquad (2.42)$$

represent the desired definitions of the assumed invariants in the linearized kinematic.

Now, we note that measures $\mathcal{L}\mathcal{M}_\alpha$ in (2.42) are independent of the rigid kinematics. Furthermore, for each measure $\mathcal{L}\mathcal{M}_\beta$, we can compute a posteriori the related mode $\mathbf{m}_\beta$ by solving the system

$$\mathbf{L}\,\mathbf{m}_\beta = \mathbf{i}_\beta M_\beta, \qquad (2.43)$$

where $\mathbf{i}_\beta$ is the unit vector in the β-th direction. In this way, the $\mathbf{m}_\beta$ mode produces the M_β value for the $\mathcal{L}\mathcal{M}_\beta$ measure and zero value for the other $\mathcal{L}\mathcal{M}_\alpha$, $\alpha \neq \beta$, considered measures. Then, the required connection between the deformative modes ($\mathbf{m}_\alpha$) and the deformative parameters (M_α) has been accomplished. $\mathcal{L}\mathcal{M}_\alpha(\mathbf{m}_\beta) = \mathcal{L}\mathcal{M}_\alpha(M_\beta)$ are the researched definitions of the invariants in the linear field while $u(\mathbf{m}_\alpha) = u(M_\alpha)$, $v(\mathbf{m}_\alpha) = v(M_\alpha)$, $w(\mathbf{m}_\alpha) = w(M_\alpha)$, are the related kinematics.

As a result of such a procedure, linear strain components are expressed in function of the deformative parameters M_α by spatial differentation of the computed $u(M_\alpha)$, $v(M_\alpha)$, $w(M_\alpha)$ kinematics while the nonlinear invariants definitions $\mathcal{M}_\alpha(u_m, v_m, w_m) = \mathcal{M}_\alpha(q_i)$ are initially given in dependence on the kinematics parameters q_i in the xyz global reference system.

For the elemental internal forces and stiffness matrix evaluation we proceed by the chain rule differentiation of the $V(\boldsymbol{\varepsilon}(\boldsymbol{M}(\boldsymbol{q})))$ potential expression. We note that non-linearities are present only in the $\boldsymbol{M}(\boldsymbol{q})$ operator. In the linear $\boldsymbol{\varepsilon}(\boldsymbol{M})$ dependence, besides, for each component of the strain tensor $\boldsymbol{\varepsilon}$, the desired M_α deformative contribution can be activated by the user through a simple switch operation.

2.4 Geometrically nonlinear statical analysis

In this section, after giving the definition of the involved energetic quantities, we describe the system of the statical motion equation and the corresponding adopted solution scheme.

2.4.1 Energetic quantities definition

The energetic quantities involved in the statical analysis are the $V(\mathbf{u})$ internal potential and the $L(\mathbf{u})$ external work:

$$V(\mathbf{u}) = \frac{1}{2} \int_\Omega \varepsilon^\mathbf{T} \mathbf{A}\, \varepsilon \, \mathbf{d\Omega}, \quad \mathbf{L(u)} = \int_{\boldsymbol{\Omega}} \mathbf{p^T u}\, \mathbf{d\Omega}. \qquad (2.44)$$

$\mathbf{A}$ is the material coefficients matrix, Ω is the domain of body and $\mathbf{p}$ is the vector of external loads.

We focus, now, on the description of the strain tensor in (2.44). We refer to the linear approximation of the tensor components, being, as abovementioned, the geometrical nonlinearity taken in to account by the definition of the deformative invariants. The tensor, then, is expressed as a linear function of the deformative parameters:

$$\begin{cases} \varepsilon_{\xi\xi} = \varepsilon_{\xi\xi}(E_\xi, E_\eta, H_\xi, H_\eta) \\ \varepsilon_{\xi\eta} = \varepsilon_{\xi\eta}(S_{\xi\eta}) \\ \varepsilon_{\eta\eta} = \varepsilon_{\eta\eta}(E_\xi, E_\eta, H_\xi, H_\eta) \end{cases} \qquad (2.45)$$

for the two-dimensional case, while

$$
\begin{cases}
\varepsilon_{\xi\xi} = \varepsilon_{\xi\xi}(E_\xi, E_\eta, E_\zeta, H_{\xi\eta}, H_{\eta\zeta}, H_{\zeta\xi}, H_{\eta\xi}, H_{\zeta\eta}, H_{\xi\zeta}, N_\xi, N_\eta, N_\zeta) \\
\varepsilon_{\xi\eta} = \varepsilon_{\xi\eta}(S_{\xi\eta}, S_{\eta\zeta}, S_{\zeta\xi}, T_\xi, T_\eta, T_\zeta) \\
\varepsilon_{\xi\zeta} = \varepsilon_{\xi\zeta}(S_{\xi\eta}, S_{\eta\zeta}, S_{\zeta\xi}, T_\xi, T_\eta, T_\zeta) \\
\varepsilon_{\eta\eta} = \varepsilon_{\eta\eta}(E_\xi, E_\eta, E_\zeta, H_{\xi\eta}, H_{\eta\zeta}, H_{\zeta\xi}, H_{\eta\xi}, H_{\zeta\eta}, H_{\xi\zeta}, N_\xi, N_\eta, N_\zeta) \\
\varepsilon_{\eta\zeta} = \varepsilon_{\eta\zeta}(S_{\xi\eta}, S_{\eta\zeta}, S_{\zeta\xi}, T_\xi, T_\eta, T_\zeta) \\
\varepsilon_{\zeta\zeta} = \varepsilon_{\zeta\zeta}(E_\xi, E_\eta, E_\zeta, H_{\xi\eta}, H_{\eta\zeta}, H_{\zeta\xi}, H_{\eta\xi}, H_{\zeta\eta}, H_{\xi\zeta}, N_\xi, N_\eta, N_\zeta)
\end{cases}
\tag{2.46}
$$

for the three-dimensional case. Locking effects are overcome by a selective choice of the modes in the (2.45) and (2.46) expressions. This selective reduction of the strain components, as said before, can be carried out by a simple zeroing of the undesired deformative parameters. In particular, in (2.45) and (2.46) we have omitted the shearing and torsional terms in the normal strain components while extension, hourglass and non-physical modes have been cancelled in the shear strain components.

We note that, the eigenvalues problem solution shows that spurious zero energy modes are not contained in the element stiffness matrix. In effect, this situation is verified because all the deformative parameters appear at least once in the strain tensor definitions.

The potential V, then, results defined by the deformative parameters that are in function of the unknown nodal displacements. As we said, by chain rule we can compute the element internal forces vector and stiffness matrix. The computational cost required by the storage and evalutation of this vectorial quantities results small. In effect, we observe that this is about equal to one-third of the computational cost required by the formulation with classical nonlinear deformations tensor.

2.4.2 Statical motion equation and adopted solution scheme

By referring to (2.44) definitions, the internal $\mathbf{N(u)}$ and the external $\mathbf{P}$ forces are expressed by:

$$
\mathbf{N(u)} = \frac{\partial \mathbf{V(u)}}{\partial \mathbf{u}}, \quad \mathbf{P} = \frac{\partial \mathbf{L(u)}}{\partial \mathbf{u}},
\tag{2.47}
$$

In the finite element approach the displacements in the body are described by the $\mathbf{q}$ vector of the global parameters. With this spatial discretization and by including the boundary conditions, we obtain the following statical equilibrium equation:

$$
\mathbf{N(u)} - \lambda \mathbf{P} = 0,
\tag{2.48}
$$

where λ is the external force parameter.

A predictor-corrector scheme as described in[48],[49] for the equilibrium path individualization is used in the statical analysis. It is characterized by a predictor step obtained by an asymptotic extrapolation and by a corrector scheme Newton's method based with minimization of the distance between approximate and equilibrium points as a constraint equation. Here we adopt a first order asymptotic extrapolation in the predictor phase. The length $\mu^{(k)}$ of the extrapolation parameter in the k-th predictor-corrector step is chosen as a function of the iterations $N_{it}^{(k-1)}$ performed in the previous corrector step:

$$\mu^{(k)} = \mu^{(k-1)} \frac{\bar{N}_{it}}{N_{it}^{(k-1)}}, \tag{2.49}$$

where $\bar{N}_{it} = 3$ is taken as target iteration count. The corrector process computes the i-th approximation of the force parameter $\lambda_{(i)}^{(k)}$ and vector of discretization parametes $\mathbf{q}_{(i)}^{(k)}$. It is stopped when the convergence criterion

$$\frac{\|\mathbf{q}_{(i)}^{(k)} - \mathbf{q}_{(i-1)}^{(k)}\|}{\|\mathbf{q}_{(i)}^{(k)}\|} < 10^{-8} \tag{2.50}$$

is satisfied.

Chapter 3

Projectors based method

Existing finite element formulations for finite rotation problems are solely based on various types of rotational parameters, inevitably used as kinematic variables. These techniques, however, suffer from the singularities in the transformation matrices for several angles and requires complex manipulations to overcome nonconservative descriptions due to the noncommutativity of rotations. The interpolation of rotations to measure deformations then requires the use of incremental solution procedures when large rotations are considered. In effect, small rotation increments are hypothesized for the linearization of the configuration space. Consequently, small steps in the continuation process are allowed and a slow convergence is intrinsic to the formulation. To overcome these limitations, a completely different approach is taken in this chapter. The suggested formulation, based on the total Lagrangian description, abandons the classical assumption because the use of the rotation parameters is bypassed. *Projectors* are used instead of rotation parameters to compute the nonlinear representations of the strain measures in the inertial frame of reference.

In particular, based on the Euler-Bernoulli beam theory, the actual configuration of the element is rigidly translated and rotated, and deformed according to the selected linear modes. Rigid and deformative modes are referred to the nodes of the element. The nonlinear rigid motion is recovered by referring to three unit and mutually orthogonal vectors attached to the nodes of the beam element. All nine components of such vectors in the global inertial frame of reference are assumed as unknown. As will be demonstrated, the rotational degree of freedom of the element is reduced to only three by six well-posed constraint conditions.

Afterward, for each deformative mode, a characteristic measure that is an invariant of the rotations is defined. As the deformation modes are reciprocally independent, they can be summed up in the strain tensor definition. The invariant measures are then computed by requiring the following two

features for each of them: not zero for the examined deformative mode and equal to zero for the other modes in the initial configuration; independent of the rigid kinematics value. We note that, boundary conditions on rotations are simply imposed by assuming as known the related nodal slopes while applied moments are modeled as forces following the motions, as will be discussed later.

In the chapter we first describe the kinematics of the beam element and related deformative energy. Subsequently we discuss the constraint conditions imposed on the unknown components of vectors representative of the rigid rotations and finally we describe the nonlinear equilibrium equations and of the related solution algorithm.

3.1 Kinematics and strain energy of the beam element

We refer to the referential coordinate ξ along the element beam centerline $-h \le \xi \le +h$. In the following, we denote with n and m the nodes respectively in $\xi = -h$ and $\xi = +h$, Latin indices i, j and k have the values [1,...,3] while δ_{ij} is the Kronecker delta. In the global inertial frame of reference (x_i) and for each n node we define three unknown displacement components u_i^n and three unknown vectors

$$\mathbf{E_1^n} = \{E_{1,1}^n, E_{1,2}^n, E_{1,3}^n\},$$
$$\mathbf{E_2^n} = \{E_{2,1}^n, E_{2,2}^n, E_{2,3}^n\},$$
$$\mathbf{E_3^n} = \{E_{3,1}^n, E_{3,2}^n, E_{3,3}^n\}, \tag{3.1}$$

or in a compact form $\mathbf{E_i^n} = \{E_{i,j}^n\}$ (see Fig.3.2). Even though the components of such vectors are unknowns, at the solution points vector $\mathbf{E_1^n}$ is in the ξ direction while vectors $\mathbf{E_2^n}$ and $\mathbf{E_3^n}$ are along the principal axes of inertia of the cross-section.

In the beam element, global displacement vector $\mathbf{u}(\xi) = \{u_i(\xi)\}$ is composed of rigid and deformative components.
In particular we refer to the deformative $\tilde{\mathbf{u}}(\xi) = \{\tilde{u}_i(\xi)\}$ displacement vectors defined in the local rigidly rotated frame of reference. The deformative kinematics is assumed by the simplest interpolations

$$\tilde{u}_1(\xi) = e_1 \xi/h,$$
$$\tilde{u}_2(\xi) = f_{12}\xi^2/2h + s_{12}\xi^3/2h^2,$$
$$\tilde{u}_3(\xi) = f_{13}\xi^2/2h + s_{13}\xi^3/2h^2. \tag{3.2}$$

Based on the assumptions (3.2), constant axial and shear stress resultants and linear bending moments are expected. Unknowns e_1, f_{12}, s_{12}, f_{13}, s_{13}
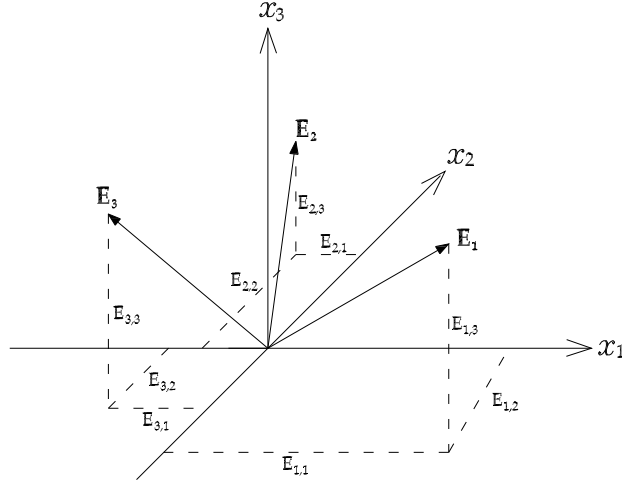
Fig. 3.1: generical unknown three nodal vectors.

in (3.2) are local deformative components. The kinematics of the element is then completed by defining the local θ rotation about the beam centerline

$$\tilde{\theta}(\xi) = t_1\xi/h, \qquad (3.3)$$

where t_1 is the related deformative component. Constant torsional stress resultant is expected here.

We note that rigid kinematics will be implicitly represented by the nodal displacement components and the degrees of freedom of the vectors $\mathbf{E_i}$ attached to the beam element.

As the beam element kinematics is defined, in order to formulate the equilibrium equations using matrix formulation, the following stress $\{S\}$ and deformation $\{\gamma\}$ vectors are introduced:

$$\{S\}^t = \{N \;\; M_2 \;\; M_3 \;\; M_{sv} \;\; M_R\},$$
$$\{\gamma\}^t = \{\varepsilon(\xi) \;\; -k_2(\xi) \;\; -k_3(\xi) \;\; \tilde{\theta}'(\xi) \;\; \frac{1}{2}\tilde{\theta}'(\xi)^2\}.$$

where $\{\}^t$ denotes the transpose operator and the prime ($'$) the derivative with respect to the ξ coordinate. By referring to stress quantities, N is the axial force, M_2 and M_3 are the bending moments, M_{sv} is the St-Venant torsion moment and M_R is the Wagner's moment. By referring to deformation quantities, $\varepsilon(\xi) = \tilde{u}_1'(\xi)$ denotes the membrane component, $k_2(\xi) = \tilde{u}_2''(\xi)$ and $k_3(\xi) = \tilde{u}_3''(\xi)$ are the beam curvatures about the main axis while $\tilde{\theta}'(\xi)$, sometimes called shortening term, is a rotation per unit length.

38

The relationships between the stress vector components in terms of deformation vector components are the following in the principal axes:

$$N = \int_A E\varepsilon_{11} dA = EA\varepsilon(\xi) + \frac{1}{2}EAJ_o\tilde{\theta}'(\xi)^2,$$

$$M_2 = \int_A E\varepsilon_{11}\xi_3 dA = -EJ_2 k_2(\xi),$$

$$M_3 = \int_A E\varepsilon_{11}\xi_2 dA = -EJ_3 k_3(\xi), \tag{3.4}$$

$$M_{sv} = 2\int_A (G\varepsilon_{13}(\xi_2 - \xi_2^c) - G\varepsilon_{12}(\xi_3 - \xi_3^c)) dA = GJ_1\tilde{\theta}'(\xi),$$

$$M_R = EAJ_o\varepsilon(\xi) + \frac{1}{2}EJ_p\tilde{\theta}'(\xi)^2,$$

where ε_{ij} denotes the strain tensor components and ξ_i^c are the shear centre coordinates. The above relationships (3.4) are also functions of elastic and geometric characteristics. E and G are the Young and shear moduli, A denotes the section area, J_2 and J_3 are the second moments of area about the principal axes of inertia, J_1 is the St-Venant torsion constant while J_o and J_p are the polar moment and the fourth moment of the area about the shear centre, respectively. We note that the warping effect, further nonlinear coupling terms and the Wagner coefficients are not taken into account because only rectangular section was analyzed. Different section shapes, however, can also be introduced (Mohri et al. [56], [57], can be referred for details of this).

These equilibrium equations written in matrix formulation lead to

$$\{S\} = \begin{Bmatrix} N \\ M_2 \\ M_3 \\ M_{sv} \\ M_R \end{Bmatrix} = \begin{bmatrix} EA & 0 & 0 & 0 & EAJ_o \\ 0 & EJ_2 & 0 & 0 & 0 \\ 0 & 0 & EJ_3 & 0 & 0 \\ 0 & 0 & 0 & GJ_1 & 0 \\ EAJ_o & 0 & 0 & 0 & EJ_p \end{bmatrix} \begin{Bmatrix} \tilde{u}_1'(\xi) \\ -\tilde{u}_2''(\xi) \\ -\tilde{u}_3''(\xi) \\ \tilde{\vartheta}'(\xi) \\ \frac{1}{2}\tilde{\vartheta}'(\xi)^2 \end{Bmatrix} = [D]\{\gamma\}.$$

where [D] is the material matrix behaviour. Using relations (3.4), the expression of the strain energy is easy to obtain. To this end the flexural strain energy of the element is defined as

$$\begin{aligned} \Pi_f &= \frac{1}{2}\int_{-h}^{+h}\{M_2\tilde{u}_2''(\xi) + M_3\tilde{u}_3''(\xi)\}d\xi \\ &= \frac{1}{2}\int_{-h}^{+h}\{EJ_2\tilde{u}_2''(\xi)^2 + EJ_3\tilde{u}_3''(\xi)^2\}d\xi. \end{aligned} \tag{3.5}$$

The pure torsional strain energy is written as

$$
\begin{aligned}
\Pi_t &= \frac{1}{2} \int_{-h}^{+h} M_{sv} \tilde{\theta}'(\xi) d\xi \\
&= \frac{1}{2} \int_{-h}^{+h} G J_1 \tilde{\theta}'(\xi)^2 d\xi.
\end{aligned}
\tag{3.6}
$$

In addition, the axial and torsional strain energies were coupled in the non-linear form

$$
\begin{aligned}
\Pi_{at} &= \frac{1}{2} \int_{-h}^{+h} \{ N \tilde{u}_1'(\xi) + M_R \tilde{\theta}'(\xi)^2 / 2 \} d\xi \\
&= \frac{1}{2} \int_{-h}^{+h} \{ [EA \tilde{u}_1'(\xi) + EAJ_o \tilde{\theta}'(\xi)^2 / 2] \tilde{u}_1'(\xi) + \\
&\quad + [EAJ_o \tilde{u}_1'(\xi) + EJ_p \tilde{\theta}'(\xi)^2 / 2] \tilde{\theta}'(\xi)^2 / 2 \} d\xi.
\end{aligned}
\tag{3.7}
$$

Finally, the total strain energy of the beam element is obtained by the sum

$$
\Pi = \Pi_f + \Pi_t + \Pi_{at}.
$$

To compute the deformative components we refer to the beam element centered in the origin of the (ξ_i) reference system (see Fig. 3.2) where ξ_1 represents the ξ beam centerline. The deformative modes have been computed by the interpolations in (3.2)-(3.3) and are shown in Fig. 3.3. In particular we refer to: e_1 expansion mode along the ξ_1 direction; f_{12} and s_{12}, respectively, flexural and shearing modes in the $\xi_1 \xi_2$ plain; f_{13} and s_{12}, respectively, flexural and shearing modes in the $\xi_1 \xi_3$ plain; t_1 torsional mode around the ξ_1 axis.
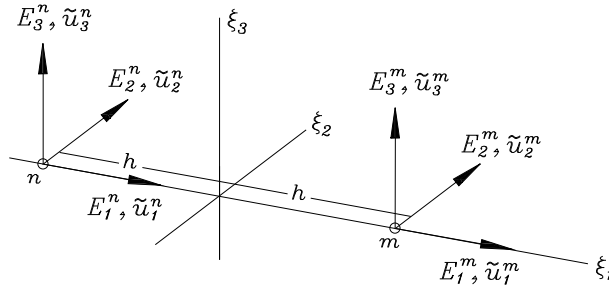
Fig. 3.2: beam element definition.
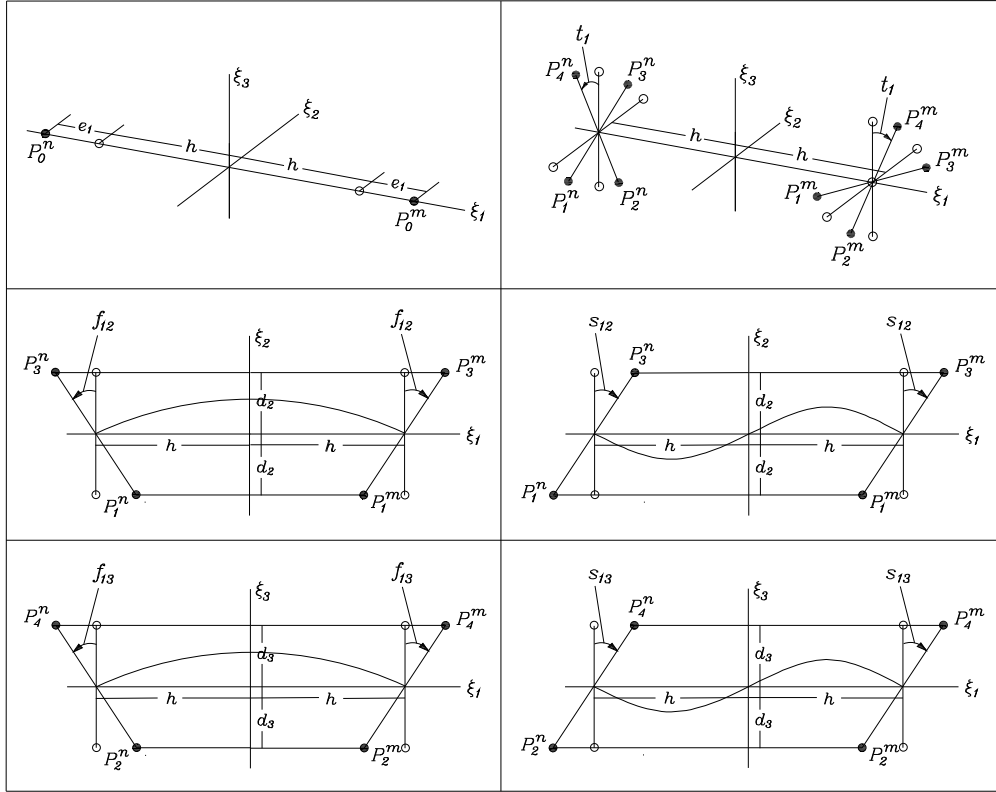
Fig. 3.3: selected points for the linear deformative modes representation.

3.2 Deformative components in the global reference system

As stated, for each deformative mode, we identify a measure with the following two features: not zero for the examined mode and equal to zero for the other modes in the initial configuration; independent of the rigid kinematics value. Such a measure uniquely describes the deformation associated with the mode itself in the generic configuration, so, these definitions make the deformative modes reciprocally independent and, then, they can be summed up in the strain tensor definitions.

The measures just described, denoted in the following as deformative invariants $\mathcal{I}$, represent here relative distances between points of the generic configuration and they are a function of the unknown elemental parameters. We refer to the $\mathcal{D}^2(P_\alpha^n, P_\beta^m)$ square of the Euclidean distance between the
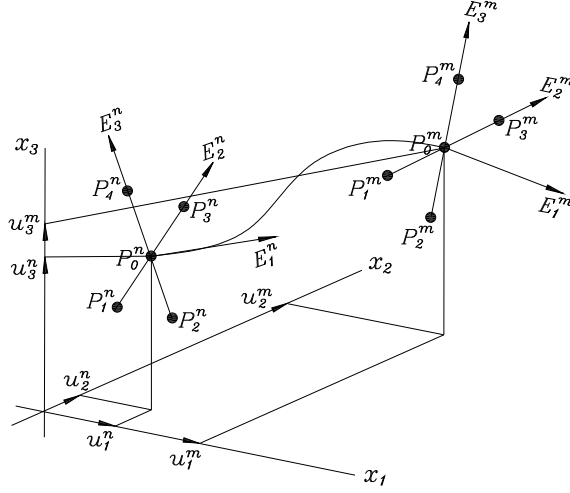
Fig. 3.4: selected points for the nonlinear deformative modes representation.

points P_α^n, P_β^m of the element (see Fig. 3.4) in the generic configuration:

$$\mathcal{D}^2(P_\alpha^n, P_\beta^m) = \sum_{i=1}^{3} \left[\xi_i(P_\alpha^n) + u_i(P_\alpha^n) - \xi_i(P_\beta^m) - u_i(P_\beta^m) \right]^2. \qquad (3.8)$$

In (3.8) $\xi_i(P_\alpha^n)$ are the initial ξ_i coordinates of the point P_α^n while $u_i(P_\alpha^n)$ are the respective displacements.

For each deformative parameter, we list the assumed invariants by:

$$\mathcal{I}e_1 = \mathcal{D}^2(P_0^n, P_0^m) - (2h)^2,$$

$$\mathcal{I}f_{12} = \mathcal{D}^2(P_3^n, P_3^m) - \mathcal{D}^2(P_1^n, P_1^m),$$

$$\mathcal{I}s_{12} = \mathcal{D}^2(P_1^n, P_3^m) - \mathcal{D}^2(P_3^n, P_1^m),$$

$$\mathcal{I}f_{13} = \mathcal{D}^2(P_4^n, P_4^m) - \mathcal{D}^2(P_2^n, P_2^m),$$

$$\mathcal{I}s_{13} = \mathcal{D}^2(P_2^n, P_4^m) - \mathcal{D}^2(P_4^n, P_2^m),$$

$$\mathcal{I}t_1 = [\mathcal{D}^2(P_1^n, P_4^m) + \mathcal{D}^2(P_2^n, P_1^m) + \mathcal{D}^2(P_3^n, P_2^m) + \mathcal{D}^2(P_4^n, P_3^m)]/(2h)^2.$$

Now, we denote with $\mathcal{I}^L$ and $\mathcal{I}^{NL}$ the deformative invariant definitions in the local (linear) and global (nonlinear) representation, respectively. By using the above definitions, for each deformative parameter, we compute the explicit expressions of the invariant representations summarized below:

$$\mathcal{I}^L e_1 = (2h + 2e_1)^2 - (2h)^2 \approx 8he_1,$$

$$\mathcal{I}^{NL} e_1 = (u_1^n - u_1^m - 2h)^2 + (u_2^n - u_2^m)^2 + (u_3^n - u_3^m)^2 - (2h)^2$$

42

$$\mathcal{I}^L f_{12} = (2h + 2d_2 f_{12})^2 - (2h - 2d_2 f_{12})^2 = 16hd_2 f_{12}$$

$$\mathcal{I}^{NL} f_{12} = 4d_2[(u_1^n - u_1^m - 2h)(E_{2,1}^n - E_{2,1}^m) + (u_2^n - u_2^m)(E_{2,2}^n - E_{2,2}^m)+$$

$$+(u_3^n - u_3^m)(E_{2,3}^n - E_{2,3}^m)]$$

$$\mathcal{I}^L s_{12} = (2h + 2d_2 s_{12})^2 - (2h - 2d_2 s_{12})^2 = 16hd_2 s_{12}$$

$$\mathcal{I}^{NL} s_{12} = 4d_2[(u_1^n - u_1^m - 2h)(E_{2,1}^n + E_{2,1}^m) + (u_2^n - u_2^m)(E_{2,2}^n + E_{2,2}^m)+$$

$$+(u_3^n - u_3^m)(E_{2,3}^n + E_{2,3}^m)]$$

$$\mathcal{I}^L f_{13} = (2h + 2d_3 f_{13})^2 - (2h - 2d_3 f_{13})^2 = 16hd_3 f_{13}$$

$$\mathcal{I}^{NL} f_{13} = 4d_3[(u_1^n - u_1^m - 2h)(E_{3,1}^n - E_{3,1}^m) + (u_2^n - u_2^m)(E_{3,2}^n - E_{3,2}^m)+$$

$$(u_3^n - u_3^m)(E_{3,3}^n - E_{3,3}^m)]$$

$$\mathcal{I}^L s_{13} = (2h + 2d_3 s_{13})^2 - (2h - 2d_3 s_{13})^2 = 16hd_3 s_{13}$$

$$\mathcal{I}^{NL} s_{13} = 4d_3[(u_1^n - u_1^m - 2h)(E_{3,1}^n + E_{3,1}^m) + (u_2^n - u_2^m)(E_{3,2}^n + E_{3,2}^m)+$$

$$+(u_3^n - u_3^m)(E_{3,3}^n + E_{3,3}^m)]$$

$$\mathcal{I}^L t_1 = [16h^2 + 2d_2^2 + 2d_3^2 + 2(d_2 + t_1 d_3)^2 + 2(d_3 + t_1 d_2)^2]/(2h)^2 \approx$$

$$(4h^2 + d_2^2 + d_3^2 + 2t_1 d_2 d_3)/h^2$$

$$\mathcal{I}^{NL} t_1 = [d_2^2 + d_3^2 + (u_1^n - u_1^m - 2h)^2 + (u_2^n - u_2^m)^2 + (u_3^n - u_3^m)^2+$$

$$(E_{2,1}^n E_{3,1}^m + E_{2,2}^n E_{3,2}^m + E_{2,3}^n E_{3,3}^m - E_{3,1}^n E_{2,1}^m - E_{3,2}^n E_{2,2}^m - E_{3,3}^n E_{2,3}^m)d_2 d_3]/h^2 \approx$$

$$[4h^2 + d_2^2 + d_3^2 + (E_{2,1}^n E_{3,1}^m + E_{2,2}^n E_{3,2}^m+$$

$$+E_{2,3}^n E_{3,3}^m - E_{3,1}^n E_{2,1}^m - E_{3,2}^n E_{2,2}^m - E_{3,3}^n E_{2,3}^m)d_2 d_3]/h^2$$

In the $\mathcal{I}^{NL} t_1$ evaluation, simplifications deriving from the $\mathbf{E_i}^T \mathbf{E_i} = 1$ and $[\mathcal{D}^2(P_0^n, P_0^m) - (2h)^2]/(2h)^2 \approx 0$ estimates have been carried out. Finally, by equating $\mathcal{I}^L$ expressions with the related $\mathcal{I}^{NL}$ we compute the global representations of the deformative parameters used in (3.2)-(3.3):

$$e_1 = [(u_1^n - u_1^m - 2h)^2 + (u_2^n - u_2^m)^2 + (u_3^n - u_3^m)^2 - (2h)^2]/8h,$$

$$f_{12} = [(u_1^n - u_1^m - 2h)(E_{2,1}^n - E_{2,1}^m)$$

43

$$+(u_2^n - u_2^m)(E_{2,2}^n - E_{2,2}^m) + (u_3^n - u_3^m)(E_{2,3}^n - E_{2,3}^m)]/4h,$$

$$s_{12} = [(u_1^n - u_1^m - 2h)(E_{2,1}^n + E_{2,1}^m)$$
$$+(u_2^n - u_2^m)(E_{2,2}^n + E_{2,2}^m) + (u_3^n - u_3^m)(E_{2,3}^n + E_{2,3}^m)]/4h,$$

$$f_{13} = [(u_1^n - u_1^m - 2h)(E_{3,1}^n - E_{3,1}^m)$$
$$+(u_2^n - u_2^m)(E_{3,2}^n - E_{3,2}^m) + (u_3^n - u_3^m)(E_{3,3}^n - E_{3,3}^m)]/4h,$$

$$s_{13} = [(u_1^n - u_1^m - 2h)(E_{3,1}^n + E_{3,1}^m)$$
$$+(u_2^n - u_2^m)(E_{3,2}^n + E_{3,2}^m) + (u_3^n - u_3^m)(E_{3,3}^n + E_{3,3}^m)]/4h,$$

$$t_1 = [E_{2,1}^n E_{3,1}^m + E_{2,2}^n E_{3,2}^m + E_{2,3}^n E_{3,3}^m - E_{3,1}^n E_{2,1}^m - E_{3,2}^n E_{2,2}^m - E_{3,3}^n E_{2,3}^m]/2.$$

We note that, as it should be, these representations are independent of the transversal lengths d_2 and d_3.

3.3 Constraint conditions

The nine $E_{i,j}$ unknown components of the $\mathbf{E_i}$ vectors are subject to six constraint conditions. We demonstrate here that the rotational degrees of freedom are reduced just to three. Of course, six conditions being imposed, the degrees of freedom are at least three. To show also that the degrees of freedom are at most three we refer to the definitions $i_- = i-1$ and $i_+ = i+1$ for the cyclic sequence of the Latin indices.

The constraint equations are

$$\mathbf{E_2} \cdot \mathbf{E_2} - 1 = 0,$$
$$\mathbf{E_3} \cdot \mathbf{E_3} - 1 = 0,$$
$$\mathbf{E_2} \cdot \mathbf{E_3} = 0,$$
$$\mathbf{E_2} \times \mathbf{E_3} = \mathbf{E_1}, \tag{3.9}$$

where the related Jacobian matrix is denoted by $\mathbf{G}$. We show that nullity($\mathbf{G}$) is at most three in the solution point. The open mapping theorem then gives the result. The Jacobian matrix of the system (4.12) is

$$\mathbf{G} = \begin{bmatrix} 0 & 0 & 0 & E_{2,1} & E_{2,2} & E_{2,3} & 0 & 0 & 0 \\ 0 & 0 & 0 & 0 & 0 & 0 & E_{3,1} & E_{3,2} & E_{3,3} \\ 0 & 0 & 0 & E_{3,1} & E_{3,2} & E_{3,3} & E_{2,1} & E_{2,2} & E_{2,3} \\ 1 & 0 & 0 & 0 & -E_{3,3} & E_{3,2} & 0 & E_{2,3} & -E_{2,2} \\ 0 & 1 & 0 & E_{3,3} & 0 & -E_{3,1} & -E_{2,3} & 0 & E_{2,1} \\ 0 & 0 & 1 & -E_{3,2} & E_{3,1} & 0 & E_{2,2} & -E_{2,1} & 0 \end{bmatrix}. \tag{3.10}$$

Then, in the solution point and for a given known vector $\mathbf{z}$, we must verify that six of the nine $y_{i,j}$ components of the unknown vector $\mathbf{y}$ are uniquely determinable from the system $\mathbf{Gy} = \mathbf{z}$.

From the last three rows of the system, as we can see in (3.10), the $y_{1,i}$ unknowns are easy to calculate. Therefore the system is reduced to the form

$$
\begin{bmatrix}
E_{2,1} & E_{2,2} & E_{2,3} & 0 & 0 & 0 \\
0 & 0 & 0 & E_{3,1} & E_{3,2} & E_{3,3} \\
E_{3,1} & E_{3,2} & E_{3,3} & E_{2,1} & E_{2,2} & E_{2,3}
\end{bmatrix}
\begin{Bmatrix}
y_{2,1} \\ y_{2,2} \\ y_{2,3} \\ y_{3,1} \\ y_{3,2} \\ y_{3,3}
\end{Bmatrix}
=
\begin{Bmatrix}
z_2 \\ z_3 \\ z_{2,3}
\end{Bmatrix} . \quad (3.11)
$$

For at least one i and one j is $E_{2,i} \neq 0$ and $E_{3,j} \neq 0$, respectively. Then, from the first two rows of (3.11) we obtain

$$
y_{2,i} = \frac{1}{E_{2,i}}(z_2 - E_{2,i-}y_{2,i-} - E_{2,i+}y_{2,i+}), \quad (3.12)
$$

$$
y_{3,i} = \frac{1}{E_{3,j}}(z_3 - E_{3,j-}y_{3,j-} - E_{3,j+}y_{3,j+}). \quad (3.13)
$$

By inserting (3.12) and (3.13) in the third row of system (3.11) and multiplying by $E_{2,i}E_{3,j}$ it follows that

$$
[E_{2,i}E_{3,i-} - E_{2,i-}E_{3,i}]E_{3,j}y_{2,i-} + [E_{2,i}E_{3,i+} - E_{2,i+}E_{3,i}]E_{3,j}y_{2,i+}
$$

$$
+[E_{2,j-}E_{3,j} - E_{2,j}E_{3,j-}]E_{2,i}y_{3,j-} + [E_{2,j+}E_{3,j} - E_{2,j}E_{3,j+}]E_{2,i}y_{3,j+}
$$

$$
= c_1 E_{3,j}y_{2,i-} + c_2 E_{3,j}y_{2,i+} + c_3 E_{2,i}y_{3,j-} + c_4 E_{2,i}y_{3,j+} = \bar{z}, \quad (3.14)
$$

with coefficients $c_1, ..., c_4$ and $\bar{z}$.

At the solution, the last three equations in (4.12) give

$$
E_{2,k}E_{3,k+} - E_{2,k+}E_{3,k} = E_{1,k-}. \quad (3.15)
$$

In particular, (3.15) with

$$
k = i- \quad \Rightarrow E_{2,i-}E_{3,i} - E_{2,i}E_{3,i-} = E_{1,i+} \quad \Rightarrow c_1 = -E_{1,i+};
$$

$$
k = i \quad \Rightarrow E_{2,i}E_{3,i+} - E_{2,i+}E_{3,i} = E_{1,i-} \quad \Rightarrow c_2 = E_{1,i-};
$$

$$
k = j- \quad \Rightarrow E_{2,j-}E_{3,j} - E_{2,j}E_{3,j-} = E_{1,j+} \quad \Rightarrow c_3 = E_{1,j+};
$$

$$
k = j \quad \Rightarrow E_{2,j}E_{3,j+} - E_{2,j+}E_{3,j} = E_{1,j-} \quad \Rightarrow c_4 = -E_{1,j-};
$$

so (3.14) becomes

$$-E_{1,i+}E_{3,j}y_{2,i-} + E_{1,i-}E_{3,j}y_{2,i+} + E_{1,j+}E_{2,i}y_{3,j-} - E_{1,j-}E_{2,i}y_{3,j+} = \bar{z}.$$
(3.16)

In the case of $i \neq j$, as all components of $\mathbf{E_1}$ are present at least one coefficient in (3.16) is not zero and an unknown is definite.

The case $i = j$ implies that if $E_{1,i-} \neq 0$ or $E_{1,i+} \neq 0$, as before, an unknown is definite. Otherwise, if $E_{1,i-} = E_{1,i+} = 0$ we have that $E_{1,i} \neq 0$. Then, from (3.15) with $k = i+$ we have

$$E_{2,i+}E_{3,i-} - E_{2,i-}E_{3,i+} = E_{1,i} \neq 0,$$
(3.17)

while with $k = i$ and $k = i-$ is

$$E_{2,i}E_{3,i+} - E_{2,i+}E_{3,i} = E_{1,i-} = 0$$
(3.18)

and

$$E_{2,i-}E_{3,i} - E_{2,i}E_{3,i-} = E_{1,i+} = 0,$$
(3.19)

respectively. But, by computing $E_{3,i+}$ and $E_{3,i-}$ from (3.18) and (3.19) respectively, and inserting this in (3.17) we have

$$E_{2,i+}\frac{E_{2,i-}E_{3,i}}{E_{2,i}} - E_{2,i-}\frac{E_{2,i+}E_{3,i}}{E_{2,i}} \neq 0,$$

that is, the false condition

$$E_{3,i}(E_{2,i+}E_{2,i-} - E_{2,i-}E_{2,i+}) \neq 0.$$

3.4 Geometrically nonlinear statical analysis

In this section, after giving the definition of the involved energetic functional, we describe the system of the nonlinear equations. The treatment of the external loads and the adopted solution scheme are also discussed.

The formulation is based on the stationary problem for the functional Π defined in Section 1. We denote with $\mathbf{H_E} = \mathbf{0}$ the constraint conditions in (4.12). These conditions are added to the stationary problem by Lagrange multiplier vector $\mathbf{\Lambda_E}$. In particular, we refer to the extended functional

$$W(\mathbf{u}, \mathbf{E_i}, \mathbf{\Lambda_E}) = \Pi(\mathbf{u}, \mathbf{E_i}) + \mathbf{\Lambda_E} \cdot \mathbf{H_E}(\mathbf{E_i}),$$
(3.20)

where $\mathbf{u}$ is the displacement parameter vector.

The variation of the functional W in (3.20), then, leads to a system of nonlinear equations in the displacement parameters, the components of the cross-section vectors and the Lagrange multipliers. After discretization and

inclusion of the boundary conditions, we group these unknowns in the vector $\mathbf{q}$. Therefore, by denoting with $\mathbf{N}(\mathbf{q})$ the internal force vector, the nonlinear equations are expressed by

$$\mathbf{N}(\mathbf{q}) - \lambda\mathbf{P} = \frac{\partial W(\mathbf{q})}{\partial\mathbf{q}} - \lambda\frac{\partial L(\mathbf{q})}{\partial\mathbf{q}} = 0. \tag{3.21}$$

In (3.21), $L(\mathbf{q})$ is external work while $\mathbf{P}$ and λ are the external force vector and the external force parameter, respectively.

We outlined that external force vector $\mathbf{P}$ can be a linear function of the unknown vector $\mathbf{q}$. In effect, because no rotations are used in the present formulation, moments are modelled as forces following the motion of the $\mathbf{E_i}$ vectors. As an example, an applied pure bending moment M around the x_2 global axis can be modelled with

$$L = P_3 E_{1,3} - P_1 E_{1,1}, \tag{3.22}$$

where P_3 and P_1 will be defined respectively as $ME_{1,1}$ and $ME_{1,3}$ after differentiation in (3.21). The modelling was obtained by considering an ϵ line segment of the element subject to an M/ϵ force couple applied at the end points. Such a force couple is multiplied by related global displacements to give the external work. (3.22) and linked P_1 and P_3 expressions are then found by the limit of external work as ϵ approaches zero and by following the motion of the line segment.

A predictor-corrector scheme as described in [48], [49] for the equilibrium path individualization is used in the analysis. It is characterized by a predictor step obtained by a first order asymptotic extrapolation and by a Newton's method based corrector scheme with minimization of the distance between approximate and equilibrium points as a constraint equation. The length $\mu^{(k)}$ of the extrapolation parameter in the k-th predictor-corrector step is chosen as a function of the iterations $N_{it}^{(k-1)}$ performed in the previous corrector step by $\mu^{(k)} = \mu^{(k-1)}\bar{N}_{it}/N_{it}^{(k-1)}$, where $\bar{N}_{it} = 3$ is taken as a target iteration count. The corrector process computes the increments of the approximation of the force parameter $\Delta\lambda^{(k)}$ and vector of discretization parameters $\Delta\mathbf{q}^{(k)}$. It is stopped when the convergence criterion

$$\frac{\|\Delta\mathbf{q}^{(k)}\|}{\|\mathbf{q}^{(k)}\|} < 10^{-8} \tag{3.23}$$

is satisfied.

3.5   Comparison with other formulations

In this section we compare the suggested formulation and a corotational approach to show the effectivenees of the proposed approach in terms of quality

of results and computing time. The comparison was realised developing a corotational analysis of the three dimensional elastic beams motion. The analysis was based on a Total Lagrangian description of motion for both formulations. According to the corotational approach, the motion of the continuous medium is decomposed into a rigid body motion followed by a pure deformation performed in a local corotational frame that rotates and translates with each element.

We briefly focus now on the kinematics and strain energy of the beam element in the conducted corotational analysis based on the Euler-Bernoulli beam theory, pointing out the different description of finite rotations. While in the proposed approach the description of motion is a function of the nine $\{E_{i,j}\}$ unknown component of the $\mathbf{E_i}$ vectors that substitute rotation parameters, in the corotational approach these $\mathbf{E_i}$ vectors are obtained by rotating the corresponding known vectors $\mathbf{e_i}$ of the initial configuration. In this way the main difficulty is the presence of finite rotations in finite kinematics that noticeably complicates the algebra for obtaining kinematics expressions. In particular finite 3D rotations must be described through rotation matrices which lie in a nonlinear manifold. In fact to define the used rotation tensor $\mathbf{R}$ we refer to the Rodrigues formula which allows $\mathbf{R}$ to be expressed in terms of the quantities lying in a vector space:

$$R[\theta] = I + \frac{sin(\theta)}{\theta} W[\theta] + \frac{1 - cos(\theta)}{\theta^2} W[\theta]^2 \qquad (3.24)$$

which used the rotation vector $\theta = [\theta_1, \theta_2, \theta_3]$. Eq.(3.24) is equivalent to the exponential map:

$$R_\theta = I + W_\theta + \frac{W_\theta^2}{2!} + \ldots = \sum_n^\infty \frac{W_\theta^n}{n!} = exp(W_\theta) \qquad (3.25)$$

Then, the displacements of the element in the frame of reference is represented by

$$u_1 = \bar{u}_1 + \tilde{u}_1 E_{1,1} + \tilde{u}_2 E_{2,1} + \tilde{u}_3 E_{3,1},$$
$$u_2 = \bar{u}_2 + \tilde{u}_1 E_{1,2} + \tilde{u}_2 E_{2,2} + \tilde{u}_3 E_{3,2},$$
$$u_3 = \bar{u}_3 + \tilde{u}_1 E_{1,3} + \tilde{u}_2 E_{2,3} + \tilde{u}_3 E_{3,3}, \qquad (3.26)$$

where $\bar{u}_i$ and $\tilde{u}_i$ refer to rigid and deformative kinematics respectively. In particular, in a reference system centered in the origin of the element, rigid kinematics of the beam element is represented by

$$\bar{u}_1 = u_1^o + x E_{1,1} - x,$$
$$\bar{u}_2 = u_2^o + x E_{1,2},$$
$$\bar{u}_3 = u_3^o + x E_{1,3}, \qquad (3.27)$$

while with regard to deformative kinematics we can assume the same simple interpolation (3.2) and (3.3) of the proposed formulation.

Through simple algebraic manipulations and using the orthonormality of the $\mathbf{E_i}$ vectors it is possible to define the rigid and deformative displacement of the beam element centered in the origin as a function of nodal displacements. In particular by denoting with n and m the left and right element node, respectively, deformative measures e_1, f_{12}, s_{12}, f_{13}, s_{13}, t_1 in (3.2) and (3.3) are evaluated as

$$e_1 = \frac{1}{2h}[(u_m - u_n + h)(E_{1,1}^n + E_{1,1}^m) + (v_m - v_n)(E_{1,2}^n + E_{1,2}^m) + (w_m - w_n)(E_{1,3}^n + E_{1,3}^m)] - 1,$$

$$f_{12} = \frac{1}{4h}(\mathbf{E_2}^n \cdot \mathbf{E_1}^m - \mathbf{E_1}^n \cdot \mathbf{E_2}^m),$$

$$f_{13} = \frac{1}{4h}(\mathbf{E_3}^n \cdot \mathbf{E_1}^m - \mathbf{E_1}^n \cdot \mathbf{E_3}^m),$$

$$s_{12} = -\frac{1}{h^3}[(u_m - u_n + h)(E_{2,1}^n + E_{2,1}^m) + (v_m - v_n)(E_{2,2}^n + E_{2,2}^m) + (w_m - w_n)(E_{2,3}^n + E_{2,3}^m)],$$

$$s_{13} = -\frac{1}{h^3}[(u_m - u_n + h)(E_{3,1}^n + E_{3,1}^m) + (v_m - v_n)(E_{3,2}^n + E_{3,2}^m) + (w_m - w_n)(E_{3,3}^n + E_{3,3}^m)],$$

$$t_1 = \frac{1}{2h}(\mathbf{E_3}^n \cdot \mathbf{E_2}^m - \mathbf{E_2}^n \cdot \mathbf{E_3}^m), \qquad (3.28)$$

Finally with regard to the total strain energy of the beam element we refer to the description given in Section 2. Now we show a classical benchmark to illustrate the results obtained using the described corotational approach and the new proposed approach.

The narrow cantilever beam shown in Fig. 3.5 was analysed. The numerical results obtained in Battini and Pacoste[7] can be taken as reference ($\circ$). The $\lambda - w_c$ vertical load parameter - lateral tip displacement curves have been computed for the proposed approach and for the corotational approach in the case of expansion series, in Rodrigues formula, stopped at the second and third order. Load parameter and lateral displacement are displayed with normalizing values $Po = \sqrt{EJ_2 GJ_1}/L^2$ and L, respectively. Meshes with 8, 12 and 16 elements are used and displayed in Fig. 3.6 - 3.7 - 3.8 respectively. The analyses were stopped when the value $\lambda = 12$ was reached.

It should be emphasized that the computation time between the two approaches is comparable if we stop the exponential map, in the Rodrigues formula, at the second order. In this case, as we can see in the numerical results, the accuracy of corotational approach results is very poor. To obtain more acceptable results it is necessary to extend the expansion series at least up to third order with much more extensive computing time. On the contrary, the new approach converges rapidly and its curves show its close agreement with results in the literature.
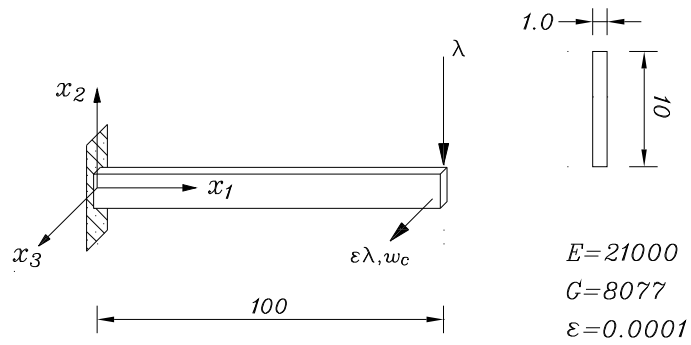
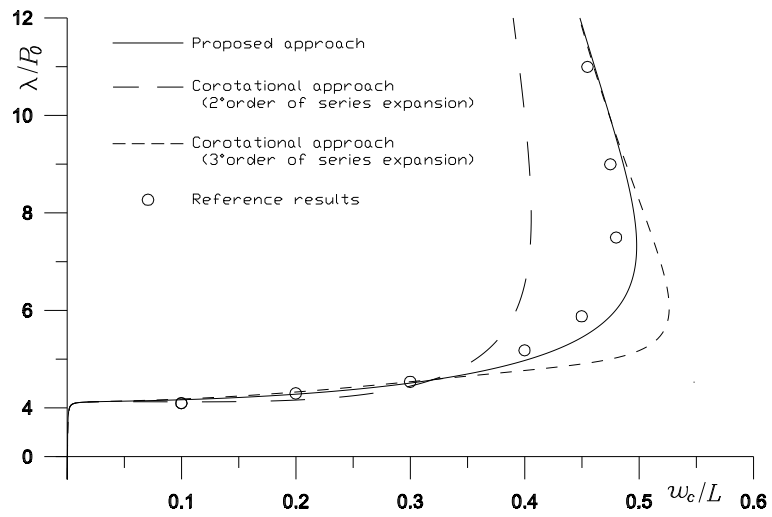**Fig. 3.5:** Example 1: model problem definitions.

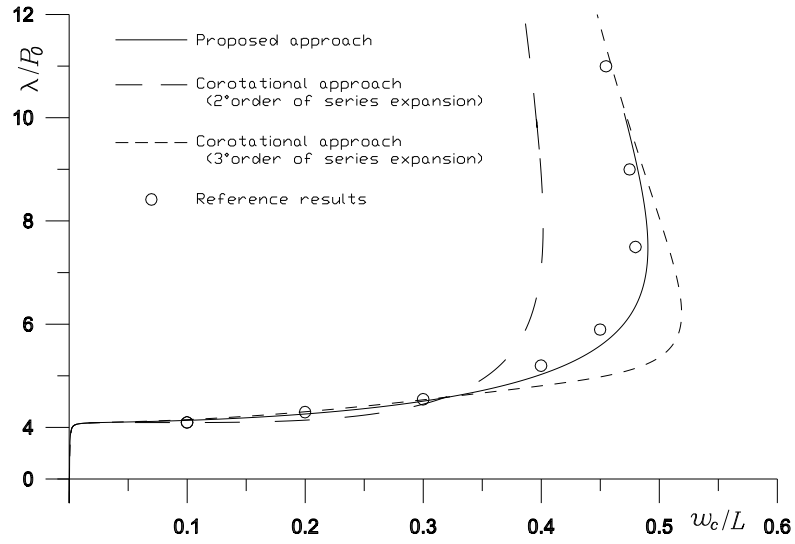**Fig. 3.6:** Statical solution curves: mesh with 8 elements

Fig. 3.7: Statical solution curves: mesh with 12 elements
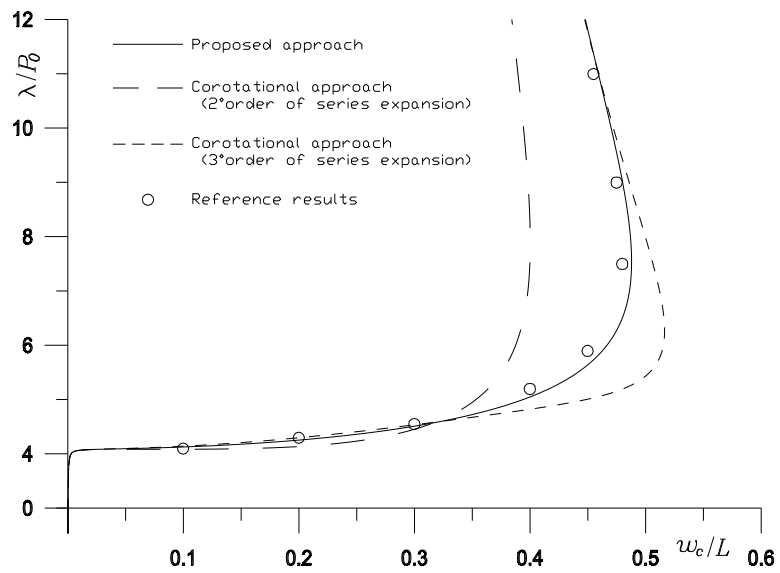

Fig. 3.8: Statical solution curves: mesh with 16 elements

Chapter 4

Dynamical analysis

Non-linear elastodynamics is an important field in structural analysis, and in the last 30 years, there has been extensive research into time-integration algorithms. In particular, stability is a dominant topic because, while unconditionally stable schemes can be recovered in linear dynamics, numerical instability frequently appears in non-linear regimes.

In order to obtain stable solutions schemes which demand the conservation or decrease in the total energy of the Hamiltonian system within each time step are extensively used. Energy-conserving algorithms in elastodynamics have already appeared in the works of Belytschko and Schoeberle [10] and Hughes et al. [33]. The energy-momentum method introduced by Simo and Tarnow [71], [72] preserves energy, as well as linear and angular momentum, in the time interval. Conservation properties are enforced into the equation of motion via Lagrange multipliers. Armero and Petĺocz [1] have introduced a modification of the energy-momentum method which allows us to include numerical dissipation. The application of this unconditionally stable energy decaying algorithm to the non-linear dynamics of three-dimensional beams was presented by Crisfield et al.[21]. Adaptive time-stepping procedures (Kuhl and Ramm [42]) and controllable numerical dissipation (Hoff and Pahl [30], Chung and Hulbert [18]) can also be introduced to permit larger time steps and, consequently, to obtain better computational efficiency. Although finite difference methods appear to prevail in the literature on the numerical treatment of initial value problems, a number of alternative finite-element methods have been developed for the temporal discretization process. Weighted residual statement and the Galerkin finite-element approach for the numerical solution of the equations of motion has been employed by Zienkiewicz et al. [77], and by Lasaint and Raviart [44]. More recently, time finite elements, where the Newmark family formulas can be recovered by the choice of representative constants and the algorithmic energy conservation is implicitly preserved, have been carried out (see Betsch and Steinmann [11]

and related bibliography). In all cases, it seems that an appropriate representation and discretization of the motion equation leads to an appreciable difference in the time-integration schemes with regard to stability. Argyris et al. [4], in particular, noted a significant increase in the range of stability of the classical Newmark method if the natural mode finite-element discretization and lumped mass matrices are used. Of course, all the above mentioned time-stepping algorithms can take additional advantage of these opportune representations.

In this chapter we consider the behaviour of the average acceleration Newmark scheme in the application to motion equations obtained by two different descriptions. In particular we present the extension to the dynamical case of the *lengths based method* and *projectors based method* already described in Chapters 2 and 3 respectively.

4.1 The dynamical problem and the Newmark integration algorithm

The topics arise the study of the evolution of a structure submitted as to forces inherent the deformations as to forces involved the temporal evolution of the same body, like to the strengths of inertia. We schematize the steps to get the solution of the system of the motion equations. We consider the vector of the displacements $\mathbf{u}$ of three spatial-components u, v, w that depend from the original position of the body $\mathbf{x} = (x, y, z)$ and from the time $\mathbf{x} = (x, y, z)$.

The principal involved energetic quantities are:
the potential energy:
$$V(\mathbf{u}) = \frac{1}{2} \int_{\Omega} \boldsymbol{\varepsilon}^T \mathbf{A} \, \boldsymbol{\varepsilon} \, d\Omega, \qquad (4.1)$$

in which $\boldsymbol{\varepsilon} = \boldsymbol{\varepsilon}(\mathbf{u})$ is the deformations vector of the body and $\mathbf{A}$ is the bidimensional domain of body;
the kinetic energy:
$$T(\dot{\mathbf{u}}) = \frac{1}{2} \int_{\Omega} \rho \, \dot{\mathbf{u}}^2 \, d\Omega, \qquad (4.2)$$

that through the mass density ρ is tied to the derivative of the displacements with respect to the time t (the velocities);
the external energy:
$$L(\mathbf{u}) = \int_{\Omega} \mathbf{p}^T \mathbf{u} \, d\Omega, \qquad (4.3)$$

to which the external loads $\mathbf{p}$ and the displacements u appear.
By means an approach to finite element the displacements of the body are located in n displacements in discreet form. With this spatial discretization

and including the boundary conditions, we get to the following semi-discrete formulation of the equations of the motion:

$$\begin{cases} \mathbf{M}\ddot{\mathbf{u}}(t) + \mathbf{N}(\mathbf{u}(t)) - \mathbf{P}(t) = 0 \\ \mathbf{u}(0) = \mathbf{u}_0 \\ \dot{\mathbf{u}}(0) = \dot{\mathbf{u}}_0 \end{cases} \tag{4.4}$$

in which $\ddot{\mathbf{u}}$ denote the accelerations, $\mathbf{u}_0$ and $\dot{\mathbf{u}}_0$ represent the initial displacements and initial velocities respectively. The inertia forces $\mathbf{M}\ddot{\mathbf{u}}(t)$, the internal forces $\mathbf{M}\ddot{\mathbf{u}}(t)$ and the external forces $\mathbf{P}(t)$ are defined as follows:

$$\begin{aligned} \mathbf{M}\ddot{\mathbf{u}}(t) &= \frac{\partial}{\partial t}\left(\frac{\partial T(\dot{\mathbf{u}}(t))}{\partial \dot{\mathbf{u}}}\right), \\[2mm] \mathbf{N}(\mathbf{u}(t)) &= \frac{\partial V(\mathbf{u}(t))}{\partial \mathbf{u}}, \\[2mm] \mathbf{P}(t) &= \frac{\partial L(\mathbf{u}(t))}{\partial \mathbf{u}}. \end{aligned} \tag{4.5}$$

We procede now at the time-integration of the non-linear semi-discrete initial value problem (4.4). In the following, we assume that the time step $\Delta t = t_{n+1} - t_n =$ is constant and that the displacement, velocity and acceleration vectors at the time t_n, denoted by $\mathbf{u}_n, \dot{\mathbf{u}}_n, \ddot{\mathbf{u}}_n$, respectively, are known. The time-integration is restricted to the successive solution of the state variables at the end for each step $\mathbf{u}_{n+1}, \dot{\mathbf{u}}_{n+1}, \ddot{\mathbf{u}}_{n+1}$. In order to realize this step by step integration, the set of variables is reduced to the displacement $\mathbf{u}_{n+1}$ alone by the Newmark approximations:

$$\begin{aligned} \dot{\mathbf{u}}_{n+1} &= \frac{\gamma}{\beta\Delta t}(\mathbf{u}_{n+1} - \mathbf{u}_n) + \left(1 - \frac{\gamma}{\beta}\right)\dot{\mathbf{u}}_n + \left(1 - \frac{\gamma}{2\beta}\right)\Delta t\ddot{\mathbf{u}}_n, \\[2mm] \ddot{\mathbf{u}}_{n+1} &= \frac{1}{\beta\Delta t^2}(\mathbf{u}_{n+1} - \mathbf{u}_n) - \frac{1}{\beta\Delta t}\dot{\mathbf{u}}_n + \left(1 - \frac{1}{2\beta}\right)\ddot{\mathbf{u}}_n. \end{aligned} \tag{4.6}$$

So this method relies on the interpolations (4.6) that relate positions, velocities, and accelerations from step n to $n+1$. γ and β are parameters that define the method.

4.2 Geometrically nonlinear dynamical analysis in lengths based method

In Chapter 2 we presented a lengths-based description of the small strains in the finite displacements regime. As we have seen in this approach, applied to low order elements and based on the total Lagrangian kinematic description,

the use of the rotation matrices is bypassed. In this Chapter we present an extension of the described approach to the dynamic range.

We refer to the semi-discrete formulation of the equations of the motion (4.4), where we suppose we have determined the inertia,internal and external forces as defined in (4.5). In the time-integration scheme of the (4.4), we assume that the time step $\Delta t = t_{n+1} - t_n =$ is constant and that the displacement, velocity and acceleration vectors at the time t_n, denoted by $\mathbf{u}_n, \dot{\mathbf{u}}_n, \ddot{\mathbf{u}}_n$, respectively, are known.

We use the Newmark average acceleration for which $\beta = 1/4$ and $\gamma = 1/2$. This case also corresponds to the assumption that the acceleration is constant over the time interval $[t_n, t_{n+1}]$ and equal to $(\ddot{\mathbf{u}}_n + \ddot{\mathbf{u}}_{n+1})/2$. method:

$$
\begin{aligned}
\dot{\mathbf{u}}_{n+1} &= \ \frac{2}{\Delta t}(\mathbf{u}_{n+1} - \mathbf{u}_n) - \dot{\mathbf{u}}_n, \\
\ddot{\mathbf{u}}_{n+1} &= \ \frac{4}{\Delta t^2}(\mathbf{u}_{n+1} - \mathbf{u}_n) - \frac{4}{\Delta t}\dot{\mathbf{u}}_n - \ddot{\mathbf{u}}_n.
\end{aligned}
\tag{4.7}
$$

where the successive solution points are the unknown state variables at the end of each step $\mathbf{u}_{n+1}, \dot{\mathbf{u}}_{n+1}, \ddot{\mathbf{u}}_{n+1}$.

By replacing relations (4.7) in the initial value problem (4.4), we obtain the nonlinear system of algebraic equations defined at the time t_{n+1} with unknown vector u_{n+1}:

$$
\mathbf{M}\left(\frac{4}{\Delta t^2}(\mathbf{u}_{n+1} - \mathbf{u}_n) - \frac{4}{\Delta t}\dot{\mathbf{u}}_n - \ddot{\mathbf{u}}_n\right) + \mathbf{N}(\mathbf{u}_{n+1}) - \mathbf{P}_{n+1} = 0.
\tag{4.8}
$$

More concisely, the system (4.8) can be placed in the following form:

$$
\mathbf{F}(\mathbf{u}_{n+1}) = 0.
\tag{4.9}
$$

We use the Newton-like iteration scheme for the solution of nonlinear equations (4.9) by linearization:

$$
\mathbf{F}(\mathbf{u}_{n+1}^{(k+1)}) \approx \mathbf{F}(\mathbf{u}_{n+1}^{(k)}) + \frac{\partial \mathbf{F}(\mathbf{u}_{n+1}^{(k)})}{\partial \mathbf{u}_{n+1}}(\mathbf{u}_{n+1}^{(k+1)} - \mathbf{u}_{n+1}^{(k)}).
\tag{4.10}
$$

As predictor points $\mathbf{u}_{n+1}^{(0)}$ we choose the linear extrapolation of the previously computed $\mathbf{u}_n$ and $\mathbf{u}_{n-1}$ vectors when $n > 0$, while the formula $\mathbf{u}_1^{(0)} = \mathbf{u}_0 + \Delta t \dot{\mathbf{u}}_0$ is used when $n = 0$. The iteration is stopped when the convergence criterion

$$
\frac{\|\mathbf{u}_{n+1}^{(k+1)} - \mathbf{u}_{n+1}^{(k)}\|}{\|\mathbf{u}_{n+1}^{(k+1)} - \mathbf{u}_n\|} \leq 10^{-8}.
\tag{4.11}
$$

is satisfied.

4.3 Geometrically nonlinear dynamical analysis in projectors based method

In Chapter 3 a vectorial approach for the rotation parameterizations and linear strain definitions based on slope unknowns has been suggested. The analyzed models do not use angle measures because slopes are used instead of rotation parameters to compute the nonlinear representations of the strain measures in the inertial frame of reference. In particular for each n node we define three unknown vectors $\mathbf{E_i^n} = \{E_{i,j}^n\}$ where the nine $E_{i,j}$ unknown components of the $\mathbf{E_i}$ vectors are subject to six constraint conditions:

$$\mathbf{E_2} \cdot \mathbf{E_2} - 1 = 0,$$
$$\mathbf{E_3} \cdot \mathbf{E_3} - 1 = 0,$$
$$\mathbf{E_2} \cdot \mathbf{E_3} = 0,$$
$$\mathbf{E_2} \times \mathbf{E_3} = \mathbf{E_1}, \tag{4.12}$$

to reduce the rotational degrees of freedom just to three.

So these constraint equations represent the nonlinear definition of the internal strains as a function of the rotational descriptors and they are established by the use of Lagrangian multipliers.

In this section our aim is to extend this approach to the dynamical field. As we refer here to the Timoshenko beam theory (unlike the static case in which we referred to the Benoulli model), again we need to describe the kinematics and to evaluate the energetic quantities of the beam element to finally write the dynamical solution scheme.

4.3.1 Kinematics of the beam element

We refer to the referential coordinate ξ along the element beam centerline $-h_\xi/2 \leq \xi \leq +h_\xi/2$. In the following, we denote with i, j and o the nodes respectively in $\xi = -h_\xi/2$, $\xi = +h_\xi/2$ and $\xi = 0$. Along the beam centerline we define the displacement vector $\mathbf{u}(\xi) = \{u(\xi), v(\xi), w(\xi)\}$ and three mutually orthogonal vectors $\mathbf{E_1}(\xi) = \{E_{1,1}(\xi), E_{1,2}(\xi), E_{1,3}(\xi)\}$, $\mathbf{E_2}(\xi) = \{E_{2,1}(\xi), E_{2,2}(\xi), E_{2,3}(\xi)\}$, $\mathbf{E_3}(\xi) = \{E_{3,1}(\xi), E_{3,2}(\xi), E_{3,3}(\xi)\}$, in the global inertial frame of reference (x, y, z). Director vectors $\mathbf{E_2}$ and $\mathbf{E_3}$ are along the principal axes of inertia of the cross-section. Let $\mathbf{E_1}$, $\mathbf{E_2}$ and $\mathbf{E_3}$ vectors be the columns of the matrix $\mathbf{E}(\xi)$:

$$\mathbf{E}(\xi) = \left[\begin{array}{c|c|c} \mathbf{E_1}(\xi) & \mathbf{E_2}(\xi) & \mathbf{E_3}(\xi) \end{array} \right]. \tag{4.13}$$

The $\mathbf{E}(\xi)$ orthonormal matrix is obtained by using director vectors at the i, j and o nodes and constrained to the (4.12) conditions. In particular, we will use unknown $\mathbf{E}^o = \mathbf{E}(0)$ to represent the large three-dimensional rotations of the local frame of reference of the beam element. As mentioned, the initial unit vector in the ξ, η and ζ element direction, finally, will be denoted by $\mathbf{e_1}$, $\mathbf{e_2}$ and $\mathbf{e_3}$ respectively.

In the beam element, global displacement vector $\mathbf{u}(\xi)$ is composed of rigid and deformation components. In particular, we refer to the $\bar{\mathbf{u}} = (\bar{u}(\xi), \bar{v}(\xi), \bar{w}(\xi))$ rigid displacements defined in the initial frame of reference while the deformation $\tilde{\mathbf{u}}(\xi) = (\tilde{u}(\xi), \tilde{v}(\xi), \tilde{w}(\xi))$ displacements and $\tilde{\boldsymbol{\theta}} = (\tilde{\theta}_1(\xi), \tilde{\theta}_2(\xi), \tilde{\theta}_3(\xi))$ rotations are defined in the local rigidly rotated frame of reference. The deformation kinematics is assumed by the linear interpolations

$$\tilde{u} = \varepsilon^o \xi, \quad \tilde{v} = \varphi_2^o \xi, \quad \tilde{w} = \varphi_3^o \xi, \tag{4.14}$$

for displacements and the quadratic interpolations

$$\tilde{\theta}_2 = \frac{\theta_2^j - \theta_2^i}{h_\xi}\xi + 2\frac{\theta_2^i + \theta_2^j}{h_\xi^2}\xi^2, \quad \tilde{\theta}_3 = \frac{\theta_3^j - \theta_3^i}{h_\xi}\xi + 2\frac{\theta_3^i + \theta_3^j}{h_\xi^2}\xi^2, \tag{4.15}$$

for flexural rotations. The kinematics of the element is then completed by defining the local $\tilde{\theta}_1$ torque rotation about the beam centerline. As in (4.15), we assume

$$\tilde{\theta}_1 = \frac{\theta_1^j - \theta_1^i}{h_\xi}\xi + 2\frac{\theta_1^i + \theta_1^j}{h_\xi^2}\xi^2. \tag{4.16}$$

Note that zero local rotations at the center of the element are assumed. Rigid kinematics, then, will be represented by the nodal displacement components and the degrees of freedom of the vectors $\mathbf{E}_1^o$ attached to the central node.

Based on the above definitions, local rotations and director components are now linked by the field vector operations

$$\begin{aligned} \mathbf{E_1}(\xi) &= \mathbf{E}_1^o + \tilde{\theta}_2(\xi)\mathbf{E}_2^o + \tilde{\theta}_3(\xi)\mathbf{E}_3^o, \\ \mathbf{E_2}(\xi) &= -\tilde{\theta}_2(\xi)\mathbf{E}_1^o + \mathbf{E}_2^o + \tilde{\theta}_1(\xi)\mathbf{E}_3^o, \\ \mathbf{E_3}(\xi) &= -\tilde{\theta}_3(\xi)\mathbf{E}_1^o - \tilde{\theta}_1(\xi)\mathbf{E}_2^o + \mathbf{E}_3^o. \end{aligned} \tag{4.17}$$

As proven, vectors $\mathbf{E}_1^o$, $\mathbf{E}_2^o$ and $\mathbf{E}_3^o$ are unit and mutually orthogonal at the solution points. Then, at the first order, $\mathbf{E_1}(\xi)$, $\mathbf{E_2}(\xi)$ and $\mathbf{E_3}(\xi)$ there are also three unit and mutually orthogonal vectors and they completely define the global orientation of the cross-section. We note that the first order accuracy of the (4.17) representations leads to local evaluations consistent with the small strains hypotheses.

By evaluating (4.17) relations for $\xi = -h_\xi/2$ and $\xi = h_\xi/2$, respectively in the i and j nodes, and by using orthonormality of the directors, we can

write

$$\theta_1^j - \theta_1^i = \tfrac{1}{2}(\mathbf{E}_3^i \cdot \mathbf{E}_2^j - \mathbf{E}_2^i \cdot \mathbf{E}_3^j),$$
$$\theta_2^j - \theta_2^i = \tfrac{1}{2}(\mathbf{E}_2^i \cdot \mathbf{E}_1^j - \mathbf{E}_1^i \cdot \mathbf{E}_2^j), \qquad (4.18)$$
$$\theta_3^j - \theta_3^i = \tfrac{1}{2}(\mathbf{E}_3^i \cdot \mathbf{E}_1^j - \mathbf{E}_1^i \cdot \mathbf{E}_3^j),$$

and

$$\theta_1^j + \theta_1^i = \tfrac{1}{2}[\mathbf{E}_3^o \cdot (\mathbf{E}_2^i + \mathbf{E}_2^j) - \mathbf{E}_2^o \cdot (\mathbf{E}_3^i + \mathbf{E}_3^j)],$$
$$\theta_2^j + \theta_2^i = \tfrac{1}{2}[\mathbf{E}_2^o \cdot (\mathbf{E}_1^i + \mathbf{E}_1^j) - \mathbf{E}_1^o \cdot (\mathbf{E}_2^i + \mathbf{E}_2^j)], \qquad (4.19)$$
$$\theta_3^j + \theta_3^i = \tfrac{1}{2}[\mathbf{E}_3^o \cdot (\mathbf{E}_1^i + \mathbf{E}_1^j) - \mathbf{E}_1^o \cdot (\mathbf{E}_3^i + \mathbf{E}_3^j)].$$

Furthermore, by referring to the centerline points, we now define rigid and deformation components in the initial frame of reference by

$$\bar{u}(\xi) = u^o + \xi E_{1,1}^o - \xi, \quad \bar{v} = v^o + \xi E_{2,1}^o, \quad \bar{w} = w^o + \xi E_{3,1}^o, \qquad (4.20)$$

and

$$\hat{u}(\xi) = \varepsilon^o \xi E_{1,1}^o + \varphi_2^o \xi E_{2,1}^o + \varphi_3^o \xi E_{3,1}^o,$$
$$\hat{v}(\xi) = \varepsilon^o \xi E_{1,2}^o + \varphi_2^o \xi E_{2,2}^o + \varphi_3^o \xi E_{3,2}^o, \qquad (4.21)$$
$$\hat{w}(\xi) = \varepsilon^o \xi E_{1,3}^o + \varphi_2^o \xi E_{2,3}^o + \varphi_3^o \xi E_{3,3}^o,$$

respectively. Then, in the vectorial notation, the motion of the ξ point is described as

$$\mathbf{u} = \mathbf{u}^o + \xi \mathbf{E}_1^o - \xi \mathbf{e}_1 + \varepsilon^o \xi \mathbf{E}_1^o + \varphi_2^o \xi \mathbf{E}_2^o + \varphi_3^o \xi \mathbf{E}_3^o. \qquad (4.22)$$

Also here, by evaluating (4.22) relations for nodal coordinates $\xi = -h_\xi/2$, $\xi = h_\xi/2$, and by using orthonormality of the directors, we deduce that

$$\mathbf{u}^o = \frac{1}{2}(\mathbf{u}^i + \mathbf{u}^j) \qquad (4.23)$$

is the central point displacement and

$$\varepsilon^o = \tfrac{1}{h_\xi}[\mathbf{E}_1^o \cdot (\mathbf{u}_j - \mathbf{u}_i) - h_\xi + h_\xi E_{1,1}^o],$$
$$\varphi_2^o = \tfrac{1}{h_\xi}[\mathbf{E}_2^o \cdot (\mathbf{u}_j - \mathbf{u}_i) + h_\xi E_{2,1}^o], \qquad (4.24)$$
$$\varphi_3^o = \tfrac{1}{h_\xi}[\mathbf{E}_3^o \cdot (\mathbf{u}_j - \mathbf{u}_i) + h_\xi E_{3,1}^o],$$

are the expressions of the axial and shear deformations as a function of nodal displacement and director components.

As can be seen, unknown nodal components completely define the (4.14)-(4.16) linearized deformation kinematics of the beam element by (4.18)-(4.19) and (4.24) expressions. Nonlinear rigid kinematics, instead, is described by the displacement vector in (4.23) and the unknown director vectors $\mathbf{E}^o$ at the central node. The remaining unknown components of the element are the displacements $\mathbf{u}^i$, $\mathbf{u}^j$ and the director vectors $\mathbf{E}^i$, $\mathbf{E}^j$ at the boundary nodes.

4.3.2 Evaluation of energetic quantities of the beam element

We consider the referential coordinates (ξ, η, ζ) in the element, where η and ζ are the thickness coordinates in the $\mathbf{e}_2$ and $\mathbf{e}_3$ directions, respectively. By denoting with $\mathbf{u}_P(\xi, \eta, \zeta) = \{u_P(\xi, \eta, \zeta), v_P(\xi, \eta, \zeta), w_P(\xi, \eta, \zeta)\}$ the displacement of the generic point P in the element represented in the global reference frame, we can refer respectively to the expression

$$\bar{\mathbf{u}}_P = \mathbf{u}^o + \xi(\mathbf{E}_1^o - \mathbf{e}_1) + \eta(\mathbf{E}_2^o - \mathbf{e}_2) + \zeta(\mathbf{E}_3^o - \mathbf{e}_3) \qquad (4.25)$$

for the rigid and to expression

$$\hat{\mathbf{u}}_P = \tilde{u}\mathbf{E}_1^o + \tilde{v}\mathbf{E}_2^o + \tilde{w}\mathbf{E}_3^o - (\tilde{\theta}_3\eta + \tilde{\theta}_2\zeta)\mathbf{E}_1^o + \tilde{\theta}_1(\eta\mathbf{E}_3^o - \zeta\mathbf{E}_2^o) \qquad (4.26)$$

for the deformation components of the motion $\mathbf{u}_P = \bar{\mathbf{u}}_P + \hat{\mathbf{u}}_P$.

The principal energetic quantities involved are the kinetic, potential and external energy:

$$T = \frac{1}{2}\int_V \rho\dot{\mathbf{u}}_P \cdot \dot{\mathbf{u}}_P dV, \quad U = \frac{1}{2}\int_V \boldsymbol{\varepsilon}_P : \boldsymbol{\sigma}_P dV, \quad W = \int_V \mathbf{p} \cdot \mathbf{u}_P dV, \quad (4.27)$$

respectively. In (4.27) the dot denotes derivatives with respect to time t, V the volume of beam, $\mathbf{p}$ the vector of external loads and ρ the mass density. Furthermore, $\boldsymbol{\varepsilon}_P$ and $\boldsymbol{\sigma}_P$ are the infinitesimal strain and stress tensors in the body, respectively.

Kinetic energy is now evaluated by referring to the following expression of the velocity vector:

$$\dot{\mathbf{u}}_P = \dot{\mathbf{u}}^o + \xi\dot{\mathbf{E}}_1^o + \eta\dot{\mathbf{E}}_2^o + \zeta\dot{\mathbf{E}}_3^o + \dot{\tilde{u}}\mathbf{E}_1^o + \dot{\tilde{v}}\mathbf{E}_2^o + \dot{\tilde{w}}\mathbf{E}_3^o - (\dot{\tilde{\theta}}_3\eta + \dot{\tilde{\theta}}_2\zeta)\mathbf{E}_1^o + \dot{\tilde{\theta}}_1(\eta\mathbf{E}_3^o - \zeta\mathbf{E}_2^o),$$
$$(4.28)$$

obtained by time differentiation of $\mathbf{u}_P$ and by truncation of the deformation measures to the zero order. The integration over the section area A of the square of the velocity in (4.28) leads to:

$$\int_A \dot{\mathbf{u}}_P \cdot \dot{\mathbf{u}}_P dA = A\dot{\mathbf{u}}^o \cdot \dot{\mathbf{u}}^o + \xi^2 A\dot{\mathbf{E}}_1^o \cdot \dot{\mathbf{E}}_1^o + J_3\dot{\mathbf{E}}_2^o \cdot \dot{\mathbf{E}}_2^o + J_2\dot{\mathbf{E}}_3^o \cdot \dot{\mathbf{E}}_3^o + 2\xi A\dot{\mathbf{u}}^o \cdot \dot{\mathbf{E}}_1^o$$
$$+ A\dot{\tilde{\mathbf{u}}} \cdot \dot{\tilde{\mathbf{u}}} + J_o\dot{\tilde{\theta}}_1^2 + J_2\dot{\tilde{\theta}}_2^2 + J_3\dot{\tilde{\theta}}_3^2 + 2A(\dot{\tilde{u}}\mathbf{E}_1^o + \dot{\tilde{v}}\mathbf{E}_2^o + \dot{\tilde{w}}\mathbf{E}_3^o) \cdot (\dot{\mathbf{u}}^o + \xi\dot{\mathbf{E}}_1^o)$$
$$+ 2\dot{\tilde{\theta}}_1(J_3\dot{\mathbf{E}}_2^o \cdot \mathbf{E}_3^o - J_2\dot{\mathbf{E}}_3^o \cdot \mathbf{E}_2^o) - 2(J_2\dot{\tilde{\theta}}_2\dot{\mathbf{E}}_3^o + J_3\dot{\tilde{\theta}}_3\dot{\mathbf{E}}_2^o) \cdot \mathbf{E}_1^o,$$
$$(4.29)$$

where J_2 and J_3 are the second moments of area about the related principal axes while J_o is the polar moment. By defining the vector $\boldsymbol{\gamma} = (\varepsilon^o, \varphi_2^o, \varphi_3^o)$, kinetic energy is now computed by further integration over the beam center-

line:

$$\frac{1}{2}\int_{-h_\xi/2}^{h_\xi/2}\int_A \rho\dot{\mathbf{u}}_P\cdot\dot{\mathbf{u}}_P dAd\xi =$$
$$\frac{1}{2}\rho\{h_\xi A\dot{\mathbf{u}}^o\cdot\dot{\mathbf{u}}^o + AJ_1\dot{\mathbf{E}}_1^o\cdot\dot{\mathbf{E}}_1^o + h_\xi J_3\dot{\mathbf{E}}_2^o\cdot\dot{\mathbf{E}}_2^o + h_\xi J_2\dot{\mathbf{E}}_3^o\cdot\dot{\mathbf{E}}_3^o$$
$$+AJ_1\dot{\boldsymbol{\gamma}}\cdot\dot{\boldsymbol{\gamma}} + 2AJ_1\dot{\mathbf{E}}_1^o\cdot\mathbf{E}^o\cdot\dot{\boldsymbol{\gamma}}$$
$$+\frac{h_\xi}{12}(J_oD\dot{\theta}_1^2 + J_2D\dot{\theta}_2^2 + J_3D\dot{\theta}_3^2) + \frac{h_\xi}{20}(J_oS\dot{\theta}_1^2 + J_2S\dot{\theta}_2^2 + J_3S\dot{\theta}_3^2)$$
$$+\frac{h_\xi}{3}[S\dot{\theta}_1(J_3\dot{\mathbf{E}}_2^o\cdot\mathbf{E}_3^o - J_2\dot{\mathbf{E}}_3^o\cdot\mathbf{E}_2^o) - (J_2S\dot{\theta}_2\dot{\mathbf{E}}_3^o + J_3S\dot{\theta}_3\dot{\mathbf{E}}_2^o)\cdot\mathbf{E}_1^o]\},$$
$$\tag{4.30}$$

with the positions $J_1 = h_\xi^3/12$, $\boldsymbol{D\theta} = (\theta_1^j - \theta_1^i, \theta_2^j - \theta_2^i, \theta_3^j - \theta_3^i)$ and $\boldsymbol{S\theta} = (\theta_1^i + \theta_1^j, \theta_2^i + \theta_2^j, \theta_3^i + \theta_3^j)$.

Finally, by introducing the geometrical coefficient matrices $\mathbf{J}_A = \mathrm{diag}(J_o, J_2, J_3)$ and $\mathbf{J}^V = \mathrm{diag}(AJ_1, h_\xi J_2, h_\xi J_3)$ we can write:

$$T = \frac{1}{2}\rho\{V\dot{\mathbf{u}}^o\cdot\dot{\mathbf{u}}^o + \dot{\mathbf{E}}^o\cdot\mathbf{J}_V\cdot\dot{\mathbf{E}}^o$$
$$+AJ_1(\dot{\boldsymbol{\gamma}} + 2\dot{\mathbf{E}}_1^o\cdot\mathbf{E}^o)\cdot\dot{\boldsymbol{\gamma}} + \frac{h_\xi}{12}\boldsymbol{D\theta}\cdot\mathbf{J}_A\cdot\boldsymbol{D\dot\theta} + \frac{h_\xi}{20}\boldsymbol{S\theta}\cdot\mathbf{J}_A\cdot\boldsymbol{S\dot\theta}$$
$$+\frac{h_\xi}{3}[S\dot{\theta}_1(J_3\dot{\mathbf{E}}_2^o\cdot\mathbf{E}_3^o - J_2\dot{\mathbf{E}}_3^o\cdot\mathbf{E}_2^o) - (J_2S\dot{\theta}_2\dot{\mathbf{E}}_3^o + J_3S\dot{\theta}_3\dot{\mathbf{E}}_2^o)\cdot\mathbf{E}_1^o]\}.$$
$$\tag{4.31}$$

In (4.31) the rigid, deformation and mixed kinetic terms can be recognized. In particular note how the term $\dot{\mathbf{E}}^o\cdot\mathbf{J}_V\cdot\dot{\mathbf{E}}^o$ reproduces the rigid inertial components of the angular momentum of the element.

The estimation of the potential energy can be carried out by extracting the contributions due to the deformation from the $\mathbf{u}_P$ motion. Then, the projection of $\hat{\mathbf{u}}_P$ in (4.26) in the $\mathbf{E}_1^o$, $\mathbf{E}_2^o$ and $\mathbf{E}_3^o$ directions gives the infinitesimal displacements:

$$\tilde{u} = \hat{\mathbf{u}}_P\cdot\mathbf{E}_1^o = \varepsilon^o\xi - \tilde{\theta}_3\eta - \tilde{\theta}_2\zeta,$$
$$\tilde{v} = \hat{\mathbf{u}}_P\cdot\mathbf{E}_2^o = \varphi_2^o\xi - \tilde{\theta}_1\zeta, \tag{4.32}$$
$$\tilde{w} = \hat{\mathbf{u}}_P\cdot\mathbf{E}_3^o = \varphi_3^o\xi + \tilde{\theta}_1\eta.$$

By using this deformation kinematics, we define the following infinitesimal strain components of the $\boldsymbol{\varepsilon}_P$ tensor:

$$\varepsilon_{11} = \varepsilon^o - \tilde{\theta}_{3,1}\eta - \tilde{\theta}_{2,1}\zeta, \quad \varepsilon_{12} = \frac{1}{2}(\varphi_2^o - \tilde{\theta}_3 - \omega_3\tilde{\theta}_{1,1}), \quad \varepsilon_{13} = \frac{1}{2}(\varphi_3^o - \tilde{\theta}_2 + \omega_2\tilde{\theta}_{1,1}),$$
$$\tag{4.33}$$

and $\varepsilon_{23} = 0$. In (4.33) shearing contributions due to the torsional mode are modelled by the $\omega_2(\eta,\zeta)$ and $\omega_3(\eta,\zeta)$ functions. Here, because $h_\eta \times h_\zeta$ rectangular sections were analyzed, we assume the distributions:

$$\omega_2 = \frac{\eta^3}{(h_\eta/2)^2}(1 - \frac{\zeta^2}{(h_\zeta/2)^2}), \quad \omega_3 = \frac{\zeta^3}{(h_\zeta/2)^2}(1 - \frac{\eta^2}{(h_\eta/2)^2}), \tag{4.34}$$

where $\varepsilon_{12} = 0$ and $\varepsilon_{13} = 0$ is realized on the boundaries $|\zeta| = h_\zeta/2$ and $|\eta| = h_\eta/2$ of the cross section, respectively.

Extensional components ε_{22} and ε_{33} are then obtained by imposing the statical assumptions $\sigma_{22} = \sigma_{33} = 0$ on the $\boldsymbol{\sigma}_P$ stress tensor. Then we have

$$\varepsilon_{22} = \varepsilon_{33} = -\frac{\lambda}{2(\lambda + \mu)}\varepsilon_{11}, \tag{4.35}$$

where λ and μ are the Lamé coefficients. By using the (4.35) expressions, the remaining stress components are:

$$\begin{aligned}
\sigma_{11} &= 2\mu\varepsilon_{11} + \lambda(\varepsilon_{11} + \varepsilon_{22} + \varepsilon_{33}) = \tfrac{2\mu+3\lambda}{\lambda+\mu}\mu\varepsilon_{11} = E\varepsilon_{11}, \\
\sigma_{12} &= 2\mu\varepsilon_{12} = 2G\varepsilon_{12}, \\
\sigma_{13} &= 2\mu\varepsilon_{13} = 2G\varepsilon_{13}
\end{aligned} \tag{4.36}$$

and $\sigma_{23} = 0$. In (4.36), E and G are the Young and shear moduli, respectively.

By integrating over the section area the potential energy contribution we have:

$$\begin{aligned}
\int_A \boldsymbol{\varepsilon}_P : \boldsymbol{\sigma}_P dA &= \int_A (E\varepsilon_{11}^2 + 4G\varepsilon_{12}^2 + 4G\varepsilon_{13}^2)dA = \\
&\quad E(A\varepsilon_2^o + J_2\tilde{\theta}_{2,1}^2 + J_3\tilde{\theta}_{3,1}^2) \\
&\quad + G[A(\varphi_2^o - \tilde{\theta}_3^o)^2 + \tilde{\theta}_{1,1}^2 \int_A \omega_3^2 dA - 2(\varphi_2^o - \tilde{\theta}_3^o)\tilde{\theta}_{1,1} \int_A \omega_3 dA] \\
&\quad + G[A(\varphi_3^o - \tilde{\theta}_2^o)^2 + \tilde{\theta}_{1,1}^2 \int_A \omega_2^2 dA + 2(\varphi_3^o - \tilde{\theta}_2^o)\tilde{\theta}_{1,1} \int_A \omega_2 dA].
\end{aligned} \tag{4.37}$$

Note that in (4.37), to overcome locking effects, the central value of the $\tilde{\theta}_2(\xi)$ and $\tilde{\theta}_3(\xi)$ interpolations are used in the shear energy computation. Besides, assuming this, $\int_A \omega_2 dA = \int_A \omega_3 dA = 0$ is obtained. Then, by defining $J_{\omega 2} = \int_A \omega_2^2 dA$ and $J_{\omega 3} = \int_A \omega_3^2 dA$, we can write:

$$\int_A \boldsymbol{\varepsilon}_P : \boldsymbol{\sigma}_P dA = E(A\varepsilon^{o2} + J_2\tilde{\theta}_{2,1}^2 + J_3\tilde{\theta}_{3,1}^2) + G[A(\varphi_2^{o2} + \varphi_3^{o2}) + (J_{\omega 2} + J_{\omega 3})\tilde{\theta}_{1,1}^2], \tag{4.38}$$

with $\tilde{\theta}_2^o = \tilde{\theta}_3^o = 0$. Then, the potential energy is computed by further integration over the beam centerline:

$$\begin{aligned}
U &= \tfrac{1}{2} \int_{-h_\xi/2}^{h_\xi/2} \int_A \boldsymbol{\varepsilon}_P : \boldsymbol{\sigma}_P dA d\xi = \\
&\quad \tfrac{1}{2}E[V\varepsilon^{o2} + \tfrac{1}{h_\xi}J_2(D\tilde{\theta}_2^2 + \tfrac{4}{3}S\tilde{\theta}_2^2) + \tfrac{1}{h_\xi}J_3(D\tilde{\theta}_3^2 + \tfrac{4}{3}S\tilde{\theta}_3^2)] \\
&\quad \tfrac{1}{2}G[+V(\varphi_2^{o2} + \varphi_3^{o2}) + \tfrac{1}{h_\xi}(J_{\omega 2} + J_{\omega 3})(D\tilde{\theta}_1^2 + \tfrac{4}{3}S\tilde{\theta}_1^2)].
\end{aligned} \tag{4.39}$$

External work W, finally, is defined in (4.27) by the (4.25) and (4.26) expressions of the displacement vector. Note that, kinematics of the element being modelled as a three dimensional body, only external forces must be assigned. Besides, because finite rotations are replaced by products $\tilde{\theta}\mathbf{E}^o$ in the present formulation, we can see from (4.26) that the external force vector is a linear function of the assumed unknowns.

4.3.3 Multibody systems

By referring to the previous beam element model, we can study the dynamical behaviour of multibody systems. In particular, prismatic bodies linked by spherical joints and free mass particles are analyzed.

A prismatic $h_\xi \times h_\eta \times h_\zeta$ element is assumed such that only the ξ axial deformation ε is present. Springs in the joint point between elements produce, furthermore, restraint moments proportional to the relative rotations. In particular, we refer now to the $\mathbf{E}^n$ and $\mathbf{E}^m$ directors attached to the central points of the n and m elements and we denote with $D\theta_1$, $D\theta_2$ and $D\theta_3$ the small relative rotations. We have:

$$\begin{aligned}
\mathbf{E}_1^m &= \mathbf{E}_1^n + D\theta_2\mathbf{E}_2^n + D\theta_3\mathbf{E}_3^n, \\
\mathbf{E}_2^m &= -D\theta_2\mathbf{E}_1^n + \mathbf{E}_2^n + D\theta_1\mathbf{E}_3^n, \\
\mathbf{E}_3^m &= -D\theta_3\mathbf{E}_1^n - D\theta_1\mathbf{E}_2^n + \mathbf{E}_3^n.
\end{aligned} \tag{4.40}$$

Then, by the usual manipulations, we obtain

$$\begin{aligned}
D\theta_1 &= \tfrac{1}{2}(\mathbf{E}_3^n \cdot \mathbf{E}_2^m - \mathbf{E}_2^n \cdot \mathbf{E}_3^m), \\
D\theta_2 &= \tfrac{1}{2}(\mathbf{E}_2^n \cdot \mathbf{E}_1^m - \mathbf{E}_1^n \cdot \mathbf{E}_2^m), \\
D\theta_3 &= \tfrac{1}{2}(\mathbf{E}_3^n \cdot \mathbf{E}_1^m - \mathbf{E}_1^n \cdot \mathbf{E}_3^m).
\end{aligned} \tag{4.41}$$

With the expression of the rigid component (4.25) and by zeroing the absent deformation measures in (4.26), the motion of the body is defined as

$$\mathbf{u}_P = \mathbf{u} + \xi(\mathbf{E}_1 - \mathbf{e}_1) + \eta(\mathbf{E}_2 - \mathbf{e}_2) + \zeta(\mathbf{E}_3 - \mathbf{e}_3) + \xi\varepsilon\mathbf{E}_1, \tag{4.42}$$

where $\mathbf{u}$ is the central point displacement vector computed by the nodal values as in (4.23).

As before, the integration over the section area of the square of the velocity leads to

$$\begin{aligned}
\int_A \dot{\mathbf{u}}_P \cdot \dot{\mathbf{u}}_P dA ={}& A\dot{\mathbf{u}} \cdot \dot{\mathbf{u}} + \xi^2 A\dot{\mathbf{E}}_1 \cdot \dot{\mathbf{E}}_1 + J_3\dot{\mathbf{E}}_2 \cdot \dot{\mathbf{E}}_2 + J_\eta\dot{\mathbf{E}}_3 \cdot \dot{\mathbf{E}}_3 + 2\xi A\dot{\mathbf{u}} \cdot \dot{\mathbf{E}}_1 \\
&+ \xi^2 A\dot{\varepsilon}^2 + 2\xi A\dot{\varepsilon}\mathbf{E}_1 \cdot (\dot{\mathbf{u}} + \xi\dot{\mathbf{E}}_1)
\end{aligned} \tag{4.43}$$

and, then, to the kinetic energy evaluation by further integration on the ξ elemental domain

$$T = \tfrac{1}{2}\rho[V\dot{\mathbf{u}} \cdot \dot{\mathbf{u}} + \dot{\mathbf{E}} \cdot \mathbf{J}_V \cdot \dot{\mathbf{E}} + AJ_1(\dot{\varepsilon}^2 + 2\dot{\varepsilon}\mathbf{E}_1 \cdot \dot{\mathbf{E}}_1)]. \tag{4.44}$$

In the potential energy definition we refer to the EV axial rigidity and to the like type k_2, k_3 flexural and k_1 torque stiffness:

$$U = \frac{1}{2}(EV\varepsilon^2 + k_1 D\theta_1^2 + k_2 D\theta_2^2 + k_3 D\theta_3^2), \tag{4.45}$$

where the relative rotations are defined in (4.41) while axial deformation is defined in the first of (4.24) expressions:

$$\varepsilon = \frac{1}{h_\xi}[\mathbf{E}_1 \cdot (\mathbf{u}^j - \mathbf{u}^i) - h_\xi + h_\xi E_1]. \qquad (4.46)$$

Finally, external energy W can be computed by the expression (4.42) of the displacement vector of the body.

In the three-dimensional mass particles motion we refer to the ith particle of m_i mass. Potential energy of interaction of the particles i and j depends on the interbody distance $h_{ij} = (1+\varepsilon_{ij})h$, where h is the initial distance and ε_{ij} is the related elongation. Then, by denoting with $\mathbf{u}_i$ the displacement vector of the particle and with k_a the interaction rigidity, kinetic and potential energy are computed by referring to

$$T = \frac{1}{2}m_i\dot{\mathbf{u}}^i \cdot \dot{\mathbf{u}}^i, \quad U = \frac{1}{2}k_a\varepsilon_{ij}^2. \qquad (4.47)$$

4.3.4   Nonlinear dynamical analysis

We refer to dynamical systems with $L(\dot{\mathbf{q}}(t), \mathbf{q}(t))$ Lagrangian function obtained by summing the described energetic contributions, where $\mathbf{q}$ is the vector of the unknown components of the element. We denote with $\mathbf{g}_E = \mathbf{0}$ the constraint conditions in (4.12) relating the unknown components of the $\mathbf{E}_1$, $\mathbf{E}_2$ and $\mathbf{E}_3$ vectors. Related Lagrange multiplier vectors are denoted with $\boldsymbol{\lambda}_E$.

Then we obtain the extended functional

$$L^S(\mathbf{q}, \dot{\mathbf{q}}, \boldsymbol{\lambda}) = T(\dot{\mathbf{q}}, \mathbf{q}) - U(\mathbf{q}) + W(\mathbf{q}) + \boldsymbol{\lambda}_E \cdot \mathbf{g}_E(\mathbf{q}). \qquad (4.48)$$

In particular, for the beam element model we refer to the contributions given in (4.31) and (4.39)Unknown vector $\mathbf{q}$ is composed of the three u^i, v^i, w^i, displacements and the nine components of the directors $\mathbf{E}_1^i, \mathbf{E}_2^i, \mathbf{E}_3^i$, at the nodes plus the nine components of the directors $\mathbf{E}_1^o, \mathbf{E}_2^o, \mathbf{E}_3^o$, for each element. Six $\boldsymbol{\lambda}_E$ values for each $\mathbf{E}^i$ and $\mathbf{E}^o$ orthonormal system complete the group of the unknowns. For the prismatic element model we use the expressions (4.44). The unknown vector is composed of the three u^i, v^i, w^i, nodal displacements and the nine components of the directors $\mathbf{E}_1, \mathbf{E}_2, \mathbf{E}_3$, at the center of the element. As multipliers, then, we have six $\boldsymbol{\lambda}_E$ unknown components. Mass particles motion, finally, is described by the three u^i, v^j, w^i, displacements of the ith mass and the three E^{ij} components for each i-j connection. The semidiscrete formulation of the motion can be written in the form:

$$\frac{\partial L}{\partial \mathbf{q}} - \frac{\partial}{\partial t}\frac{\partial L}{\partial \dot{\mathbf{q}}} = 0, \quad \frac{\partial L}{\partial \boldsymbol{\lambda}} = 0, \quad \mathbf{q}(\mathbf{0}) = \mathbf{q}^*, \quad \dot{\mathbf{q}}(\mathbf{0}) = \dot{\mathbf{q}}^*, \qquad (4.49)$$

63

where $\mathbf{q}^*$ and $\dot{\mathbf{q}}^*$ represent the initial values and velocities, respectively.

For the time integration of the semidiscrete initial value problem (4.49) we refer to the constant time step $\Delta t = t_{n+1} - t_n$. Unknown components of the $\mathbf{q}$ and $\boldsymbol{\lambda}$ vectors also collected in the $\mathbf{d}$ vector. By assuming the state variables $\mathbf{d}_n$, $\dot{\mathbf{d}}_n$, $\ddot{\mathbf{d}}_n$, as known at the time t_n and making the external forces $\mathbf{p}(t)$ for all t, the time integration is restricted to the subsequent solution of the state variables at the end of each step $\mathbf{d}_{n+1}$, $\dot{\mathbf{d}}_{n+1}$, $\ddot{\mathbf{d}}_{n+1}$. In order to realize this step by step integration, the set of variables is reduced to the unknowns $\mathbf{d}_{n+1}$ only by the Newmark approximations

$$\dot{\mathbf{d}}_{n+1} = \frac{\gamma}{\beta \Delta t}(\mathbf{d}_{n+1} - \mathbf{d}_n) + (1 - \frac{\gamma}{\beta})\dot{\mathbf{d}}_n + (1 - \frac{\gamma}{2\beta})\Delta t \ddot{\mathbf{d}}_n, \qquad (4.50)$$

$$\ddot{\mathbf{d}}_{n+1} = \frac{1}{\beta \Delta t^2}(\mathbf{d}_{n+1} - \mathbf{d}_n) - \frac{1}{\beta \Delta t}\dot{\mathbf{d}}_n + (1 - \frac{1}{2\beta})\ddot{\mathbf{d}}_n. \qquad (4.51)$$

In the following we use the average acceleration scheme by adopting $\gamma = 1/2$ and $\beta = 1/4$.

By inserting relations (4.50) and (4.51) in equations (4.49), we arrive at the nonlinear equation of the form:

$$\mathbf{F}(\mathbf{d}_{n+1}) = 0. \qquad (4.52)$$

This represents the nonlinear system of algebraic equations defined at the t_{n+1} time with the $\mathbf{d}_{n+1}$ unknown vector. The velocities and accelerations at the end of the time step can then be obtained by relations (4.50) and (4.51), respectively. Newton like iterative methods can be used to solve system (4.52) by linearization

$$\mathbf{F}(\mathbf{d}_{n+1}^{(k+1)}) = \mathbf{F}(\mathbf{d}_{n+1}^{(k)}) + \frac{\partial \mathbf{F}(\mathbf{d}_{n+1}^{(k)})}{\partial \mathbf{d}_{n+1}}(\mathbf{d}_{n+1}^{(k+1)} - \mathbf{d}_{n+1}^{(k)}) + \mathbf{O}(\Delta t^2) = \mathbf{0}. \quad (4.53)$$

The iterative process is here initialized by choosing $\mathbf{d}_{n+1}^{(0)}$ as the linear extrapolation of the previously computed $\mathbf{d}_n$ and $\mathbf{d}_{n-1}$ vectors when $n > 0$, while the formula $\mathbf{d}_1^{(0)} = \mathbf{d}^* + \Delta t \dot{\mathbf{d}}^*$ is used when $n = 0$. By choosing the fixed tolerance $\eta = 10^{-8}$, the formula

$$\| \mathbf{d}_{n+1}^{(k+1)} - \mathbf{d}_{n+1}^{(k)} \| / \| \mathbf{d}_{n+1}^{(k+1)} - \mathbf{d}_n \| \leq \eta \qquad (4.54)$$

is adopted as convergence criterion.

Chapter 5

Numerical results in lengths based method

As we learn in Chapter 2 the lengths based method is an alternative approach to formulate models for two or three-dimensional elastic structures in the case of small strains in the large displacements regime. It's based on definitions of only relative lengths in order to avoid the use of rotation measures and to overcome all the difficulties connected with the management of the rotation matrices in 3D space. In this chapter a set of examples is examined to illustrate the features of this approach. In particular, the tests analyze plane and spatial kinematics by modelling the body with the described two and three-dimensional low-order elements. Tests have been carried out both in the statical and in the dynamical context.

5.1 Statical, quasi statical and dynamical analysis

In this section we include a set of tests which have been carried out both in the statical and quasi-statical or dynamical context. We refer to quasi statical rather than dynamical analysis when the dynamics affects only the zone of mode jumping of the structure. In fact, the inertial forces of the structure are active only in the transient response of the structure from an unstable bifurcation point, on a postbuckled equilibrium path, to a second stable equilibrium state, on a new equilibrium path. In particular, the tests analyze plane and spatial kinematics by modelling the body with the described two and three-dimensional elements.

5.1.1 Clamped right angle frame

A right angled frame shown in Figure 5.1, fully restrained at one end, is analyzed both in statical and dynamical cases. Equilibrium states were computed by the three-dimensional finite element formulation. It is worth noting that the motion of the system involves large torsion and bending.
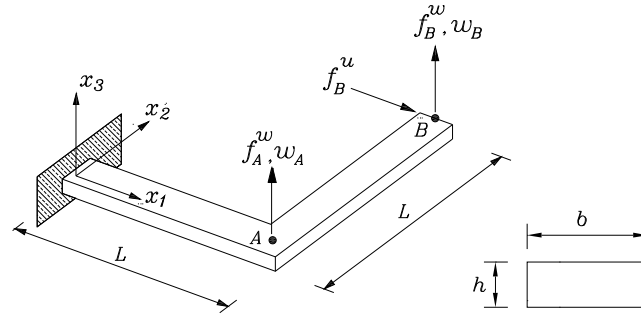
Fig. 5.1: Clamped right angle frame: geometry and loading definitions.

Statical analysis

In the statical case, the analysed frame is loaded at the free end B by $f_B^u = \lambda$ in the x_1 direction. An imperfection load $f_B^w = 10^{-4}\lambda$ in the x_3 direction is set to initiate lateral buckling along the fundamental equilibrium path. The geometrical and mechanical properties are defined by: length $L = 255$, width $b = 30$, thickness $t = 0.6$, Poisson coefficient $\nu = 0.31$ and Young's modulus $E = 7.124 \times 10^4$. The entire frame was modelled by 68 elements to test the convergence to the reference analysis.
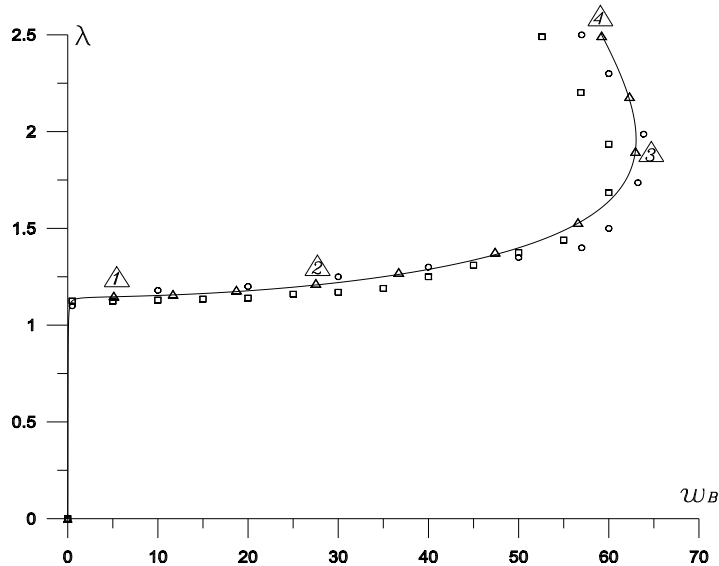
Fig. 5.2: Clamped right angle frame: statical solution curves.

66
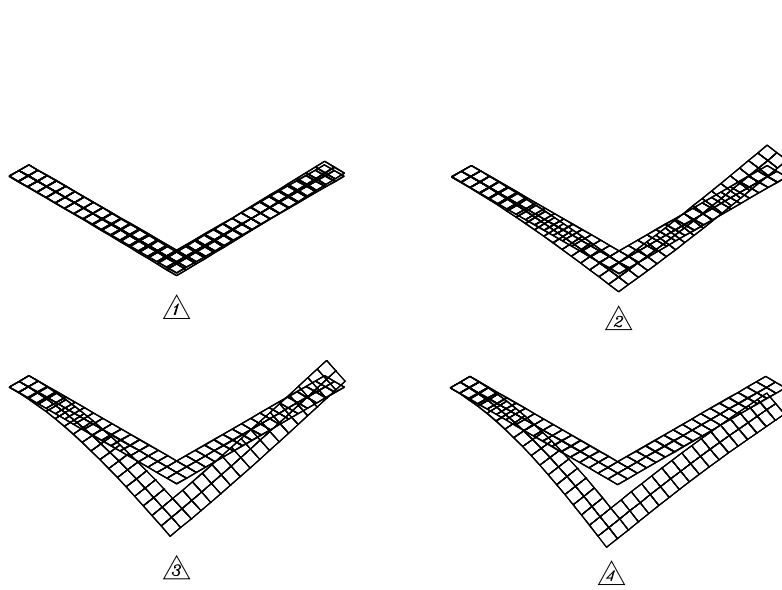
Fig. 5.3: Right angle frame: statical deformative configurations at marked solution points.

The $\lambda - w_B$ load parameter - out of plane free end displacement curve ($\triangle$) was computed and displayed in Figure 5.2 where a good agreement is observed in respect to the predictions of Izzuddin[36] ($\square$) and Yang et al.[75] ($\circ$). Figure 5.3 shows deformed shapes of the presented structure at the marked equilibrium points.

Dynamical analysis

In the dynamical case the studied frame is loaded by an out of plane force $f_A^w = \lambda$ at the elbow point A. The geometry and material properties are: $L = 10$, $b = h = 1$, $\nu = 0.2$, $E = 5.0 \times 10^4$ and mass density $\rho = 0.1$. The frame is modelled using overall 160 elements.

Figure 5.4 shows the time history of the x_3 direction displacements in the tip B and elbow A points. Indications about the shape and duration of the applied load are also indicated. A good agreement was found between the calculated results with those of Mata et al.[55] ($\circ$). Deformed configurations of the structures at the marked equilibrium points are depicted in Figure 5.5.

5.1.2   Deep circular arch under vertical load

Equilibrium states for the deep circular arch shown in Figure 5.6 were computed by the two-dimensional finite element formulation. Several authors, Simo and Vu-Quoc[73], Kouhia and Mikkola[40], Cardona and Huespe[17],
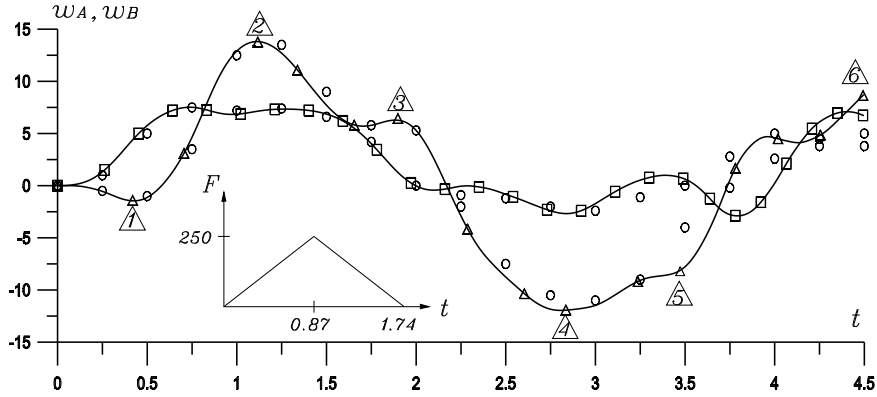
Fig. 5.4: Clamped right angle frame: dynamical solution curves.

have analyzed the equilibrium paths for such a structure by using a one-dimensional finite element in the geometrically nonlinear regime.

A 32 equally-spaced element mesh for the whole arch is employed. Here we refer to the Young modulus $E = 6 \times 10^6$ and to the Poisson ratio $\nu = 0$ while the normal area is squared with the edge equal to $\sqrt{2}$. Modejumping analysis is carried out by assuming $\rho = 0.0025$ mass density and $\lambda = 25t$ load history.

Note that, to compare the results, simply support boundary condition requires a suitable treatment because quadrilateral two-dimensional elements are used. In particular, here Lagrangian multipliers are adopted to impose zero values for the displacements at the central point of the elemental edge and for the related nodal internal forces.

The $\lambda - w_c$ vertical load parameter - deflection of the apex curve was computed for both the statical and quasi-statical analysis. The analyzes are stopped when the value $\lambda = 1000$ is traversed. For the statical case, the primary path traced in Figure 5.7 is in agreement with the results reported in the cited literature. Deformed configurations of the structure at the marked equilibrium points are depicted in Figure 5.8. For the dynamical case, again in Figure 5.7 the modejump at the first limit point can be observed while in Figure 5.9 the deformed configurations at the marked instants are reported.

5.1.3 Cylindrical shell

A cylindrical shell of constant thickness and deformed by an applied compressive load is analyzed. We consider vanishing radial and tangential dis-
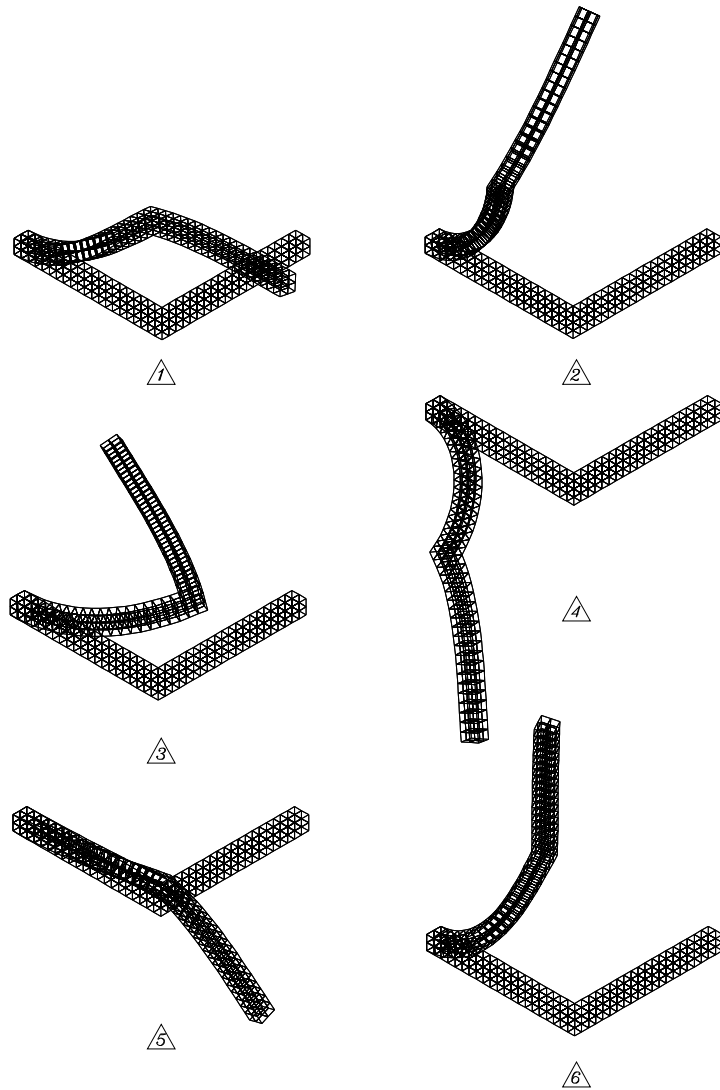
Fig. 5.5: Clamped right angle frame: dynamical deformative configurations at marked solution points.

placements on both ends and $E = 3103$, $\nu = 0.3$, as material parameters. Geometric parameters and problem definitions are given in Figure 5.10. An 8×8 mesh for the symmetric quarter of the shell was considered. Here, $v = 0$ for the nodes along the symmetric circumferential edge and $u = 0$ for the nodes along the symmetric longitudinal edge. As before, suitable treatment of the central points of the elemental edge at the boundaries is carried out.
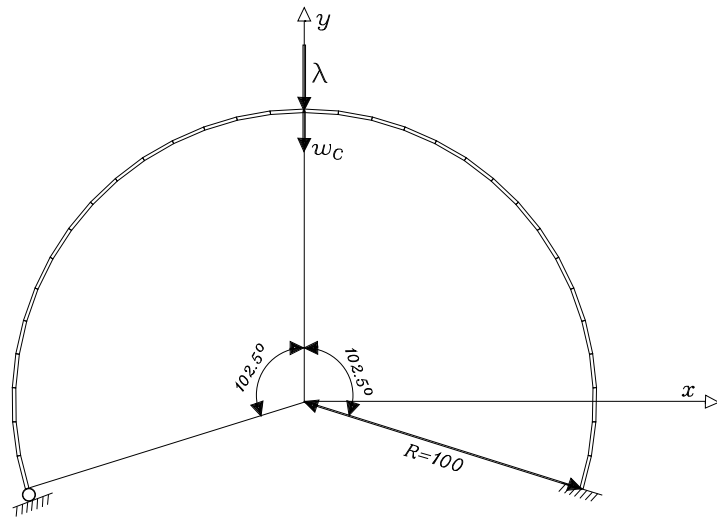
Fig. 5.6: Deep arch: geometry and loading definitions.
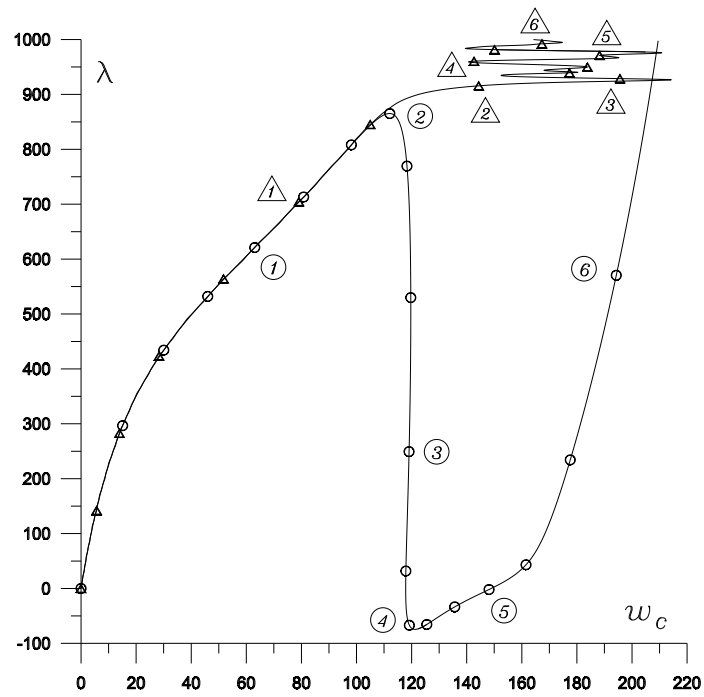
Fig. 5.7: Deep arch: statical (○) and modejumping (△) solution curves.
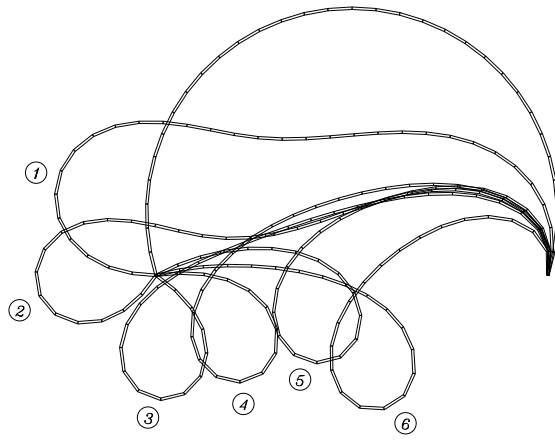
Fig. 5.8: Deep arch: statical deformative configurations at marked solution points.
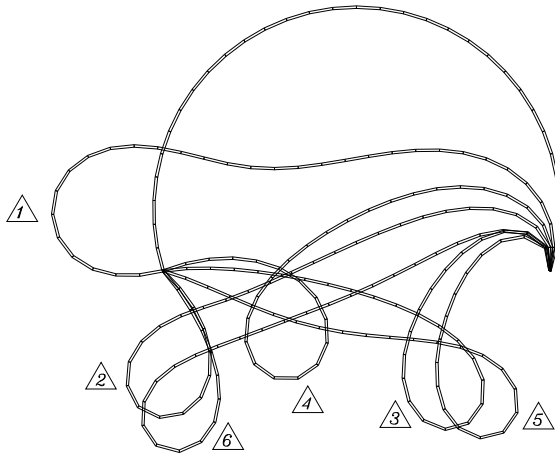
Fig. 5.9: Deep arch: dynamical deformative configurations at marked solution points.

Two cases, which differ for the values of radius R, thickness h and mass density ρ, were analyzed. The computed equilibrium curves are displayed by external load parameter λ and vertical deflection at the central point of the shell w_c. $\lambda = 0.1t$ is the load history employed in the quasi-static version.
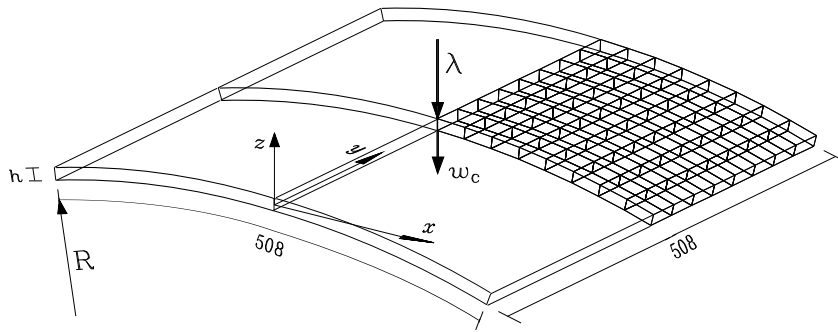
Fig. 5.10: Cylindrical shell: geometry and loading definitions.
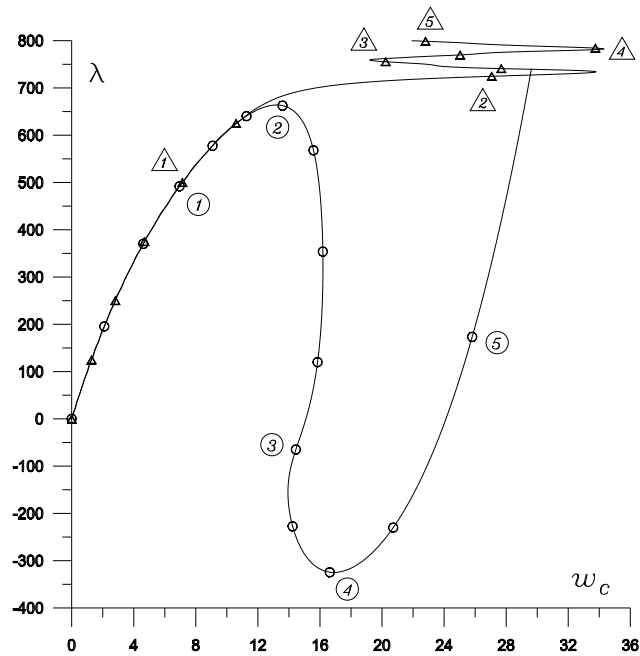
Fig. 5.11: Cylindrical shell, case I: statical ($\circ$) and modejumping ($\triangle$) solution curves.

Case I.

In the case, studied in Eriksson[24],[25] by two-dimensional thin shell elements, we make $R = 2540$ and $h = 6.35$, while we assume $\rho = 1$ for the dynamical analysis. Figure 5.11 shows the load parameter - central point deflection behavior for both the statical and quasi-statical solutions when

72
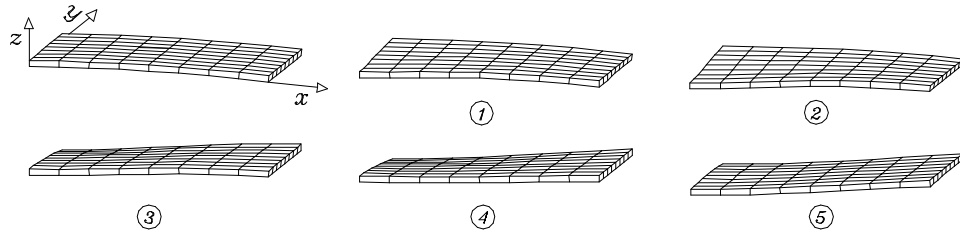
Fig. 5.12: Cylindrical shell, case I: statical deformative configurations at marked solution points.
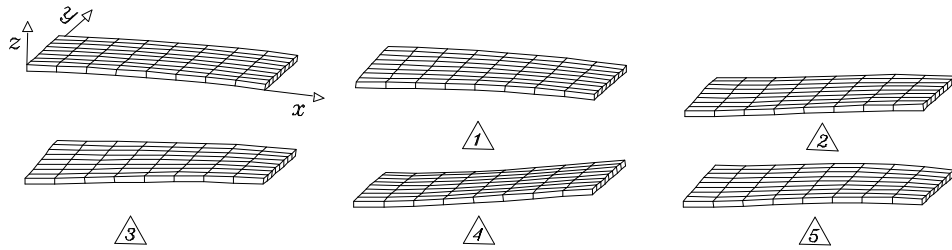
Fig. 5.13: Cylindrical shell, case I: dynamical deformative configurations at marked solution points.

the algorithm is stopped for the achieved $\lambda = 800$ value.

For the statical analysis, deformations in the pre and post-critical phase are displayed in Figure 5.12. Post modejumping deformations are also shown in Figure 5.13 for the related dynamical model.

Case II.

By assuming $R = 1000$ and $h = 12$, in this second case a greater curvature and thickness of the shell is considered. The mass density now takes the value $\rho = 1000$. The structure, therefore, proves to be stiffer and larger values of the displacements are attained. The analysis are stopped here when the algorithm traverses $\lambda = 18000$.

In Figures 5.14 and 5.15, for the statical problem, note that shearing stresses are activated in the post flexural-membranal behavior. Figures 5.14 and 5.16, in the modejumping context, illustrate a higher frequencies dominance in the post-buckling zone.
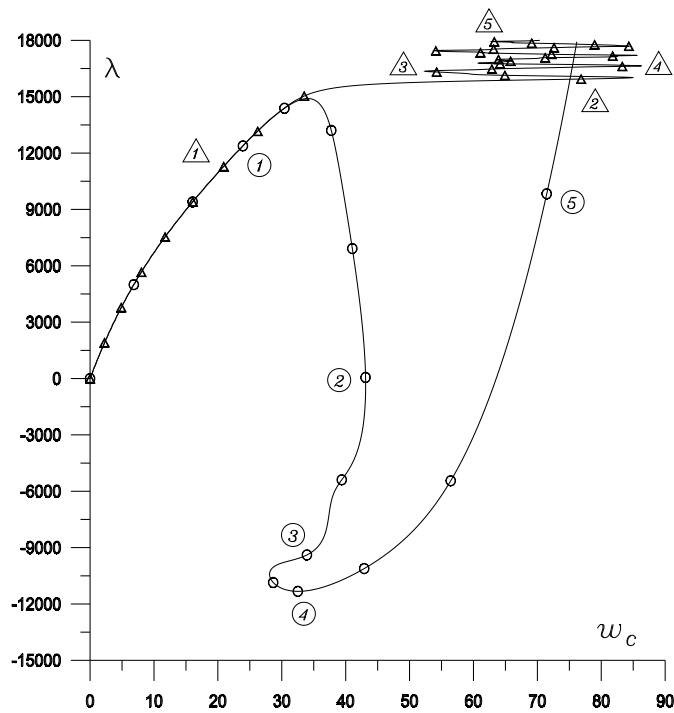
Fig. 5.14: Cylindrical shell, case II: statical (○) and modejumping (△) solution curves.
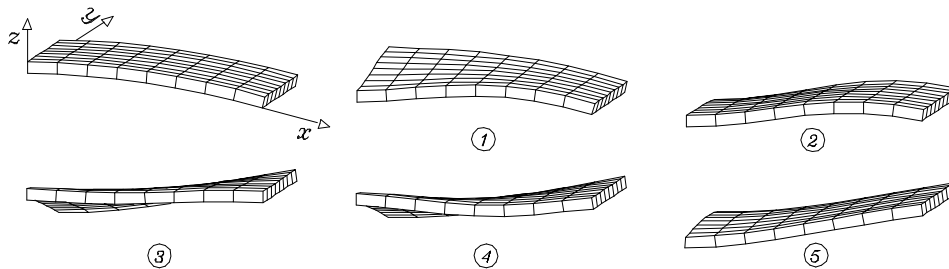
Fig. 5.15: Cylindrical shell, case II: statical deformative configurations at marked solution points.

5.1.4 Spherical cup

A spherical cup of constant thickness with a top hole, studied in Brank et al.[15], is analyzed and displayed in Figure 5.17. Force per unit area $p = 50\lambda$ is applied along the top ring in the vertical direction.

Using symmetry, only one quarter of the structure is considered and

74
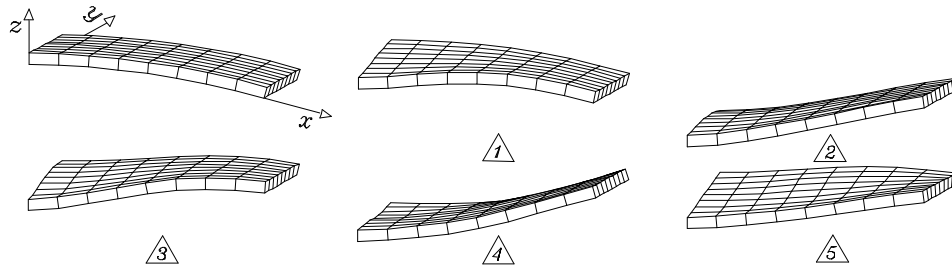
Fig. 5.16: Cylindrical shell, case II: dynamical deformative configurations at marked solution points.
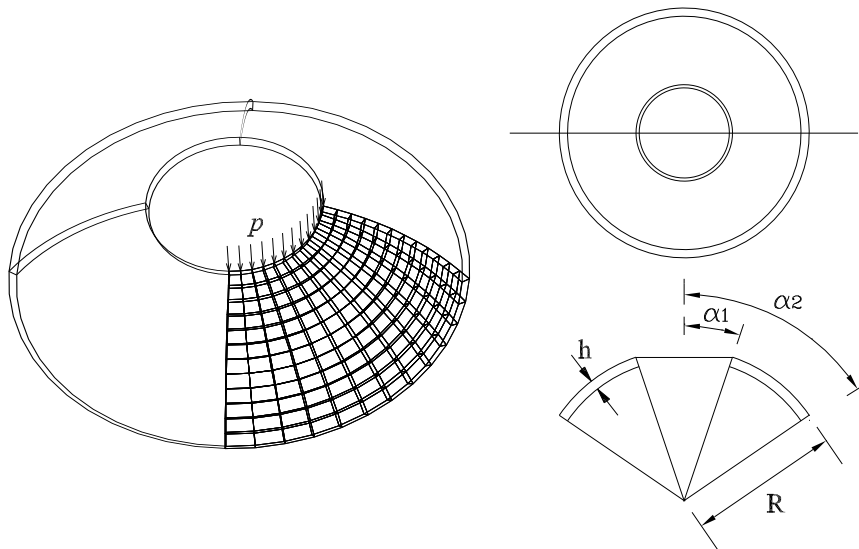
Fig. 5.17: Spherical cup: geometry and load conditions.

modeled by a 12×12 mesh. Vertical displacements are set to zero at the nodes of the bottom ring. We refer to the Young modulus $E = 1000$ and to the Poisson ratio $\nu = 0.3$. Dynamical analysis is carried out by assuming the $\rho = 0.1$ mass density, the $\lambda = 0.1t$ load history and the $\Delta t = 0.1$ time step for the Newmark scheme. For geometric parameters, we make $R = 12.16$, $h = 0.4$, $\alpha_1 = 18.594$ and $\alpha_2 = 55.668$.

Figure 5.18 shows $\lambda - \bar{w}$ vertical load parameter - deflection of the top ring points behavior for both the statical and modejumping solutions, respectively. The analysis are stopped when the value $\lambda = 1.5$ is traversed. Deformed configurations of the structure at the marked instants are depicted
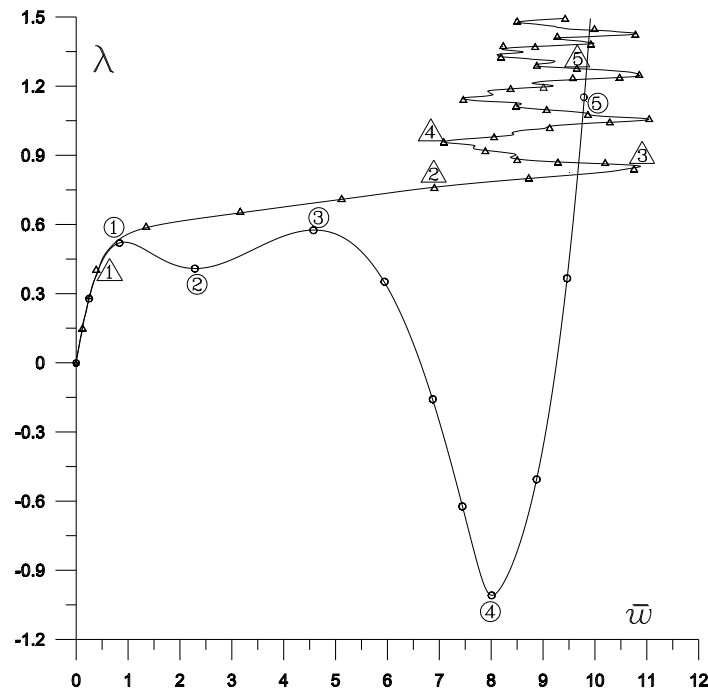
Fig. 5.18: Spherical cup: statical ($\bigcirc$) and modejumping ($\triangle$) solution curves.

in Figure 5.19 for the statical case and in Figure 5.20 for the quasi-statical one.

5.2 Dynamical analysis

In this section a set of examples is examined to analyze plane and spatial dynamical motion of bodies modeled with the presented two- and three-dimensional elements.

5.2.1 L-shaped block

The plane motion of a two-dimensional L-shaped block is analyzed by the 4-node element. The mesh is made up of 36 finite elements. The mesh configuration, p external load positions and time history are shown in Fig. 5.21.

Two different choices, $E = 10^7 \ N/m^2$ and $E = 10^4 \ N/m^2$, of the Young modulus have been adopted to analyze rigid-like and soft like motions, respectively. The Poisson modulus is assumed to be $\nu = 0.3$, while mass density $\rho = 1 kg/m^3$. Starting at the rest, a sequence of configurations have
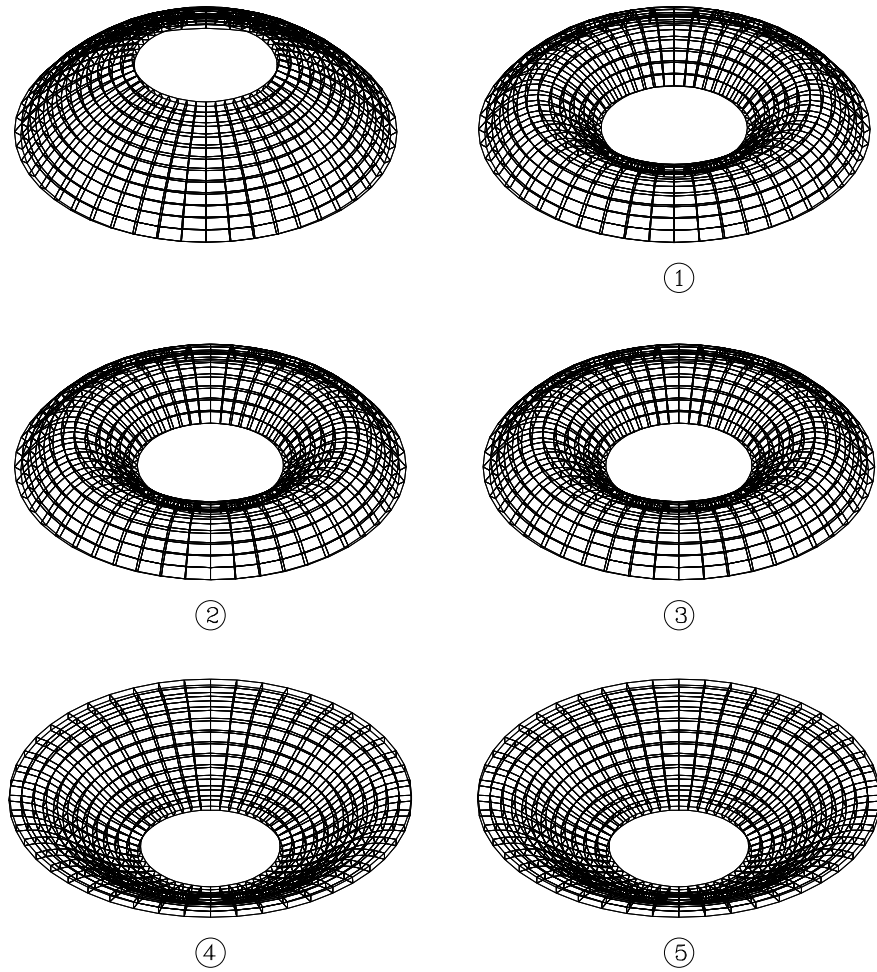
Fig. 5.19: Spherical cup: statical deformative configurations at marked so-
lution points.

been computed by using a $t = 0.01s$ time step for the observation time
$t = 0..10s$. The configurations obtained every single second for the rigid-like
motion are drawn in Fig.5.22. The results are equal to the ones reported in
Betsch and Steinmann [12] and Lopez and Russo [52] obtained by several
models of 4-node finite elements. Soft-like behavior of the L-shaped block,
by displaying the configurations every single second, is shown in Fig.5.23.
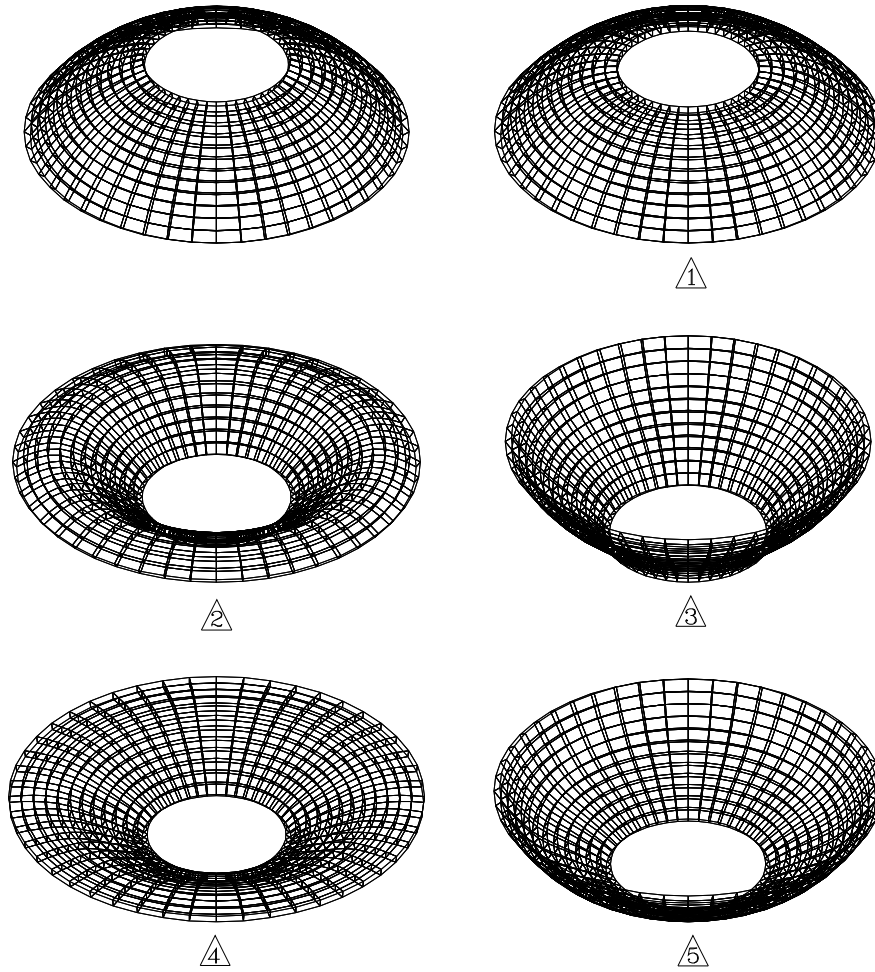
Fig. 5.20: Spherical cup: dynamical deformative configurations at marked solution points.

5.2.2 Toss rule in the plane

The plane movement of a free toss rule is analyzed by the 8-node element. The spatial discretization is made up of 30 finite elements. The material constants are $E = 2.06\,10^{11}\ N/m^2$, $\nu = 0$ and $\rho = 7.8\,10^3\ kg/m^3$. The geometry and position of distributed loads p and load function of the rule are described in Fig.5.24. With zero initial conditions, the integration time scheme computes the configurations by using a $\Delta t = 10^{-5}s$ time step. In Fig.5.25 the sequence of deformed shapes in the range $t = [0\,s, 0.1\,s]$ are shown. Similar results are obtained in Kuhl and Ramm [41] by using an

78
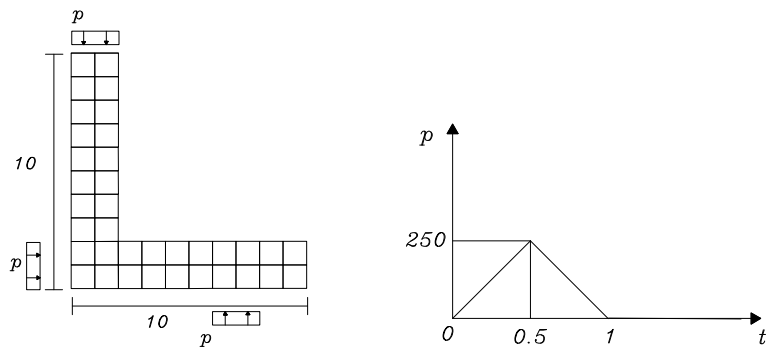
Fig. 5.21: L-shaped block: mesh configuration, external load positions and time history.
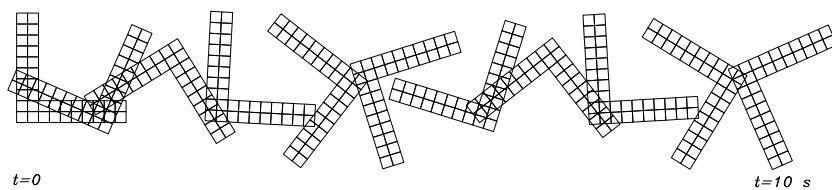
Fig. 5.22: L-shaped block $E = 10^7 \ N/m^2$: sequence of configurations.
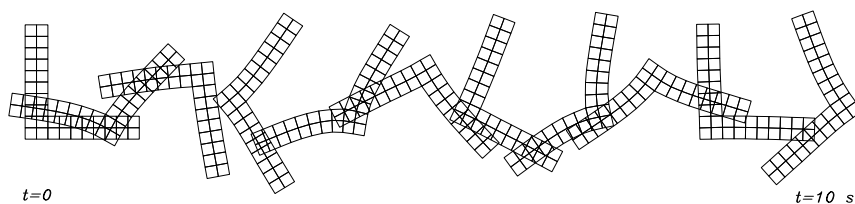
Fig. 5.23: L-shaped block $E = 10^4 \ N/m^2$: sequence of configurations.

8-node shell element and in Lopez and Russo [52] by using a 6-node plane element.
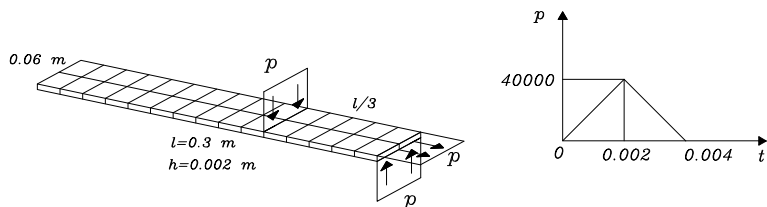
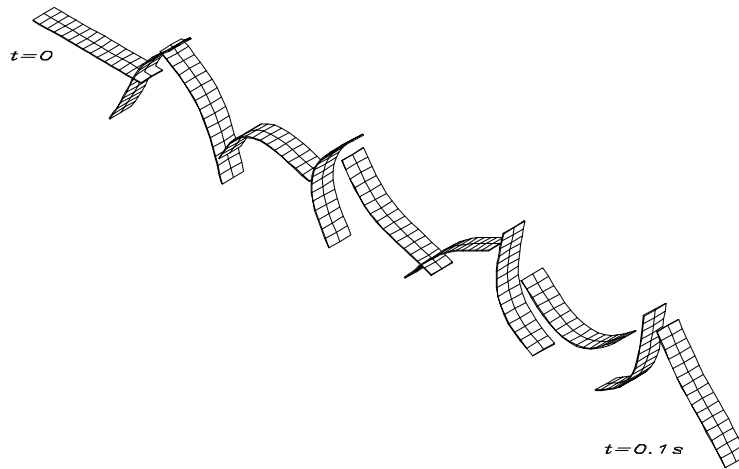**Fig. 5.24:** Toss rule nel piano: configurazione iniziale, mesh, andamento dei carichi esterni.

Fig. 5.25: Toss rule nel piano: sequenza di deformate.

5.2.3 Toss rule in space

The same rule as in the previous Section is now stimulated to fly in the space. Figure 5.26 describes the position of distributed loads p and load time function. As before, starting at the rest, the integration time scheme computes the configurations by using a $\Delta t = 10^{-5} s$. In Fig.5.27 the sequence of deformed shapes for $t = [0\,s, 0.4\,s]$ are shown. The deformed configurations are comparable with the 8-node shell element analysis reported in Kuhl and Ramm [41, 42].
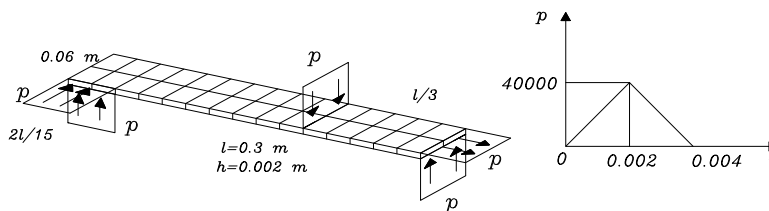
Fig. 5.26: Toss rule nello spazio: configurazione iniziale, mesh, andamento dei carichi esterni.

5.3 Conclusions

An alternative technique to analyze the motion of geometrically nonlinear structures is presented. The described formulation is applied to low-order elements and it does not use rotation measures.

The procedure involves only exact integrations and the kinematical basis is here defined by referring to natural modes. In order to avoid shear-locking
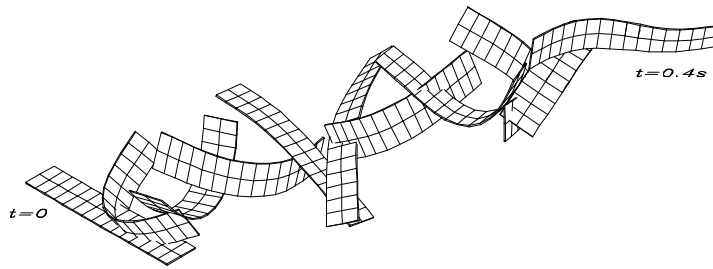
80

Fig. 5.27: Toss rule nello spazio: sequenza di deformate.

phenomena, a selective based definition of the strain tensor is carried out. This selection is carried out on the linear definition of deformation components the element reference system being independent.

In particular, the proposed approach is based on definitions of only relative lengths and it avoids adapting definitions of the element reference system. In this way:

- the finite element construction can be carried out completely in the linear field;

- we can select the deformative modes that contribute to the expressions of the strain tensor components;

- the analysis is robust because the singularities in rotation matrices are not introduced.

In addition, since the mechanical description is implicitly conservative, we can note that:

- the analysis is economical as it does not require complex manipulations to overcome the noncommutativity of rotations.

The numerical tests, finally, have shown that lower computational time and storage demand are required.

Additional benefits that arise from the aforementioned features include symmetry of the tangent stiffness matrix and insensitivity of the large displacement transformations to the size of the incremental step.

81

Chapter 6

Numerical results in projectors method

In Chapter 3 an innovative Total Lagrangian formulation of geometrically nonlinear finite elements has been proposed. The key concept is that slopes are used instead of rotation parameters to compute the nonlinear representations of the strain measures in the inertial frame of reference. So complex manipulations required to obtain conservative descriptions and well-posed transformation matrices are avoided. In this chapter numerical tests have been carried out to validate the developed technique in the frame structures context both in statical and dynamical field.

6.1 Statical analysis

In particular, the tests analyze spatial kinematics to validate the developed technique in the frame structures context. Equilibrium states were computed by the predictor-corrector scheme described Chapter 3 and compared to reference results obtained with similar beam models.

In the examples, meshes of increasing element size are used to test the convergence to the reference analyses. Numerical tests validate that the developed technique is well posed for any large rotation. The proposed formulation shows simplicity of the analysis while computational effectiveness and algorithmic reliability are retained.

6.1.1 Lateral buckling of a narrow cantilever beam

The narrow cantilever beam shown in Fig. 6.1 was analyzed. The numerical results obtained by Battini and Pacoste [7] can be taken as reference. The λ - w_c vertical load parameter - lateral tip displacement curves were computed and displayed in Fig. 6.2. The analysis were stopped when the value $\lambda = 8$ was reached.
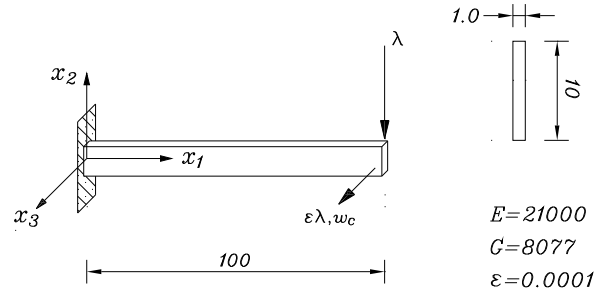
Fig. 6.1: Lateral buckling of a narrow cantilever beam: problem definition.
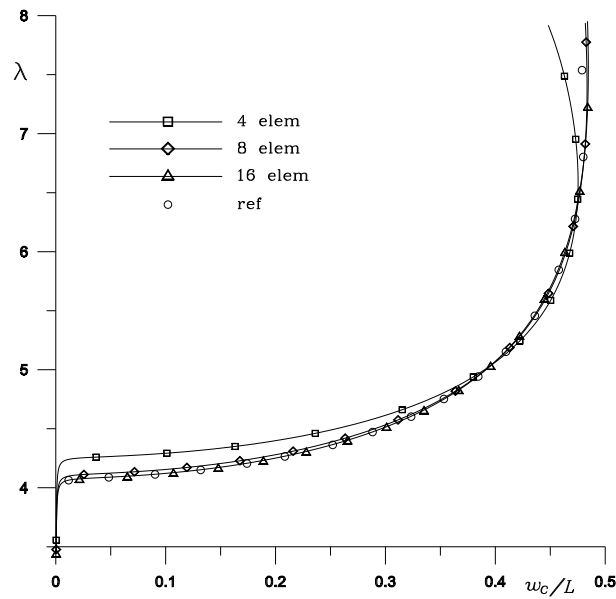

Fig. 6.2: Lateral buckling of a narrow cantilever beam: equilibrium paths.

6.1.2 Cantilever beam subject to a pure bending moment

A cantilever beam subject to a bending moment at the free end was analysed here (see Fig. 6.3). This is a classical test and the results can be compared with those obtained by Simo [70]. In Fig. 6.4 the normalized $\lambda L/\pi E J_2$ and $(L - u_c)/L$ values are used to show the computed equilibrium path.
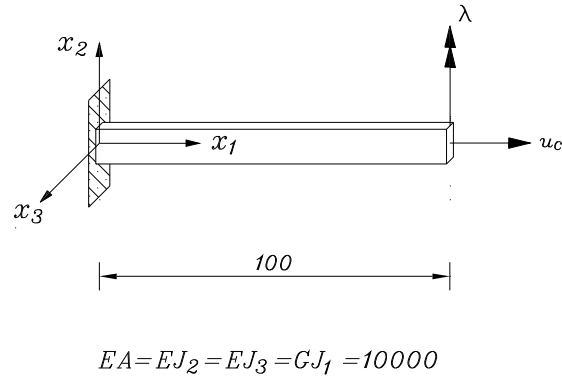
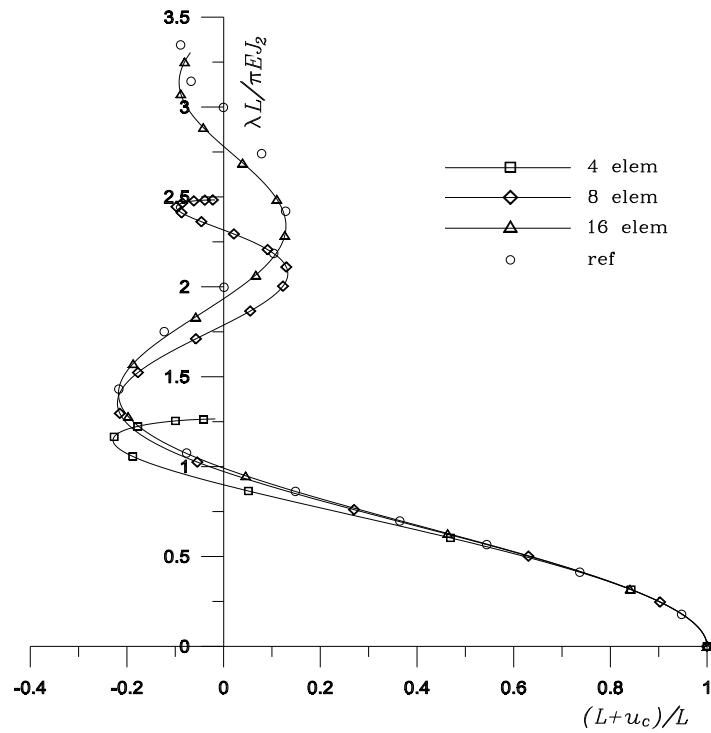**Fig. 6.3:** Cantilever beam subject to a pure bending moment: problem definition.

Fig. 6.4: Cantilever beam subject to a pure bending moment: equilibrium paths.

84

6.1.3 Cantilever beam subject to a pure torsional moment

The primary path of a cantilever beam subjected to end torsion, as shown in Fig. 6.5, was computed in this example. An analytical solution of the problem can be found in Hsiao and Lin [32]. Fig. 6.6 exhibits the λ - φ_c torque - angle of twist curves calculated until the value $\lambda = 16000$ is traversed.
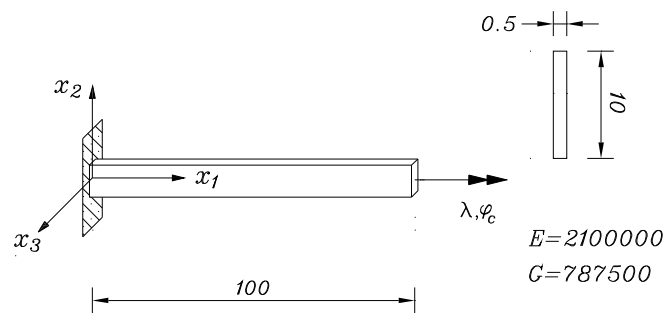

Fig. 6.5: Cantilever beam subject to a pure torsional moment: problem definition.

6.1.4 Right-angled frame under an end load

The nonlinear solution path of the L frame shown in Fig. 6.7 is analysed. The finite dimension connection between the members of the frame was modelled by Battini and Pacoste [7] with both a rigid and disregard connections. The λ - w_c horizontal load parameter - lateral tip displacement of the free end curves was computed until the $\lambda = 4$ value and displayed in Fig. 6.8. The number of elements indicated in Fig. 6.8 showing solution curves refers to the total number of used elements.

6.1.5 Right-angled frame under end moments

The last example concerns the right angle frame depicted in Fig. 6.9 where appreciable large rotations with a significant amount of twist are considered. The loading is given by a pair of concentrated moments applied at the supports. Due to the symmetry, only half of the frame is modelled. At the support only translation along x_1 and rotation around x_3 are allowed. The
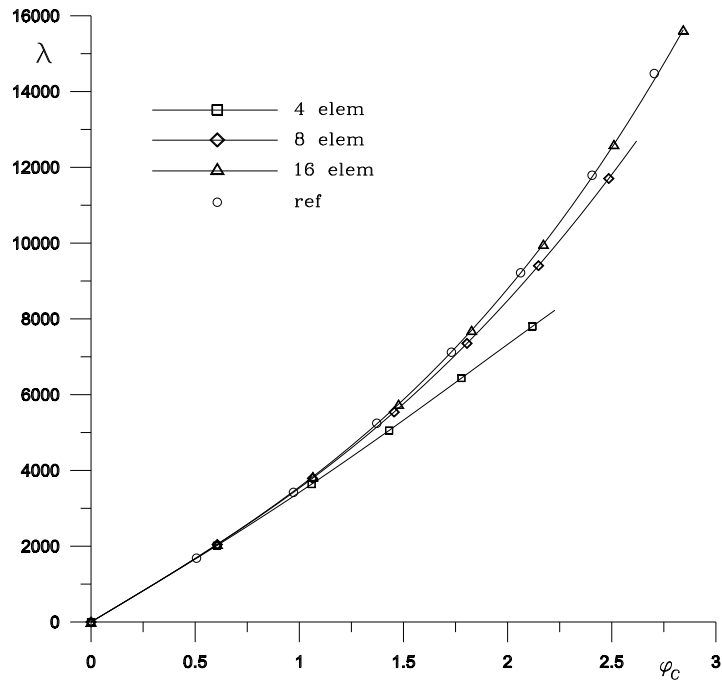
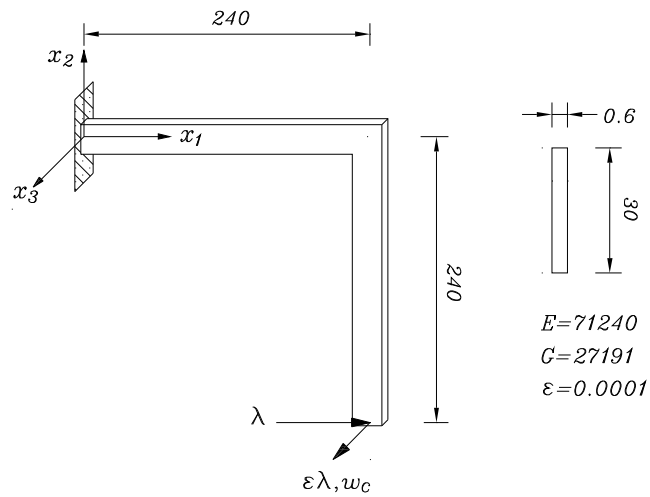**Fig. 6.6:** Cantilever beam subject to a pure torsional moment: equilibrium paths.

Fig. 6.7: Right-angled frame under an end load: problem definition.
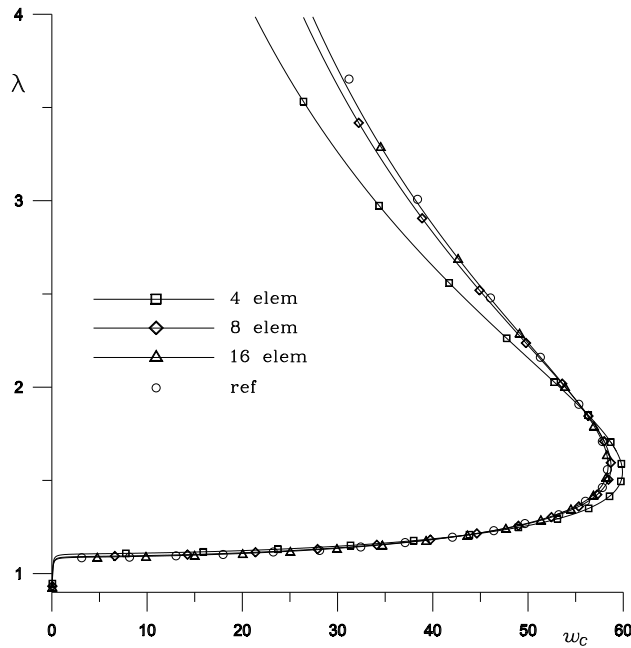
86

Fig. 6.8: Right-angled frame under an end load: equilibrium paths.

λ - w_c moment parameter - apex displacement in the x_3 direction diagram is plotted in Fig. 6.10. The results are in agreement with those found in Battini and Pacoste [7]. Meshes with 6, 8 and 10 elements are used here for the half of the frame.

The test is also carried out by removing imperfection load, now defined as $10^{-5}\lambda$, after the first buckling phase as in Simo and Vu-Quoc [73]. In the analysis, therefore, equilibrium curve traverses the negative critical point and completes a second revolution of the frame about the line connecting its hinged ends. Applied moment versus lateral displacement curves are shown in Fig. 6.11 for the first and second revolution. Afterward computed solution points traverse the positive critical point and describe the same first post-buckling behaviour as previously computed. In the formulation, then, there is no difficulty in subjecting the frame to any number of revolutions. A symmetrically intersection of the moment axis is, furthermore, obtained with ± 621.8 critical values.

6.2 Dynamical analysis

In the projectors methods context,a set of numerical examples shows the application of the proposed method for the time integration of the motion
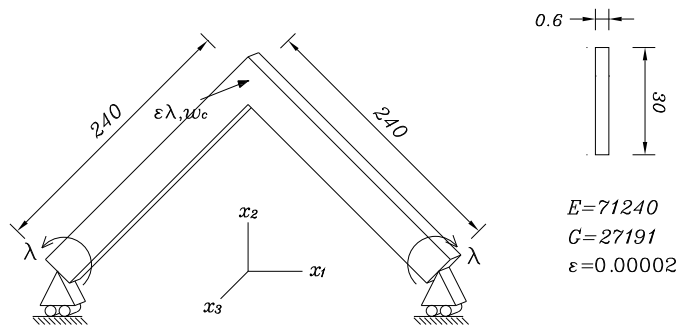
87

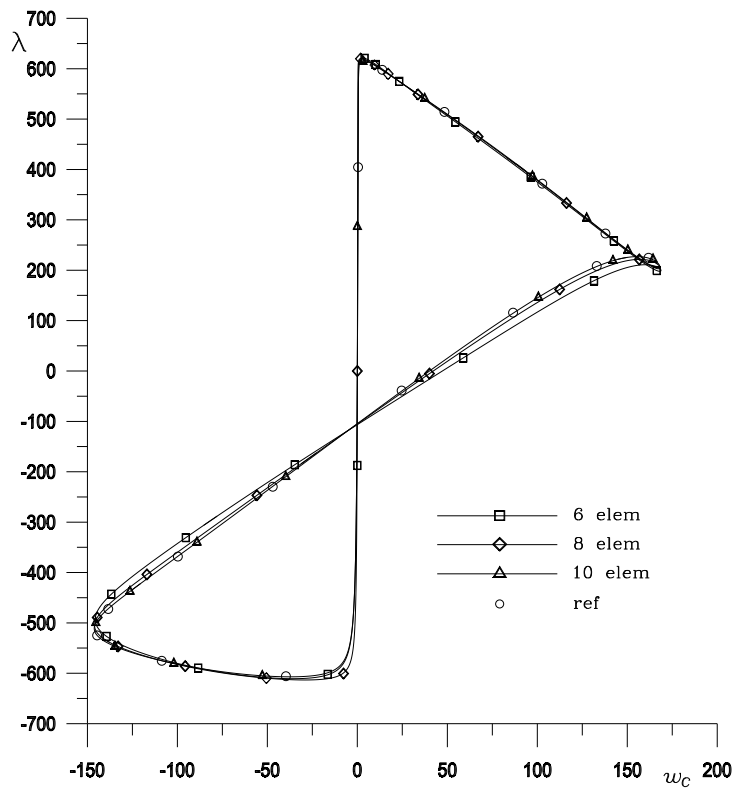**Fig. 6.9:** Right-angled frame under end moments: problem definition.

Fig. 6.10: Right-angled frame under end moments: equilibrium paths.
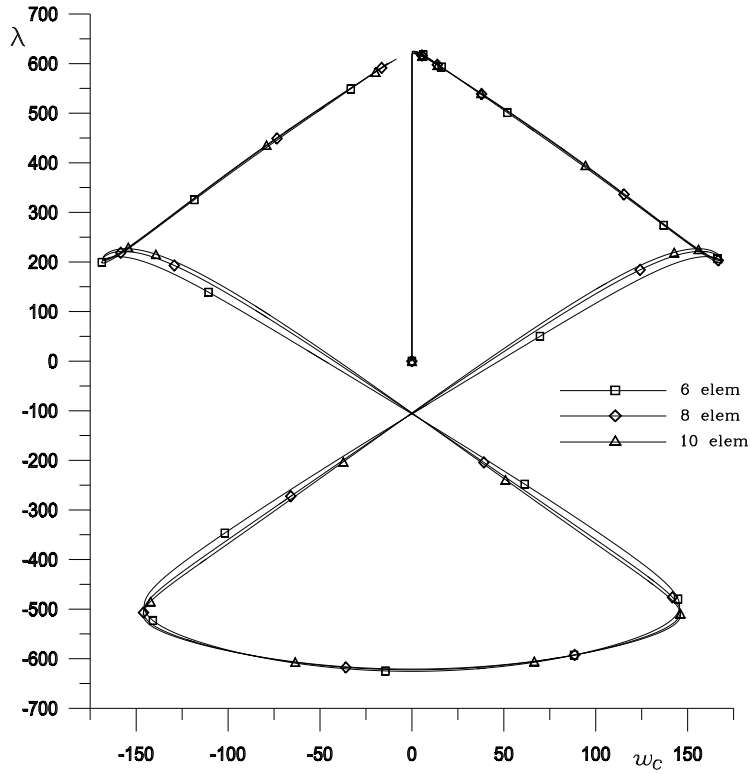
88

Fig. 6.11: Right-angled frame under end moments: first and second revolution.

equations.

In particular numerical tests were performed for increasing values of the Δt time step. Let *steps* be the number of time steps effected by the integration process to analyze the behaviour for $t = 0...T$. In the following we refer to the mean value of the Nw_i Newton iterations in the ith step

$$Nw_m = \sum_{i=1}^{step} Nw_i / steps, \tag{6.1}$$

carried out, unless it becomes unstable (div), in the process.

6.2.1 Motion of a dumbbell

We investigate the motion of a dumbbell with initial interbody distance $h = 1$ modeled as a two-particle problem and defined in the three-dimensional ambient space. We assume $m_1 = m_2 = 1$ with $\mathbf{u} = \{u_1 \ v_1 \ w_1 \ u_2 \ v_2 \ w_2\}$. The initial conditions are given by $\mathbf{u}^* = \mathbf{0}$, $\dot{\mathbf{u}}^* = \{0 \ 0 \ 2 \ 5 \ 5 \ 10\}$ and $\mathbf{E}^{ij} =$

89

{1 0 0} is the director in the x direction. Accordingly $\varepsilon_{ij} = 0$ and, by time differentiation, $\dot{\varepsilon}_{ij} = 0$ and $\dot{\mathbf{E}}^{ij} = \{0\ 3\ 5\}$ is obtained.
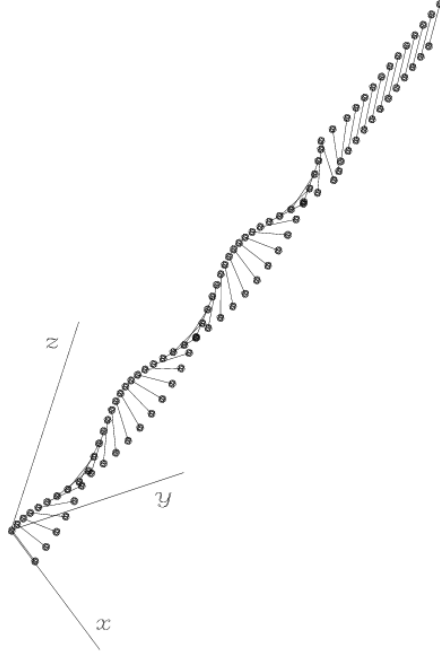

Fig. 6.12: Dumbbell $\Delta t = 0.02$ for $T = 2$: sequence of configurations obtained.

The interaction of the two bodies is assumed to be governed by a Lennard-Jones potential $U(r_{ij}) = A[(\sigma/r_{ij})^5 - (\sigma/r_{ij})^3]$ which is often employed in molecular dynamic simulations. The distance between the centers of the two particles is $r_{ij} = h + \varepsilon_{ij}$. We make $\sigma = (3/5)^{1/2}$, such that $\varepsilon_{ij} = 0$ characterizes the internal force free configuration. Here we consider the quasi-rigid connection $A = 10^6$ that classically has severe instability restrictions. In such a case, by linearization of $U(r_{ij})$ for $r_{ij} = 1$, $k_a = 6A\sigma^3$ can be interpreted as the spring stiffness. We can refer to Gonzales and Simo [29] and Crisfield and Shi [22] for the numerical instabilities which are introduced in such dynamic systems. Additional background material on the motion of a several particle system in a potential field can be found in standard books on classical mechanics, see e.g. Goldstein [28] and Arnold [2].

To illustrate the motion, Fig. 6.12 contains a sequence of configurations with $\Delta t = 0.02$ and $t = 0...2$. At about $t = 1.4$ an unphysical motion indicates the unstable behaviour of the Newmark scheme.

Tab. 6.1: Dumbbell $T = 10$: mean value Nw_m of the Newton iterations

Δt	0.002	0.005	0.01	0.02
	3.000	3.185	3.486	*div*

6.2.2 Two body system

Here we study the behaviour of a pair of equal pin-jointed elements as described in Section 4.3.3. Starting from rest, the dynamics of the two prismatic $h_\xi = 0.5$, $h_\eta = h_\zeta = 0.02$, bodies is stimulated by an impulsive force $p(t)$ acting on the system as illustrated in Fig. 6.13. We assume $\rho = 1.5 \cdot 10^4$ and $E = 5 \cdot 10^9$, $k_1 = 10^3$, $k_2 = 5 \cdot 10^2$, $k_3 = 2 \cdot 10^2$, for the evaluation of the (4.44) kinetic and (4.45) potential energy. Time-stepping schemes applied to N-body problems can be found in Betsch and Steinmann [11].
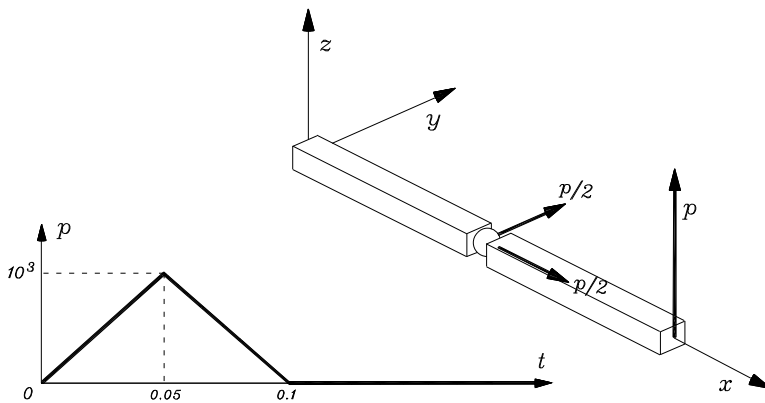

Fig. 6.13: Two body system: initial configuration and problem definition

The motion of the two body system with $\Delta t = 0.0002$ and $T = 0.3$ is shown in Fig. 6.14. The unstable motion of the system can be observed at about $t = 0.21$ where chaotic relative rotations in the joint point occur. Table 6.2 reports the Nw_m values performed in the time integation process for $T = 1$.

Tab. 6.2: Two body system $T = 1$: mean value Nw_m of the Newton iterations

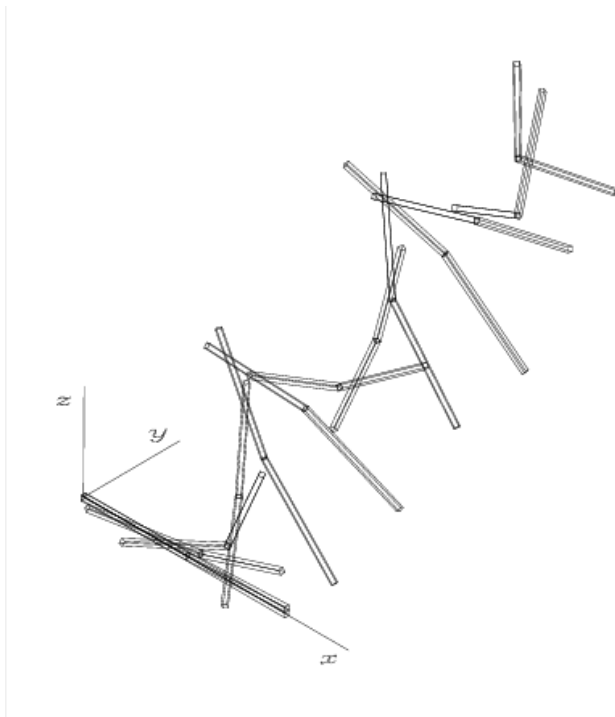| Δt	0.00002	0.00005	0.0001	0.0002
	3.010	3.312	3.665	*div*

Fig. 6.14: Two body system $\Delta t = 0.0002$ for $T = 0.3$: sequence of configurations

6.2.3 Toss rule in space

Here there is the example of the three-dimensional movement of a toss rule (see Kuhl and Ramm [41] for a solution to such a dynamical problem). The beam, with zero initial displacements and velocities, is discretized by nine described finite elements. The geometry, position of loads and load function of the rule are described in Fig. 6.15. The material is characterized by the values $\rho = 7.8 \cdot 10^3$, $E = 2.06 \cdot 10^{11}$ and $G = E/2$.

Tab. 6.3: Toss rule $T = 0.1$: mean value Nw_m of the Newton iterations.

Δt	0.00001	0.00002	0.00005
	3.202	3.635	*div*

An incipient non stable behaviour of the integration scheme at about $t = 0.026$ can be observed. Table 6.3 shows the behaviour with respect to the time integration step for $T = 0.1$.
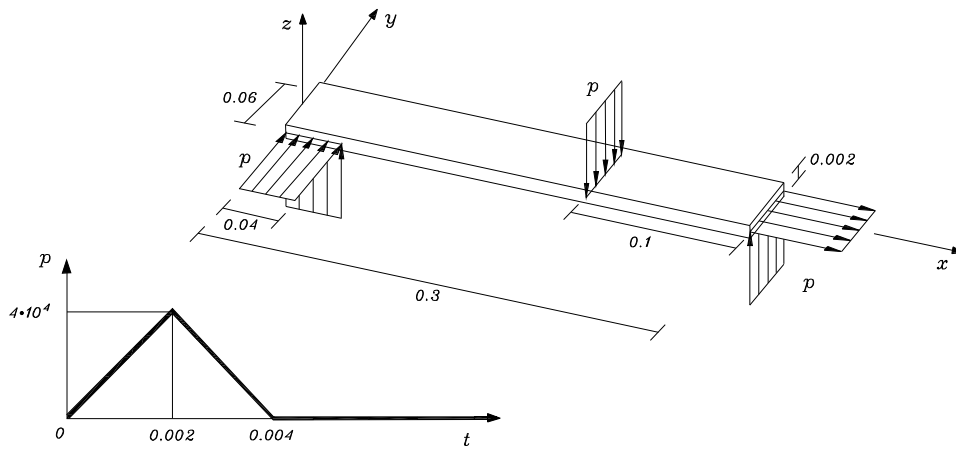
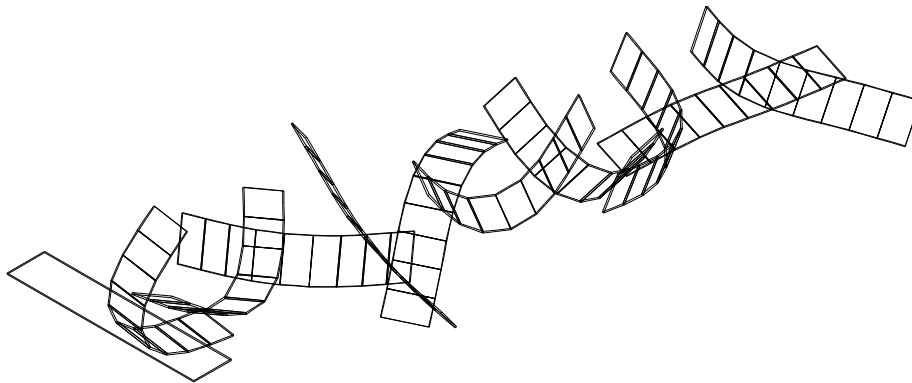**Fig. 6.15:** Toss rule: geometry, loads and load function

Fig. 6.16: Toss rule $\Delta t = 0.00005$: sequence of configurations

6.3 Conclusions

In the hypothesis of large displacements and rotations and small strains, a technique to analyze the behavior of three-dimensional finite element beam frames has been presented. A vectorial approach for the rotation parametrizations and linear strain definitions based on invariant measures has been used. The described formulation does not use angle measures and we have demonstrated that it proves to be well posed for any finite rotations. Rotation at the nodal location has been defined with two basis vectors along the cross-section, which creates nine degrees of freedom at the node.

We obtain a Lagrangian and implicitly conservative mechanical description where simple and computationally efficient expressions in the equations of the nonlinear system are preserved. Besides numerical results illustrate

93

that the present approach produces attractive properties for non-linear problems involving very large rotations compared to the conventional rotational parameter approach.

Bibliography

[1] F. Armero, E. Petocz, Formulation and analysis of conserving algorithms for frictionless dynamic contact/impact problems, *Computer Methods in Applied Mechanics and Engineering*, **158**, (1998), 269–300.

[2] V.I. Arnold, Mathematical methods of classical mechanics, *Prentice-Hall*, Englewood Cliffs, NJ (1989).

[3] J. Argyris, An excursion into large rotations, *Computer Methods in Applied Mechanics and Engineering*, **32** (1982), 85–155.

[4] J. Argyris, M. Papadrakakis, Z.S. Mauroutis, Nonlinear dynamic analysis of shells with the triangular element TRIC, *Computer Methods in Applied Mechanics and Engineering*, **192** (2003), 3005–3038.

[5] J. Argyris, L. Tenek, L. Olofsson, TRIC: a simple but sophisticated 3-node triangular element based on 6 rigid body and 12 straining modes for fast computational simulations of arbitrary isotropic and laminated composite shells, *Computer Methods in Applied Mechanics and Engineering*, **145** (1997), 11–85.

[6] K.J. Bathe, L.W. Ho, A simple and effective element for analysis of general shell structures, *Computers and Structures*, **13** (1980), 673–681.

[7] J.M. Battini, C. Pacoste, Co-rotational beam elements with warping effects in instability problems, *Computer Methods in Applied Mechanics and Engineering*, **191** (2002), 1755–1789.

[8] T. Belytschko, B.J. Hsieh, Non-linear transient finite element analysis with convected co-ordinates, *International Journal for Numerical Methods in Engineering*, **7** (1973), 255–271.

[9] T. Belytschko, J.S.J. Ong, W.K. Liu, J.M. Kennedy, Hourglass control in linear and nonlinear problems, *Computer Methods in pplied Mechanics and Engineering*, **43** (1984), 251–276.

[10] T. Belytschko, D.F. Schoeberle, On the unconditional stability of an implicit algorithm for nonlinear structural dynamics, *Journal of Applied Mechanics*, **42** (1975), 865–869.

[11] P. Betsch, P. Steinmann, Conservation properties of a time FE method. Part I: Time-stepping schemes for N-body problems , *International Journal for Numerical Methods in Engineering* , **49** (2000), 599–638.

[12] P. Betsch, P. Steinmann, Conservation properties of a time FE method. Part II: Time-stepping schemes for non-linear elastodynamics, *International Journal for Numerical Methods in Engineering*, **50** (2001), 1931–1955.

[13] P. Betsch, P. Steinmann, Constrained dynamics of geometrically exact beams, *Computational Mechanics*, **31** (2003), 49–59.

[14] P. Betsch, P. Steinmann, Constrained integration of rigid body dynamics, *Computer Methods in Applied Mechanics and Engineering*, **191** (2001), 467–488.

[15] B. Brank, J. Korelc and A. Jbrahimbegovic, Dynamics and time-stepping schemes for elastic shells undergoing finite rotations, *Computers and Structures*, **81** (2003), 1193–1210.

[16] A. Cardona, M. Geradin, A beam finite element non-linear theory with finite rotations, *International Journal for Numerical Methods in Engineering*, **26** (1988), 2403–2438.

[17] A. Cardona, A. Huespe, Evaluation of simple bifurcation points and post-critical path in large finite rotation problems, *Computer Methods in Applied Mechanics and Engineering*, **175** (1999), 137–156.

[18] J.Chung, G.M. Hulbert, A time integration algorithm for structural dynamics with improved numerical dissipation: the generalized-a method, *Journal of Applied Mechanics*, **60** (1993), 371–375.

[19] M.A. Crisfield, A consistent co-rotational formulation for nonlinear three-dimensional beam elements, *Computer Methods in Applied Mechanics and Engineering*, **81** (1990), 131–150.

[20] M.A. Crisfield, Non-linear finite element analysis of solids and structures. Volume 2: advanced topics, *John Wiley & Sons, Chichester*, 2003.

[21] M.A. Crisfield, U. Galvanetto, G. Jelenic', Dynamics of 3-D co-rotational beams, *Computational Mechanics*, **20** (1997), 507–519.

[22] M.A. Crisfield, J. Shi, An energy conserving co-rotational procedure for non-linear dynamics with finite elements, *Nonlinear Dynamics*, **9** (1996), 37–52.

[23] K.E. Dufva, J.T. Sopanen, A.K. Mikkola, Three-dimensional beam element based on a cross-sectional coordinate system approach, *Nonlinear Dynamics*, **43** (2006), 311–327.

[24] A. Eriksson, On a thin shell element for non-linear analysis based on the isoparametric concept, *Computers and Structures*, **42** (1992) 927–939.

[25] A. Eriksson, On improved predictions for structural equilibrium path evaluations, *International Journal for Numerical Methods in Engineering*, **36** (1993), 201–220.

[26] C.A. Felippa, B. Haughen, A unified formulation of small-strain corotational finite elements: I.Theory, *Computer Methods in Applied Mechanics and Engineering*, **194** (2005), 2285–2335.

[27] D.P. Flanagan, T. Belytschko, A uniform strain hexahedron and quadrilateral with orthogonal hourglass contol, *International Journal for Numerical Methods in Engineering*, **17** (1983), 679–706.

[28] H. Goldstein, Classical mechanics, *Addison-Wesley*, Reading, Massachusetts (1980).

[29] O. Gonzales, J.C. Simo, On the stability of symplectic and energy-momentum algorithms for non-linear Hamiltonian systems with symmetry, *Computer Methods in Applied Mechanics and Engineering*, **134** (1996), 197–222.

[30] C. Hoff, P.J. Pahl, Development of an implicit method with numerical dissipation for generalized single step algorithm for structural dynamics, *Computer Methods in Applied Mechanics and Engineering*, **67** (1988), 367–385.

[31] K.M. Hsiao, Nonlinear analysis of general shell structures by flat triangular shell element, *Computers and Structures*, **25** (1987), 665–675.

[32] K.M. Hsiao, W.Y. Lin, A co-rotational finite element formulation for buckling and postbuckling analyses of spatial beams, *Computer Methods in Applied Mechanics and Engineering*, **188** (2000), 567–594.

[33] T.J.R. Hughes, T.K. Caughy, W.K. Liu, Finite-element methods for nonlinear elastodynamics which conserve energy, *Journal of Applied Mechanics* , **45** (1978), 366–370.

[34] A. Ibrahimbegović, F. Frey, I. Kozar, Computational aspects of vector-like parameterization of three-dimensional finite rotations, *International Journal for Numerical Methods in Engineering*, **38** (1995), 3653–3673.

[35] A. Ibrahimbegović, H. Shakourzadeh, J.L. Batoz, M. Al Mikdad, Y.Q. Guo, On the role of geometrically exact and second-order theories in buckling and post-buckling analysis of three-dimensional beam structures, *Computers and Structures*, **61** (1996), 1101–1114.

[36] B.A. Izzuddin, An enhanced co-rotational approach for large displacement analysis of plates, *International Journal for Numerical Methods in Engineering*, **64** (2005), 1350–1374.

[37] R.N. Jazar , Advanced Dynamics: Rigid Body, Multibody, and Aerospace Applications. *John Wiley & Sons.* -

[38] K.T. Kavanagh, S.W. Key, A note on selective and reduced integration techniques in finite element method, *International Journal for Numerical Methods in Engineering*, **4** (1972), 148–150.

[39] D. Kosloff, G.A. Frazier, Treatment of hourglass patterns in loworder finite element codes, *International Journal for Numerical and Analytical Methods in Geomechanics*, **2** (1978), 57–72.

[40] R. Kouhia and M. Mikkola, Tracing the equilibrium path beyond simple critical points, *International Journal for Numerical Methods in Engineering*, **28** (1989), 2923–2941.

[41] D. Kuhl, E. Ramm, Constraint Energy Momentum Algorithm and its application to non-linear dynamics of shells, *Computer Methods in Applied Mechanics and Engineering*, **136** (1996), 293–315.

[42] D. Kuhl, E. Ramm, Generalized energy-momentum method for non-linear adaptive shell dynamics, *Computer Methods in Applied Mechanics and Engineering*, **178** (1999), 343–366.

[43] W. Lacarbonara, H. Yabuno, Refined models of elastic beams undergoing large in-plane motions: theory and experiment, *International Journal of Solid and Structures*, **43** (2006), 5066–5084.

[44] P. Lasaint, P.A. Raviart, On a finite element method for solving the neutron transport equation. In: de Boor, C. (ed.), *Mathemetical aspects of finite elements in partial differential equations*, Academic Press, New York, (1974), 89–123.

[45] R. Levy, E. Gal, The Geometric Stiffness of Thick Shell Triangular Finite Elements for Large Rotations, *International Journal for Numerical Methods in Engineering*, **65** (2006), 1378–1402.

[46] W.K. Liu, Y.K. Hu and T. Belytschko, Multiple quadrature unterintegrated finite elements, *International Journal for Numerical Methods in Engineering*, **37** (1994), 3263–3289.

[47] W.K. Liu, J.S.J. Ong and R.A. Uras, Finite element stabilization matrices-a unification approach, *Computer Methods in Applied Mechanics and Engineering*, **53** (1985), 13–46.

[48] S. Lopez, An effective parametrization for asymptotic extrapolations, *Computer Methods in Applied Mechanics and Engineering*, **189** (2000), 297–311.

[49] S. Lopez, Detection of bifurcation points along a curve traced by a continuation method, *International Journal for Numerical Methods in Engineering*, **53** (2002), 983–1004.

[50] S. Lopez, Improving stability by change of representation in time-stepping analysis of non-linear beams dynamics, *International Journal for Numerical Methods in Engineering*, **69** (2007), 822–836.

[51] S. Lopez, Structural dynamical analysis by a lengths-based description of the small strains in the finite displacements regime, *Nonlinear Dynamics*, **59** (2010), 29–44.

[52] S. Lopez, K. Russo, Improving stability in the time-stepping analysis of structural nonlinear dynamics, *International Journal of Structural Stability and Dynamics*, **8** (2008), 257–270.

[53] S. Lopez, G. La Sala, A vectorial approach for the formulation of finite element beams in finite rotations, *Proceedings Tenth International Conference on Computational Structures Technology*, Valencia (2010).

[54] S. Lopez, G. La Sala, A finite element approach to statical and dynamical analysis of geometrically nonlinear structures, *Finite Element in Analysis and Design*, **46** (2010), 1096–1105.

[55] P. Mata, S. Oller, A.H. Barbat, Dynamic analysis of beam structures considering geometric and constitutive nonlinearity, *Computer Methods in Applied Mechanics and Engineering*, **197** (2008), 857–878.

[56] F. Mohri, L. Azrar, M. Potier Ferry, Flexural-torsional post-buckling analysis of thin-walled elements with open sections, *Thin-Walled Structures*, **39** (2001), 907–938.

[57] F. Mohri, N. Damil, M. Potier Ferry, Large torsion finite element model for thin-walled beams, *Computers and Structures*, **86** (2008), 671–683.

[58] A.H. Nayfeh, Introduction to Perturbation Techniques, *John Wiley & Sons*, (1981).

[59] A.H. Nayfeh, Nonlinear Interactions. Analytical, Computational, and Experimental Methods, *John Wiley & Sons*, (2000).

[60] A.H. Nayfeh, Perturbations Methods, *John Wiley & Sons*, (1973).

[61] A.H. Nayfeh, Problems in Perturbation, *John Wiley & Sons*, (1985).

[62] A.H. Nayfeh, B. Balachandran, Applied Nonlinear Dynamics, *John Wiley & Sons*, (1995).

[63] A.H. Nayfeh, D.T. Mook, Nonlinear Oscillations, *John Wiley & Sons*, (1979).

[64] A.H. Nayfeh, P.F. Pai, Linear and Nonlinear Structural Mechanics, *John Wiley & Sons*, (2004).

[65] N.M. Newmark, A method of computation for structural dynamics, *ASCE Journal of the Engineering Mechanics Division*, **85** (1959), 67–94.

[66] C. Pacoste, Co-rotational flat facet triangular elements for shell instability analyses, *Computer Methods in Applied Mechanics and Engineering*, **156** (1998), 75–110.

[67] X. Peng, M. A. Crisfield, A consistent co-rotational formulation for shells using the constant stress/constant moment triangle, *International Journal for Numerical Methods in Engineering*, **35** (1992), 1829–1847.

[68] C.C. Rankin, B. Nour-Omid, The use of projectors to improve finite element performance, *Computers and Structures*, **30** (1988), 257–267.

[69] J. Rhim, W. Lee, A vectorial approach to computational modelling of beams undergoing finite rotations, *International Journal for Numerical Methods in Engineering*, **41** (1998), 527–540.

[70] J.C. Simo, A finite strain beam formulation. The three-dimensional dynamic problem. Part I, *Computer Methods in Applied Mechanics and Engineering*, **49** (1985), 55–70.

[71] J.C. Simo, N. Tarnow, A new energy and momentum conserving algorithm for the nonlinear dynamics of shells, *International Journal for Numerical Methods in Engineering*, **37** (1994), 2527–2549.

[72] J.C. Simo, N. Tarnow, The discrete energyŰmomentum method. Conserving algorithms for nonlinear elastodynamics, *Journal of Applied Mathematics and Physics*, **43** (1992), 757–792.

[73] J.C. Simo, L. Vu-Quoc, A three-dimensional finite-strain rod model. Part II: Computational aspects, *Computer Methods in Applied Mechanics and Engineering*, **58** (1986), 79–116.

[74] G. Wempner, Finite Elements, finite rotations and small strains of flexible shells, *International Journal of Solid and Structures*, **5** (1969), 117–153.

[75] Y.B. Yang, S. P. Lin, C.S. Chen, Rigid body concept for geometric nonlinear analysis of 3D frames, plates and shells based on the updated Lagrangian formulation, *Computer Methods in Applied Mechanics and Engineering*, **196** (2007), 1178–1192.

[76] O.C. Zienkiewicz, R.L. Taylor, J.M. Too, Reduced integration technique in general analysis af plates and shells, *International Journal for Numerical Methods in Engineering*, **3** (1971), 275–290.

[77] O.C. Zienkiewicz, W.L. Wood, N.W. Hine, R.L. Taylor, A unified set of single step algorithms. Part I. General formulation and applications, *International Journal for Numerical Methods in Engineering*, **20** (1984), 1529–1552.